SEMMELWEIS EGYETEM

DOKTORI ISKOLA

Ph.D. értekezések

3084.

SZABÓ ADRIENN

Biológiai pszichiátria

című program

Programvezető: Dr. Lazáry Judit, egyetemi tanár

Témavezető: Dr. Zelena Dóra, egyetemi tanár

EXPLORING THE PROGRESSION OF ALZHEIMER'S DISORDER THROUGH THE INTERPLAY OF ANXIETY, MOTOR DYSFUNCTION AND METABOLIC CHANGES IN THE 3xTG-AD MOUSE MODEL

PhD thesis

Adrienn Szabó

János Szentágothai Doctoral School of Neurosciences

Semmelweis University

Supervisor: Dóra Zelena, MD, DSc

Official reviewers: András Iring, Ph.D

Zsuzsanna Tóth Várnainé, Ph.D

Head of the Complex Examination Committee:

Gábor Varga, MD, DSc

Members of the Complex Examination Committee:

Krisztina Káldi, DSc

Zsuzsanna Helyes, MD, DSc

Budapest

2024

"On ne voit bien qu'avec le cœur. L'essentiel est invisible pour les yeux."
"It is only with the heart that one can see rightly; what is essential is invisible to the eye."
— *The Little Prince* by Antoine de Saint-Exupéry

I dedicate my dissertation to Stefi's memory.

Your memory lives on in my heart.

Table of Contents

3

List of Abbreviations

AD	Alzheimer's disorder
2MT	fox odour, 2-methyl-2-thiazoline
3xTg-AD mice	triple transgenic mouse model of AD
A673T	protective APP variant
AAV	adeno-associated virus
AgRP	agouti-related peptide
AICD	amyloid precursor protein intracellular domain
APP	amyloid precursor protein
APP-CTF or C99	APP C-terminal fragments
APPSwe; K670N/M671L	Swedish mutation
Arc	arcuate nucleus of the hypothalamus
Aβ	amyloid β
Aβ1–40	Aβ of the most prevalent form comprising 40 amino acids
Aβ1–42	Aβ of a less soluble variant composed of 42 amino acids
BACE	β-secretase
BAX	gene of Bcl-2 associated X protein
BAX	Bcl-2 Associated X protein
BCL2	gene of B-cell leukaemia/lymphoma 2 protein
Bcl-2	B-cell leukaemia/lymphoma 2 protein
BLA	basolateral amygdala
Br	Bregma
C	control
CAA	cerebral amyloid angiopathy
CART	cocaine and amphetamine-regulated transcript
Cas3	caspase-3
COX4	gene of cytochrome c oxidase subunit 4
COXIV	protein of cytochrome c oxidase subunit 4
CSF	cerebrospinal fluid
DIO	deiodinase enzymes
DIO1	deiodinase enzyme type 1
DIO2	deiodinase enzyme type 2
DIO3	deiodinase enzyme type 3

DMMB	dimethyl-methylene-blue staining
DSM-5-TR	Diagnostic and Statistical Manual of Mental Disorders, Fifth Edition, Text Revision
E693G	mutations like Arctic
E693Q	mutations like Dutch
EE	energy intake and expenditure
ELISA	Enzyme-Linked Immunosorbent Assay
EPM	elevated plus maze
fAD	familiar Alzheimer's disorder
fT3	serum free T3
fT4	serum free T4
FTD	frontotemporal dementia
GAPDH	glyceraldehyde-3-phosphate dehydrogenase protein
HPT	hypothalamic-pituitary-thyroid axis
HRT	hormone replacement therapy
icv	intracerebroventricular
LBD	Lewy body dementia
LD	light-dark box test
M	month
MAPT	microtubule associated protein tau
MBH	mediobasal hypothalamus
MC3R	melanocortin 3 receptor
MC4R	melanocortin 4 receptor
MCHR	melanin-concentrating hormone receptor
MCI	mild cognitive impairment
MCT8	monocarboxylate transporter 8
MWM	Morris water maze test
NfL	neurofilament light
NFT	intraneuronal/neurofibrillary tangles
Ni-DAB	nickel-diaminobenzidine tetrahydrochloride
NPY	neuropeptide Y
OB	olfactory bulb
OCT	operant condition test
OFT	open field test

PBS	phosphate-buffered saline
PET	positron emission tomography
phospho-tau	p-tau
POMC	proopiomelanocortin
proCas3	procaspase-3
PSEN1	presenilin 1
PSEN2	presenilin 2
PVN	paraventricular nucleus of the hypothalamus
qPCR	Real-time polymerase chain reaction, quantitative PCR
RAM	radial arm maze test
RER	respiratory exchange ratio
rpm	round per minute
RQ	respiratory quotient
sAD	sporadic Alzheimer's disorder
SAM	senescence-accelerated mouse model
SAMP	SAM-prone
SEZ6L	gene of membrane protein seizure 6-like
SPRT	single pellet retrieval test
T3	triiodothyronine
T4	thyroxine
TBI	traumatic brain injury
TDP-43	TAR DNA-binding protein 43
Thy-1	platelet-derived growth factor þ-chain, thymocyte differentiation antigen 1
TMT	2,4,5-trimethylthiazole
TRERM2	trigger receptor 2 expressed on myeloid cells model
TRH	thyrotropin-releasing hormone
TRβ2	gene of thyroid hormone receptor-β2
TSH	thyroid stimulating hormone
V717F	mutations like Indiana
V717I	mutations like London
VaD	vascular dementia
WB	Western Blot

I. Introduction

Alzheimer's disorder (AD) represents an age-related neurodegenerative disorder and stands as one of the most prevalent forms of dementia worldwide (1, 2). Presently, approximately 50 million individuals are afflicted by AD, which increase annually by 10 million (1). Less than 5% of AD is caused by a single genetic mutation that is transmitted through families, called familiar AD (3, 4). Thus, most of the cases have unknown, multifactorial origin, labelled as sporadic AD (sAD) (5). In the clinical picture the cardinal feature of AD is the memory loss, while histologically the diagnostic criteria is the presence of extracellular senile plaques comprised predominantly of amyloid β (Aβ) and the presence of intracellular tau aggregates within the brain (6, 7).

Early diagnosis can help slow down the progression, for which the mapping of risk factors and appropriate biomarkers is essential. Unfortunately, the therapeutic options are limited, which necessitates preclinical research on animals to identify new targets and to test new compounds. My general aim was to contribute to the understanding of disease pathology.

I.0. Dementia Overview: Types, Prevalence, and Key Characteristics

Dementia encompasses a spectrum of progressive neurodegenerative syndromes, characterized by the deterioration of cognitive functions, including memory, reasoning, and behaviour, as neurons die over time (8, 9). Primarily affecting individuals over 65, dementia symptoms lead to increasing difficulties in daily life and a loss of independence, with severe consequences on quality of life (10). Dementia is not a single disease but rather an umbrella term covering multiple subtypes, each with distinct pathological features (9, 11). This classification largely depends on the abnormal accumulation of specific proteins in various brain regions, such as tau, amyloid, alpha-synuclein, and TAR DNA-binding protein 43 (TDP-43), which collectively damage neurons, disrupt brain networks, and impair cognitive and sensorimotor functions (9). The prevalence of dementia is steadily increasing worldwide, affecting approximately 46.8 million people in 2015 and projected to reach 131.5 million by 2050 (12).

Among the major types of dementia, AD is the most common, representing around 60% of cases (13). Vascular dementia (VaD) is the second most prevalent, estimated to account for 15-20% of dementia cases (14). It develops due to damage in brain blood vessels, often following strokes or other vascular incidents, which result in cognitive

decline that typically affects attention, planning, and problem-solving abilities (15). Lewy body dementia (LBD) comprises approximately 10-15% of dementia diagnoses (16), presenting with fluctuating cognitive decline, visual hallucinations, motor symptoms, and REM sleep disturbances. This type is associated with the abnormal accumulation of alpha-synuclein protein in brain cells, forming Lewy bodies (17). Frontotemporal dementia (FTD), accounting for around 5-10% of cases, usually manifests in individuals under 65 and is characterized by significant behavioural and language changes due to progressive damage in the frontal and temporal lobes (18). Prion diseases, such as Creutzfeldt–Jakob disease, represent rare and rapidly progressing forms of dementia driven by prion protein accumulation, leading to swift cognitive decline and a short survival period post-onset (19).

Understanding the prevalence, symptoms, and pathology of these dementia subtypes is essential to advancing diagnostic and therapeutic strategies, particularly as global population aging continues to drive a rapid rise in cases.

I.1. Alzheimer's disorder (AD)

I.1.1. Gender Differences in AD

Epidemiological studies demonstrate a higher prevalence of AD among women, with a greater risk that escalates with age (20). Hormonal influences, particularly the decrease in oestrogen during menopause, are central, as this neuroprotective hormone supports mitochondrial function and genomic stability (21). The reduction in oestrogen post-menopause may heighten women's susceptibility to AD's neurodegenerative effects, especially without hormone replacement therapy (HRT) (22, 23). By contrast, although testosterone levels in men also decline with age, the cognitive implications of this decline remain less well defined (24).

Gender-specific differences are also evident in the genetic aspects of AD. The APOE ε4 allele, a key genetic risk factor for AD, confers a higher risk in women, particularly those aged 65–75 (25). Additionally, neuroinflammatory processes, autophagy, and metabolic mechanisms exhibit sex-based differences (26). Lower autophagic activity in women is associated with a greater accumulation of tau and amyloid proteins (27, 28). Moreover, differences in gut microbiota, which interact with neuroinflammation and metabolism, further underscore gender-specific variability in AD pathophysiology (29, 30).

Risk factors such as depression, cardiovascular issues, and sleep disturbances vary between genders: depression is more prevalent in women around menopause (31, 32) while traumatic brain injury (TBI) appears as a contributing AD risk factor in men (33). Clinically, cognitive impairment often manifests differently between sexes, with verbal memory decline more common in women and spatial-visual impairment more typical in men (34, 35). Biomarker studies indicate that neurofilament light (NfL) levels, a marker of neuronal degeneration, are generally higher in men, as shown in blood and cerebrospinal fluid (CSF) analyses (36, 37).

In conclusion, AD progression, risk factors, and clinical manifestations exhibit significant gender differences, whose understanding is essential for targeted diagnostics and therapeutic advancements. Research approaches incorporating sex-specific variables may open new avenues in the treatment and prevention of AD, especially by considering individualized hormonal, genetic, and social influences (26, 38).

I.1.2. Symptoms

According to the Diagnostic and Statistical Manual of Mental Disorders, Fifth Edition, Text Revision (DSM-5-TR) (American Psychiatric Association, 2022) diagnosis of AD requires a decline in memory and learning and deficit in at least one other cognitive domain (from the following six domains: complex attention, executive function, learning and memory, language, perceptual-motor, and social cognition). However, in many cases AD also interferes with the activities of daily living. Although it is generally accepted that memory decline is the core symptom, some authors suggest that AD is the disease of consciousness (39).

I.1.3. Comorbidities

I.1.3.1. Anxiety and depression

AD is often associated with other diseases that complicate the diagnosis and treatment. A meta-analysis summarizing data from 1964 to 2014 found that one of the most common comorbidities is depression: 42% of patients suffered from both (40-42). Additionally, anxiety symptoms were found to be comorbid in 39% of patients with AD (42). Moreover, anxiety and depression are not only consequences, but also risk factors for the development of AD (43). Over the course of the illness, individuals exhibit a range of anxious symptoms, such as excessive worry, restlessness, irritability, and a decreased engagement in once-enjoyable activities (44, 45). As cognitive function deteriorates,

these symptoms can escalate in severity, often having a profound impact on daily life and functional abilities (46). Moreover, anxiety appears to be intertwined with the AD diagnosis itself, as individuals grapple with the emotional implications of their condition (47, 48).

I.1.3.2. Metabolic disturbances

Weight loss is a frequent clinical finding in AD possibly due to abnormally high energy expenditure, or low energy intakes, or both (49, 50). However, hypermetabolic state or inadequate energy intake in AD patients was not confirmed, requiring further studies. Nevertheless, disturbances in energy metabolism and insulin signalling pathways have been implicated in AD (51-53).

The hypothalamic-pituitary-thyroid (HPT) axis (Figure 1.) is one of the key regulators of metabolism, energy expenditure, and thermoregulation. Recent attention has focused on exploring the potential interplay between AD and the HPT axis, a pivotal neuroendocrine system governing thyroid hormone homeostasis (54-58). The effector molecules are thyroid hormones, triiodothyronine (T3) and thyroxine (T4) (59, 60). The hypothalamic component, the paraventricular nucleus of the hypothalamus (PVN) produces thyrotropin-releasing hormone (TRH), while the pituitary releases thyroid-stimulating hormone (TSH) into the general circulation. Precise control of active T3 levels within brain tissues is executed by deiodinase enzymes (DIO), notably DIO type 2 (DIO2), responsible for converting prohormone T4 into biologically active T3 (61). They exhibit differential expression across brain regions, including the hippocampus and cerebral cortex - structures profoundly implicated in AD (62). Perturbations in thyroid hormone equilibrium have been observed in AD patients, encompassing alterations in

Figure 1. The HPT axis schematic figure, illustrating the interactions between TRH, TSH, T4, and T3. Alongside, the figure shows conversion by deiodinases (DIO1, 2, 3). TRH from the hypothalamus stimulates TSH release from the pituitary gland, which, in turn, triggers T4 and T3 production by the thyroid gland. Deiodinases convert T4 to T3 and metabolize them into inactive forms. Negative feedback loops are indicated, where T4 and T3 inhibit TRH and TSH release, respectively, to regulate hormone levels (54-58). Figure created by Adrienn Szabo, unpublished.

serum T3 and T4 levels and changes in brain thyroid hormone receptor expression (63, 64).

Additionally, the mediobasal hypothalamus (MBH), particularly its arcuate nucleus (ARC) region, plays a critical role in integrating peripheral signals and centrally regulating energy homeostasis (65). The MBH contains key genes that orchestrate nutrient uptake and energy balance, such as proopiomelanocortin (POMC) and cocaine- and amphetamine-regulated transcript (CART), which are responsible for anorexigenic pathways, as well as neuropeptide Y (NPY) and agouti-related peptide (AgRP), which are responsible for orexigenic pathways. These genes are crucial in modulating food intake and energy expenditure (66) (Figure 2.).
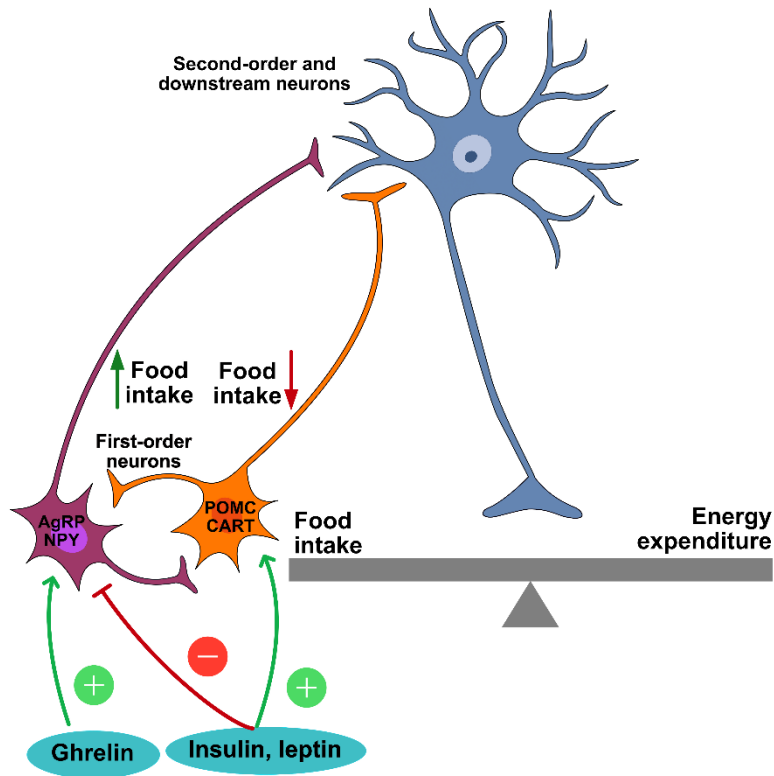
Figure 2. The energy balance schematic figure. The figure illustrates the key neuronal pathways involved in the regulation of energy homeostasis. POMC neurons and CART neurons, which are part of the anorexigenic pathway, decrease food intake and increase energy expenditure. In contrast, AgRP and NPY neurons, which constitute the orexigenic pathway, have the opposite effect. Specifically, POMC and CART neurons stimulate pathways that enhance energy expenditure, while AgRP/NPY neurons promote increased food intake. Hormones such as insulin and leptin inhibit the activity of orexigenic AgRP/NPY neurons and activate anorexigenic POMC and CART neurons, thereby reducing food intake and increasing energy expenditure. Conversely, ghrelin exerts the opposite effect by inhibiting anorexigenic POMC and CART neurons and stimulating orexigenic AgRP/NPY neurons, leading to increased food intake (66). Figure created by Adrienn Szabo, unpublished.

Disruptions in the expression of these genes and their associated neuropeptides have been linked to metabolic disorders, including obesity and insulin resistance (67, 68). Emerging evidence also suggests a connection between MBH dysfunction and AD (69-72).

Both NPY/AgRP and POMC neurons exert antagonistic effects on energy balance by projecting to second-order neurons in the PVN and other hypothalamic nuclei (73). Upon nutrient ingestion, α-melanocyte-stimulating hormone (α-MSH) from POMC neurons activates melanocortin 3 receptor (MC3R) and melanocortin 4 receptor (MC4R) receptors in the PVN, leading to reduced energy intake and increased energy expenditure

(74). The PVN is particularly important due to its high MC4R expression, positioning the melanocortin pathway as a major anorexigenic circuit in the brain (75, 76).

Studies show that deletion of POMC neurons or deficiencies in MC4R lead to obesity, highlighting their critical roles in energy regulation (77, 78). Both neuronal populations are influenced by circulating hormones such as insulin and leptin (79, 80). Leptin directly stimulates POMC neurons and inhibits AgRP neurons, promoting energy expenditure and weight loss (81, 82). Notably, while traditionally viewed as downstream mediators of leptin's effects, melanocortin signalling pathways have been shown to function independently (83).

Chronic leptin administration can reduce caloric intake and body weight (84, 85), whereas leptin deficiency or loss of leptin receptor function results in obesity (86, 87). Over-activation of leptin receptors in hypothalamic neurons can also contribute to obesity, particularly in the context of a high-fat diet (88). Thus, the interplay between metabolic disturbances, the HPT axis, and hypothalamic signalling pathways is crucial in understanding the pathophysiology of AD and its associated risks.

In the blood not only hormone levels, but also the fat concentrations (triglycerides, cholesterol) can be altered in AD patients. Indeed, metabolic syndrome (accompanied by increased levels of these lipids) significantly increased the risk of dementia (89). Controversially, higher triglyceride levels within the normal to high-normal range had a lower dementia risk and slower cognitive decline over time compared with individuals with lower triglyceride levels (90). This paradox may suggest that relatively higher triglyceride levels reflect better overall health, potentially providing a protective effect against dementia. It's important to note that these triglyceride levels were still within the normal range.

Energy intake and expenditure (EE) are the key counterbalancing factors that determine body weight change (91). On the other hand, EE together with the respiratory quotient (RQ) are known predictors of daily food intake. EE is largely determined by body size and composition, while RQ is defined as the volume of carbon dioxide released over the volume of oxygen absorbed during respiration, used in a calculation for basal metabolic rate. Interestingly, in a systematic review, EE of community-dwelling people with dementia was higher than in institutionalized groups (92).

I.1.4. Early symptoms in mild cognitive impairment (MCI)

Ronald Petersen and his colleagues found in 1999 that AD is usually preceded by a stage in which individuals have a greater degree of memory impairment than their age, but this does not yet meet the criteria for dementia. This condition has been termed "mild cognitive impairment" (MCI), of which there are several types. Classification into types also plays an important role in making a diagnosis, as MCI may be an early sign of not only AD but also other diseases (93, 94). While motor deficits were historically considered late-onset symptoms in AD, emerging evidence challenges this notion. Indeed, motor impairments might appear even in the preclinical stages, and a connection between motor skill deficits and the onset of AD has been proposed (95). There is growing evidence that changes in muscle structure and lower muscle strength are strongly associated with the risk of developing AD (96, 97). Lin et al even hypothesized that the extent of muscle mass loss may be related to the severity of cognitive deficits (98). An increase in myostatin level is known to cause a decrease in skeletal muscle mass (99, 100). Several studies have shown that inhibition of this molecule may be a promising strategy for the treatment of e.g. muscular dystrophy. Increased myostatin level was already found in a double transgene mouse model of AD (98). Follistatin is a glycoprotein widely present in both serum and tissues, known as a natural inhibitor of members of the transforming growth factor-β superfamily, including myostatin (101-104). Thus, the levels of these two molecules - myostatin and follistatin - should be jointly evaluated (105, 106) (Figure 3.).
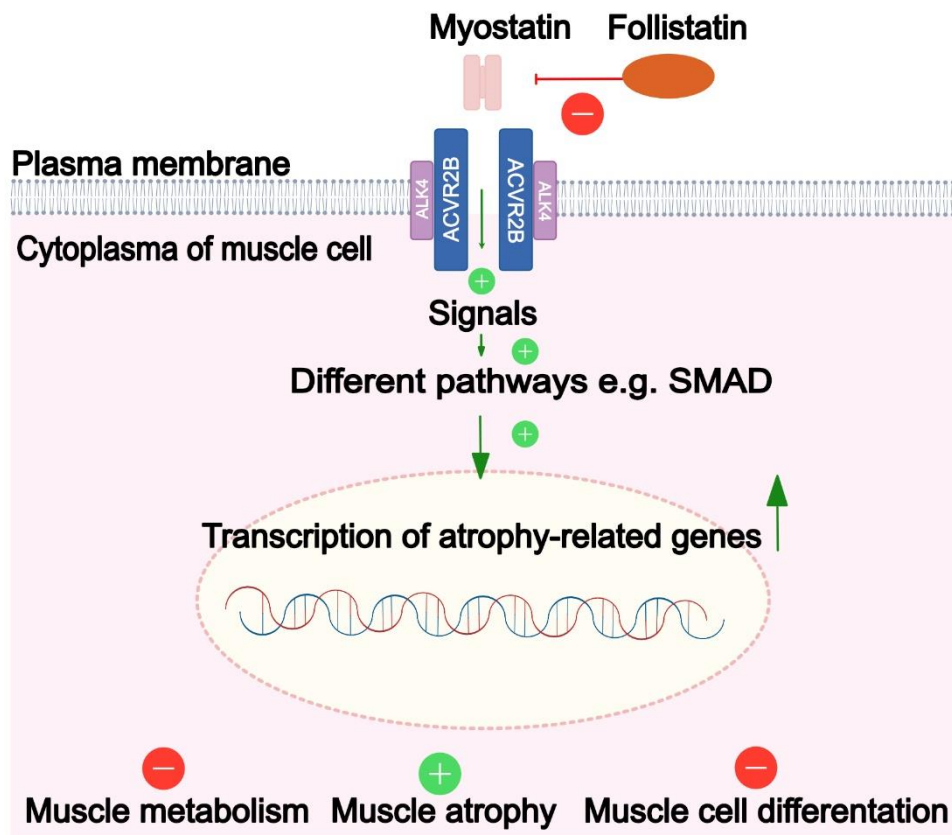
Figure 3. Illustration depicting the myostatin and follistatin system in muscle cells. Myostatin bind to their respective receptors, initiating signalling cascades that activate various SMAD pathways. This activation ultimately leads to the transcription of atrophy-related genes, resulting in muscle atrophy. However, this process is inhibited by follistatin, which blocks the binding of myostatin to its receptors, thereby preventing muscle catabolism and maintaining muscle mass (105, 106). Figure created by Adrienn Szabo, unpublished

Additionally, olfactory disfunction (problems with the sense of smell) is one of the earliest, preclinical symptoms observed in AD, thus, it is considered as an early biomarker (107). Several meta-analyses confirmed olfactory deficit in MCI (108). Interestingly olfaction worsens progressively as patients progress from MCI to AD (109) highlighting the potential for olfactory dysfunction to identify AD in the preclinical stages prior to MCI.

I.1.5. Pathomechanism

Definitive diagnosis of AD is postmortem, based upon the accumulation of Aβ and phospho-tau (p-tau) in the brain. Thus, these molecules seem to be critical in the pathomechanism. (110-116) Aβ, now recognized as a physiologically ubiquitous peptide,

serves a multitude of roles within the brain. These include the regulation of neuronal electrophysiology (117, 118), synaptic plasticity (119, 120), long-term potentiation (121), neuronal transmission (122), learning processes (123), hippocampal memory consolidation (124), neurogenesis (125) and processes contributing to neuronal survival (126). Notably, elevated levels of brain Aβ are observable in neurological and psychiatric conditions beyond AD, encompassing traumatic brain injury (127, 128), cerebral ischemia (129), and amyotrophic lateral sclerosis. It is posited that this elevation potentially acts to ameliorate neuronal damage, facilitate repair in response to insults, or mitigate the decline in neuronal functionality (130).

The amyloid cascade hypothesis postulates that the initial pathological anomaly of AD is the accumulation of Aβ, which subsequently triggers the development of plaques and the progression of neurodegeneration (131, 132) (Figure 4.).
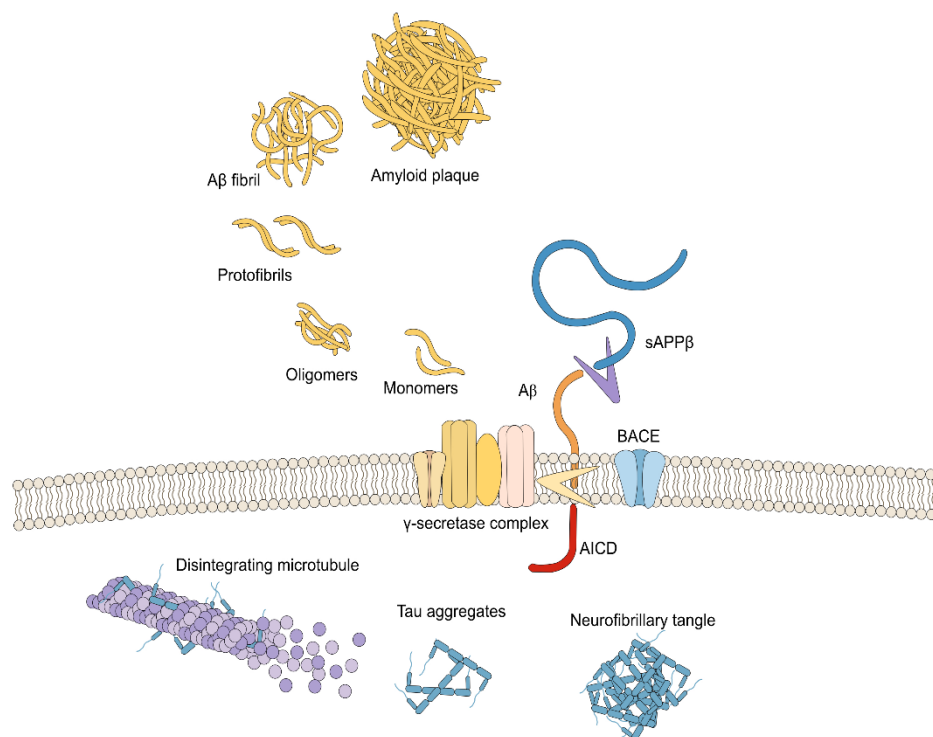
Figure 4. The amyloid cascade hypothesis suggests that the accumulation of Aβ initiates plaque formation and neurodegeneration. Aβ is generated through APP cleavage by β-secretase (BACE), producing sAPPβ and a membrane-bound fragment processed by γ-secretase, which releases both Aβ and the amyloid intracellular domain (AICD). Aβ variants aggregate into oligomers, protofibrils, fibrils, and amyloid plaques, central to AD pathology (137, 138). Figure created by Adrienn Szabo, unpublished.

The Aβ peptide emerges from the metabolic breakdown of amyloid precursor protein (APP), a transmembrane glycoprotein of type I spanning 695 to 770 amino acids (133). The cleavage of APP in close proximity to the cell membrane involves two key enzymes: α-secretase, an extracellular protease, and β-secretase (BACE), an aspartyl protease (134). This process leads to the generation of a soluble extracellular fragment referred to as soluble APPβ , alongside a membrane-bound fragment known as APP C-terminal fragments (also known as APP-CTF or C99) (4). C99 undergoes further cleavage within the cellular membrane by the action of γ-secretase. This enzymatic cleavage liberates Aβ, and an intracellular peptide recognized as the amyloid intracellular domain. Aβ exists in diverse lengths, with the most prevalent form comprising 40 amino acids ($A\beta_{1-40}$), and a less soluble variant composed of 42 amino acids ($A\beta_{1-42}$) (135). Subsequently, Aβ assembles to form oligomers, protofibrils, fibrils, and eventually coalesces into plaques (136).

Tau, a microtubule-binding protein, typically participates in the regulation of axonal transport under normal physiological circumstances (137, 138). However, in conditions such as AD and other tau pathology-related disorders, an abnormal state emerges where tau undergoes excessive phosphorylation and accumulates within neurons, forming distinctive structures termed intraneuronal tangles (neurofibrillary tangles; NFT) (139). These tangles are composed of paired helical filaments, twisted ribbons, and/or straight filaments (140) (Figure 5.). This pathological accumulation disrupts the normal microtubule assembly process and diminishes the binding capacity of tau to microtubules (141).
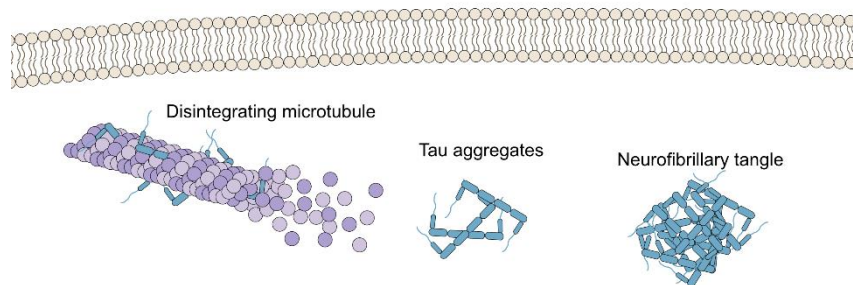
Figure 5. Schematic representation of tau pathology. Under normal conditions, tau stabilizes microtubules and supports axonal transport. In AD and related tauopathies, tau undergoes excessive phosphorylation, reducing its microtubule binding capacity and leading to structural disintegration. This hyperphosphorylated tau accumulates within neurons, forming aggregates that develop into neurofibrillary tangles (NFTs), which are composed of paired helical and other filamentous structures (140). Figure created by Adrienn Szabo, unpublished.

This hyperphosphorylated state of tau has multifaceted consequences. It results in alterations to the structure of heterochromatin (142), impairs synaptic plasticity (143), and hinders the process of anterograde axonal transport (144). NFTs, existing as intracellular lesions, exert detrimental effects on crucial physiological functions. Ultimately, this cumulative damage culminates in the destruction of neurons, contributing to the progressive degeneration characteristic of these conditions (145, 146).

These pathological deposits may induce abnormal apoptosis, characterized by various factors such as B-cell leukaemia/lymphoma 2 (Bcl-2), Bcl-2 Associated X protein (BAX) also known as Bcl-2-like protein 4 and caspases (147, 148). Oxidative stress is also connected to apoptosis leading to the mitochondrial cascade hypothesis of AD proposed already in 2004 (149). Although the correctness of the theory is still disputed, there is increasing evidence that disruption of mitochondria function is already present among the early symptoms (150-153) and may contribute to the accumulation of harmful toxic proteins, including Aβ (154). In various mouse models of AD deterioration of the mitochondrial system was repeatedly described (155, 156).

I.1.6. Clinical diagnosis

The clinical diagnosis is often made upon the symptoms and disease progression. However, positron emission tomography (PET) imaging has provided an avenue for monitoring the progression of Aβ deposition and NFT in vivo (110-112). Commencing within the temporobasal and frontomedial regions, Aβ deposition advances through the neocortex, subsequently affecting the primary sensory-motor cortex, and finally reaching the striatum (113-115). In contrast, tau pathology manifests earlier within the medial temporal lobe, basal forebrain, brainstem, and olfactory regions (bulb and cortex), often displaying a clinically benign nature, denoted at times as primary age-related tauopathy. This initial manifestation is followed by the extension of tau pathology into limbic domains and eventually into the neocortex (116).

I.2. Mouse Models of AD

I.2.1. Sporadic AD (sAD) models

AD is a complex puzzle shaped by intricate interactions between genetic susceptibilities, molecular anomalies, and environmental factors (157). To fathom this neurodegenerative enigma, diverse rodent models have emerged (158-161). These models, while not replicating full AD symptoms, provide valuable insights into disease

progression and potential treatments. Notably, sAD models, designed to emulate specific disorder aspects, signify a significant step in understanding this global healthcare challenge.

In the early 1980s, the senescence-accelerated mouse model (SAM) emerged by selecting traits within the AKR/J mouse lineage (162). This yielded nine primary SAM-prone (SAMP) strains and three SAM-resistant strains. Among these, the SAMP8 strain stands out for emulating critical AD hallmarks, Aβ deposition and tau hyperphosphorylation (163). This pivotal discovery reshaped research approaches towards unravelling the complexities of sAD.

Another research avenue in sAD involves injection models focusing on Aβ and tau aggregates. These models directly inject aggregated Aβ (164-167) or tau (168, 169) into the brain, replicating sAD pathology. They reveal the impact of aggregates on neuronal function, synaptic connectivity, and cognition. Moreover, they provide insights into the spread of aggregated proteins across brain regions, shedding light on toxicity, propagation mechanisms, and consequences of protein aggregation.

Introduced in 2009, seed injection models reveal tau transmission dynamics by injecting brain lysates from AD patients or model mice, along with recombinant tau, into mouse brains (170, 171). These models highlight synaptic connections as the primary means of spreading pathological tau, influenced by factors like age, Aβ presence, tau oligomerization, and splicing isoforms (172, 173). Rooted in the prion hypothesis, they introduce aggregated protein "seeds" into specific brain regions, triggering widespread deposition and unveiling self-propagation mechanisms of pathological protein aggregates (171).

Recent advances feature immune response models in sAD research. The trigger receptor 2 expressed on myeloid cells (TREM2) model highlights the intricate interplay of neuroinflammation, Aβ buildup, and synaptic dysfunction (174, 175). Linked to late-onset AD via the R47H variant, TREM2 expressed in brain microglia has a unique response to Aβ and induces lesions, leading to neurodegeneration (176, 177). TREM2 loss in APP model mice accelerates tau accumulation, emphasizing its role in the Aβ-tau connection (178).

Among chemical-induced sAD models, okadaic acid-induced and colchicine-induced models are noteworthy. Okadaic acid, injected either into the hippocampus or

amygdala, induced memory deficits, synaptic dysfunction, and Aβ accumulation in mice, mirroring sAD pathogenesis (179, 180). Similarly, intracerebroventricular (icv) administration of colchicine triggered cognitive impairments, neuroinflammation, and oxidative stress, offering insights into sAD-related neurodegeneration (181). Streptozotocin can destroy glucose sensitive cells. Injected icv it can be used as a model of AD replicating several aspects of AD pathology (182). This model is especially interesting as takes advantage of the connection between AD and metabolic disturbances.

Models exploring cerebral amyloid angiopathy (CAA) and vascular dementia provide insights into sAD's vascular dimension. CAA, characterized by Aβ buildup in cerebral blood vessels, contributes to vascular dysfunction and cognitive decline (183, 184).

However, these models, while insightful into specific sAD aspects, do not fully capture the disorder's intricate evolution. Crafting a model encompassing AD's full progression remains a challenge. Genetic adjustments enable researchers to target specific aspects, refining models to mirror distinct pathological features more faithfully.

I.2.2. Familiar AD (fAD) models

FAD is induced by mutations in genes encoding the secretase complex components, such as APP, presenilin 1 (PSEN1), and presenilin 2 (PSEN2) (Figure 6) (185-188) These mutations elevate Aβ levels, alter $A\beta_{42}$:$A\beta_{40}$ ratios, and promote Aβ aggregation (189-193). Typically manifesting before age 60, early-onset fAD is attributed to these mutations, impacting less than 5% of AD cases (194, 195).

APP gene mutations linked to fAD adopt geographic origin-based nomenclature and primarily occur near cleavage sites, yielding varied effects on APP processing and AD development. The Swedish mutation (APP_{Swe}; K670N/M671L) at the β-secretase cleavage site escalates β-secretase activity, boosting $A\beta_{40}$ and $A\beta_{42}$ production (196, 197). Mutations like Indiana (V717F), London (V717I) and others at γ-cleavage sites amplify $A\beta_{42}$ generation, known for heightened toxicity compared to $A\beta_{40}$ (185, 198, 199). Mutations within Aβ, such as Arctic (E693G) and Dutch (E693Q), foster Aβ aggregation, prompting stable oligomer and protofibril formation (200, 201) are linked to CAA (202-204). Mutations near the μ-cleavage site favour more toxic $A\beta_{42}$ over $A\beta_{40}$, with London (205) and Indiana (206-208) prevailing. Nearly all PSEN1 and PSEN2 mutations in fAD heighten the $A\beta_{42}/A\beta_{40}$ ratio (209-212). Additionally, a protective APP variant (A673T)

against AD and cognitive decline cuts β-secretase cleavage and total Aβ production, corroborating brain Aβ deposition as a central AD pathogenic mechanism (213, 214). The APP gene is situated on chromosome 21, which is also implicated in Down syndrome (215). Thus, it is not surprising that AD is more common in Down patients than in the general population (215).
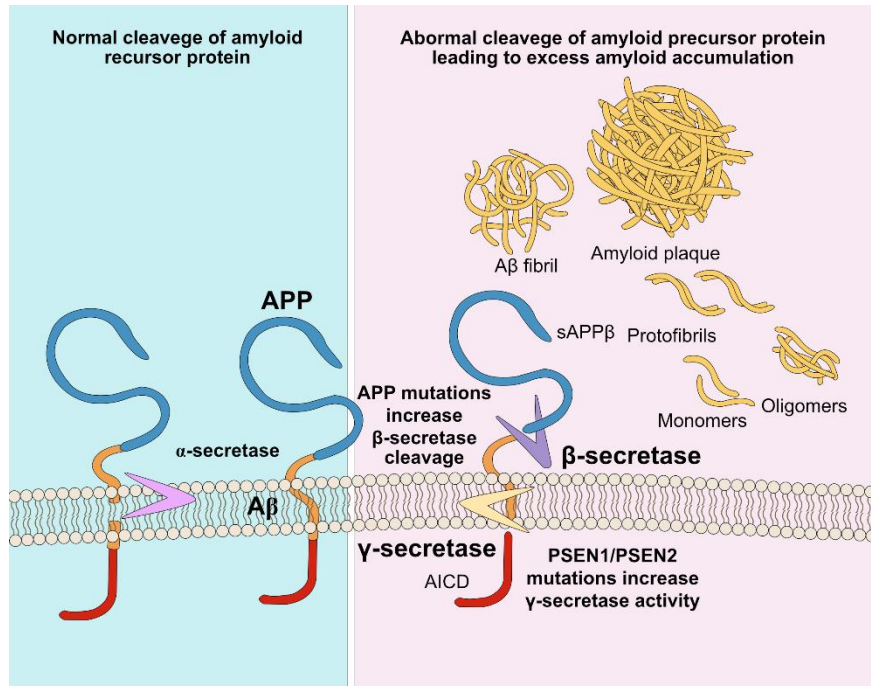
Figure 6. Normal and pathological APP cleavage. APP undergoes processing by secretase enzymes, with α-secretase cleavage preventing amyloidogenic processing. In contrast, β- and γ-secretase cleavage releases neurotoxic Aβ peptides that can accumulate into oligomers. Mutations in the APP, presenilin-1 (PSEN1), and presenilin-2 (PSEN2) genes disrupt normal cleavage, favouring β- and γ-secretase activity, which leads to increased Aβ production and aggregation. These mutations enhance Aβ accumulation, contributing to synaptic dysfunction and neuroinflammation. (185-188). Figure created by Adrienn Szabo, unpublished.

As rodents lack inherent AD features, genetic alterations are essential to replicate human AD pathology (216, 217). Transgenic organisms are produced via two possible strategies: pronuclear injection and gene-targeted replacement. Pronuclear injection introduces complementary DNA containing the transgene into zygote pronuclei, resulting in multiple random insertions into the genome. Conversely, gene-targeting modifies endogenous genes in embryonic stem cells through homologous recombination with a vector carrying desired modifications, yielding knock-in or knock-out mice (218, 219). Viral technologies, like lentiviruses and adeno-associated viruses (AAV), facilitate transgenesis, introducing human fAD genes crucial for modelling AD pathology (220,

221). Transgenic lines express mutated proteins regulated by diverse promoters like platelet-derived growth factor þ-chain, thymocyte differentiation antigen 1 (Thy-1) or prion protein (222). The choice of promoter significantly influences phenotypic outcomes (158-161). Though transgenic models replicate AD-associated proteins, broader factors beyond isoforms and mutations dictate AD-like pathology onset and progression (223).

The inaugural transgenic mouse model embodying AD-like pathology showcased a mutated human APP form, particularly APP_{Swe} at the β-cleavage site, augmenting β-secretase activity and Aβ production (159).

While familiar microtubule associated protein tau (MAPT) gene mutations do not underlie fAD, the presence of familial frontotemporal dementia-linked mutations has spurred tauopathy mouse model creation (224, 225). These tauopathy models span genetically modified and tau seed-injection types (168, 169), varying in genetic engineering methods, in the expressed tau isoforms and expression levels as well as in the targeted brain regions (226). Currently, most tauopathy models necessitate overexpressing mutant human tau protein to mimic tau pathology. A fresh strategy involves human MAPT knock-in mice, humanizing the entire MAPT gene including exons and introns (227, 228). Created by crossing MAPT knock-in mice with single APP knock-in mice, these mice unravel the role of the Aβ-tau axis in AD (226). While double knock-in mice exhibit increased tau phosphorylation, they lack tau pathology and neurodegeneration, even after aging (227). Remarkably, human tau humanization significantly hastens AD brain-derived pathological tau propagation, in the presence or absence of amyloidosis (227). This interaction underscores species-specific pathogenic protein preferences, amplifying their role in tauopathy. These mice might also facilitate the better understanding of the behavioural properties of tauopathies. Moreover, mutant MAPT knock-in mice with various pathogenic mutations exhibit aging-dependent tau aggregation and cognitive decline, and show accelerated Aβ pathology, accessible for research queries.

I.2.2.1. Triple transgenic mouse model of AD (3xTg-AD mice)

The 3xTg-AD mouse model, established in 2003, encompasses three crucial mutations linked to fAD: the Swedish $APP_{KM670/671NL}$ mutation, the $PSEN1_{M146V}$ mutation, and the $MAPT_{P301L}$ (tau_{P301L}) mutation (229) (Figure 7). The wide adoption of

the model is attributed to its ability to replicate several hallmark features of AD progression. Transgene expression is meticulously orchestrated utilizing a Thy-1 regulatory element for both human APP and MAPT, while the $PSEN1_{M146V}$ mutation is governed by the mouse PSEN1 locus (229). Typically employed in a homozygous state for both transgene insertions and the $PSEN1_{M146V}$ mutation, the 3xTg-AD model has been pivotal in unravelling the temporal dynamics of amyloid and tau pathologies (229). It offers a unique platform to delve into the intricate interplay between these two pathological markers and their potential contribution to cognitive deficits (230). Over time, changes in phenotypes have been noted, potentially originating from mixed strain backgrounds, alterations in transgene copy numbers, and other factors (231, 232). Particularly striking is the shift in the timing of plaque development and the emergence of significant sex disparities in pathology, primarily observed in female mice (231, 233-235). These sex-related distinctions have kindled interest in comprehending the complex role of sex in AD pathogenesis. Beyond its role in exploring genetic mutations and neuro-pathological shifts, the 3xTg-AD mouse model has proven indispensable in evaluating therapeutic strategies targeting amyloid and tau pathologies.
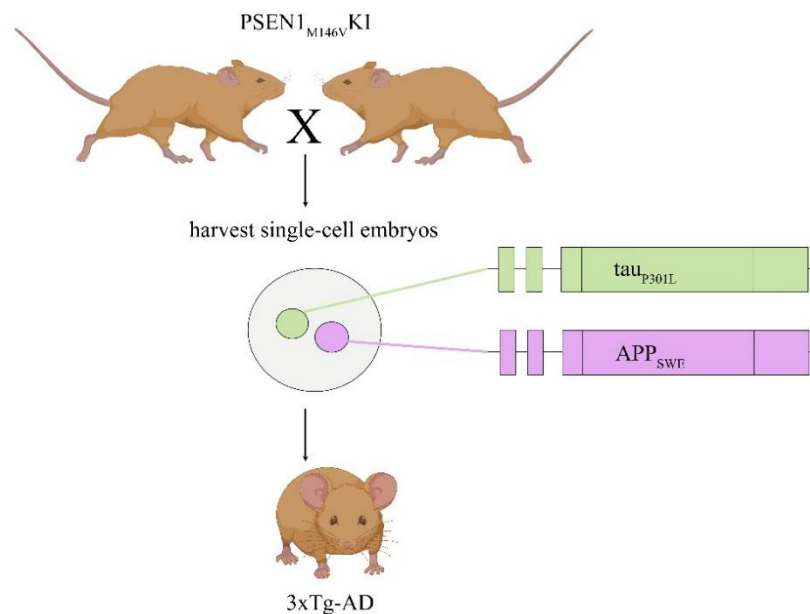
Figure 7. Triple transgenic mouse model of AD. The 3xTg AD mouse model was created using a method that involved injecting two separate transgenes, carrying human APP_{SWE} and human tau_{P301L}, into single-cell embryos from homozygous mutant PS1M146V knock-in (PS1-KI) mice. This method aimed to exploit the likelihood of the two transgene cassettes integrating at the same genomic site (229). Figure created by Adrienn Szabo, unpublished.

I.3. Behavioural alterations in AD mice models

Preclinical research investigating the neuropsychology of AD primarily focuses on the decline of spatial learning and memory using the Morris water maze test (MWM) (236, 237). However, in addition to cognitive decline other neuropsychiatric symptoms may also occur (238).

I.3.1. Anxiety

The presence of anxiety is increasingly recognized as a critical aspect of the AD progression an early symptom (239). To illuminate the intricate relationship between AD and anxiety, researchers have turned to animal models. In the 3xTg-AD mice open spaces induced anxiety was studied by open field test (OFT) (240-243), elevated plus maze (EPM) (240, 241, 243, 244), and light-dark box (LD) tests (245-247). The outcomes from various studies showed mixed results: some reported no significant difference between age-matched controls and 3xTg-AD mice (240-242, 244), while others observed increased anxiety levels in the latter group (248). Interestingly, even the same research group reported varying anxiety responses in 3xTg-AD mice using EPM at six months of age (249-251). The potential explanations for these inconsistencies point toward the temporal emergence of symptoms, prompting the need for longitudinal studies covering a wide age range, as earlier studies focused mostly on a single, specific age group (244, 249, 252, 253).

In addition to open spaces, predatory cues emerge as universal danger signals to animals, triggering behavioural responses on the approach-avoidance spectrum (254) and offering a unique opportunity to investigate the neurobiology of anxiety (255). A particular component of fox odour, 2-methyl-2-thiazoline (2MT), is frequently employed to induce negative emotional responses (254, 256, 257). It is obvious that the perception of odours requires an intact olfactory system. Aβ plaques are observed across the olfactory system in various transgenic mouse models (258-260). To further comprehend changes in fox odour avoidance, it is crucial to confirm the presence of these deposits and their potential role within the local colony. Interestingly, synaptic transmission and electrical activity of the olfactory bulb exhibit an initial increase followed by a later decrease with age, offering insight into the behavioural transition during disease progression (260-263). The temporary lull in electrical activity coincides with the known

appearance of AD hallmarks at six months of age, suggesting a possible link between molecular and behavioural changes (261-263).

I.3.2. AD and motor function changes

Locomotion is fundamental for almost all kinds of behaviour. Changes in this parameter can deeply influence the outcome of other tests and may lead to misinterpretation. Moreover, decline in fine motoric can also be an early symptom of AD (264, 265). Transgenic mouse models of AD are noteworthy for their significant motor impairments. For instance, TgCRND8 and APPswe/PS1dE9 transgenic mice exhibit motor coordination deficits even before Aβ accumulation occurs (208, 266, 267). This stands in contrast to 5xFAD mice, where motor deficits appear after cognitive impairments manifested (205). Additionally, there are AD models, like the APP23 mice, where both motor and cognitive symptoms onset simultaneously (268). The APPswe/PS1dE9 model demonstrates motor coordination deficits in the rotarod test and motor learning deficits in the Erasmus Ladder task (269). In contrast, the TgCRND8 model showcases motor coordination deficits on the balance beam test and gait impairment through the foot printing test yet exhibits no motor learning deficits on the accelerated rotarod test (270). The APP23 model also reveals motor coordination deficits on the rotarod test (268). Similarly, the 5×FAD model presents motor coordination deficits on the balance beam test, motor learning deficits on the accelerated rotarod test, and gait impairment through the foot printing test (271, 272).

As mentioned before, motor deficits do not necessarily run parallel to cognitive decline in AD models. This disparity, along with the presence or absence of motor deficits, indicates that the brain regions accountable for motor and cognitive functions might be affected in different ways (273). One of the brain areas responsible for motor-coordination is the cerebellum implicated both in fAD and sAD (273, 274). Indeed, as a possible pathomechanism, elevated levels of Aβ oligomers have been observed in the cerebellar cortex of AD patients. Especially the early-onset fAD cases, linked to mutations in PSEN1, demonstrated Aβ deposition in their cerebellum alongside the appearance of hyperphosphorylated tau, and Purkinje cell loss (269, 275). Additionally, cerebellar atrophy might contribute to motor impairments such as gait and limb coordination deficits (95). However, the relationship between cerebellar Aβ deposits and motor deficits is intricate. Some models show no motor dysfunctions despite cerebellar

Aβ accumulation and pathology (276, 277). This variability suggests that soluble forms of Aβ, like monomers or oligomers, might be more directly tied to motor symptoms.

In the broader context, AD's impact goes beyond cognitive decline (238). The intricate relationship between AD, motor deficits, and the intricate process within the cerebellum presents a fascinating avenue for understanding the disorder's multifaceted nature paving the way for enhanced insights and potential therapeutic strategies (278, 279).

I.3.3. AD and metabolism

Previous studies confirmed increased EE in 3xTg-AD mice, suggesting metabolic disturbances (280).

Additionally, mounting evidence points to the dysregulation of the HPT axis in AD, suggesting a role in disease pathogenesis (58, 281). Therefore, it is not surprising that thyroid hormone disruption has been associated with cognitive impairment, neuroinflammation, and Aβ accumulation in animal AD models (282-286). However, the relationship between AD and the HPT axis is multifaceted and bidirectional (287). On one hand, AD-induced pathophysiological changes within the brain can disturb HPT axis function, leading to perturbed thyroid hormone secretion and metabolism (288). Conversely, thyroid hormones exert a pivotal role in preserving neuronal integrity, synaptic plasticity, and cognitive function, rendering them potential modulators of AD progression (289). Moreover, both hypo- (290) and hyperthyroidism (291) were connected with AD as well as local thyroid hormone concentration can vary among tissues within the same individual (292). Further studies seem to be required to clarify molecular details as well as to address whether mice models are suitable for testing HPT-AD interaction (51-53, 71, 72).

II. Objectives

Early diagnosis of AD is crucial, as beta-amyloid plaques and hyperphosphorylated tau tangles are already present when cognitive impairments are detected. Therefore, our experiments focus on three key areas using the 3xTg-AD mouse model.

II.1. Temporal Emergence of Increased Innate Anxiety

We investigated innate anxiety in different age groups of our mouse model using the fox odour test and examined sex differences. Separate cohorts were used for each age group to avoid long-lasting trauma from fox odour exposure. Through another series of open field tests, we monitored behavioural changes monthly. To explore potential underlying mechanisms, we confirmed the progressive accumulation of classical AD markers (Aβ and p-tau) in emotionally relevant brain areas, such as the amygdala, and in the olfactory system using immunohistochemistry.

II.2. Musculoskeletal and Cerebellar Changes in the Context of Motor Alterations

We examined basic motor abilities from multiple perspectives, including environmental enrichment, handling, negative-avoidance (water), and positive-reward (pellet) during behaviour tests. Our study focused on the fine motor skills of the mice, paying particular attention to locomotor changes (such as joint structure and the changes of myostatin and follistatin in muscle tissue), as well as apoptotic and mitochondrial markers in both muscle and cerebellum. Considering that intense behavioural motor testing can act as training and that starvation (to increase motivation during testing) can affect apoptotic and oxidative parameters, we compared naïve and "training", experimental animal groups.

II.3. Disrupted HPT Axis and Imbalance in MBH Neuropeptides as a Possible Underlying Mechanism of Metabolic Shifts

This investigation was motivated by observations that 3xTg-AD animals performed paradoxically better than controls in reward-based cognitive tests. We first examined body composition using MRI-based equipment and monitored food and water intake, respiratory rate, and energy consumption with the TSE PenoMaster Metabolic Unit. Subsequently, we analysed key metabolic blood parameters (glucose, triglyceride, cholesterol, and fT3/fT4). Finally, we used PCR to study the gene expression of metabolically relevant molecules and receptors in critical regions, including the PVN, pituitary, and MBH.

III. Methods

III. 1. Animals

3xTg-AD (B6;129-Tg (APP$_{Swe}$, tau$_{P301L}$) 1Lfa PSEN1$_{tm1Mpm/Mmjax}$ #034830-JAX) and control (C57Bl6/J) mice were obtained from the local colonies of the Institute of Experimental Medicine, Budapest. Males and females were also used, and their exact age are given by the specific experiments. Adult mice were housed in groups of 3-5 in Macrolon cages (40 cm x 25 cm x 26 cm) under a reversed 12-hour light-dark cycle (lights on at 8 p.m., 21±1°C, 50-60% humidity), with food (standard mice chow, Charles River, Hungary) and water available ad libitum if not otherwise indicated. To enhance motivation to collect pellets (Dustless Precision Pellets® Rodent, Purified, 45mg, Bio-Serv, Bilaney Consultants GmbH, Germany, #F0021-J) during operant condition test (OCT), radial arm maze (RAM), single pellet reaching test (SPRT) and staircase test, mice were kept on a restricted diet to maintain 90% of their initial body weight beginning 2 days prior to the first experimental day. Bodyweight was measured every experimental day, and in case it dropped below the target body weight, the diet was adjusted.

All tests were approved by the local committee of animal health and care (PE/EA/918-7/2019) and performed according to the guidelines for the care and use of laboratory animals (2010/63/EU).

III.2. Experimental Design: Cohorts Overview

III.2.1. Temporal Emergence of Increased Innate Anxiety

Cohort 1. Innate anxiety was studied in 3Tg-AD mice across a wide age range using (2TM)-induced avoidance-approach behaviour paradigm. As fox odour might induce long lasting trauma (used also as a model for posttraumatic stress disorder (293)) inducing long-term changes in behaviour, we had to use separate cohorts for each age group. The age (in month, M) and the number of animals in different groups can be found on Figure 8.

To have a comprehensive picture, we aimed to examine the temporal resolution in 2-month "bins", however, after 12-month, due to insufficient number of animals, we switched to 3-month "bins". Our main goal was to reveal temporal differences. Therefore, sex differences were addressed only at two timepoint (2 and 15 months, i.e., before and after the presumable transient period).
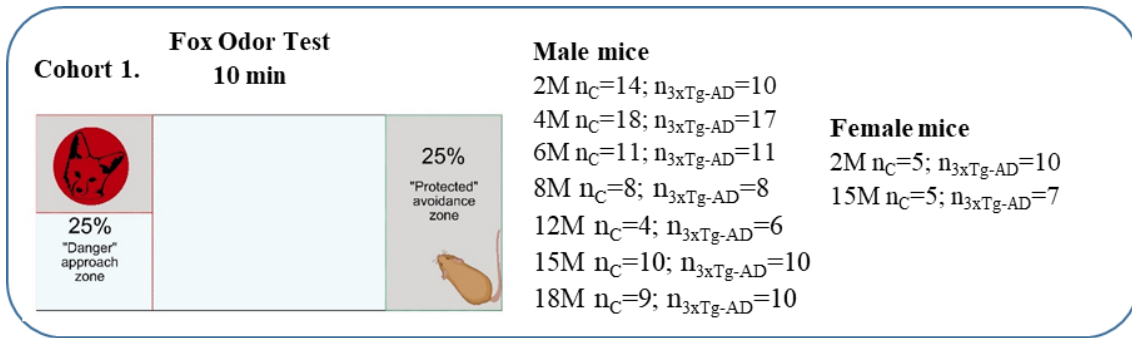
Figure 8. Schematic representation of cohort 1 in experimental series 1. Fox odour avoidance in separate age-groups. Abbreviation: M: age in month

Cohort 2. As general locomotor problems might have influenced the outcome of the previous test we conducted a serial OFT. As spending 5 min in an open arena does not have long term behavioural consequences, the same animals were examined repeatedly. To maintain interest, the animals were tested monthly in slightly different environments (size, colour, and smell) to avoid habituation to the arena. During these observations we could also detect anxiety from open spaces. The number and sex of the animals can be found on Figure 9.
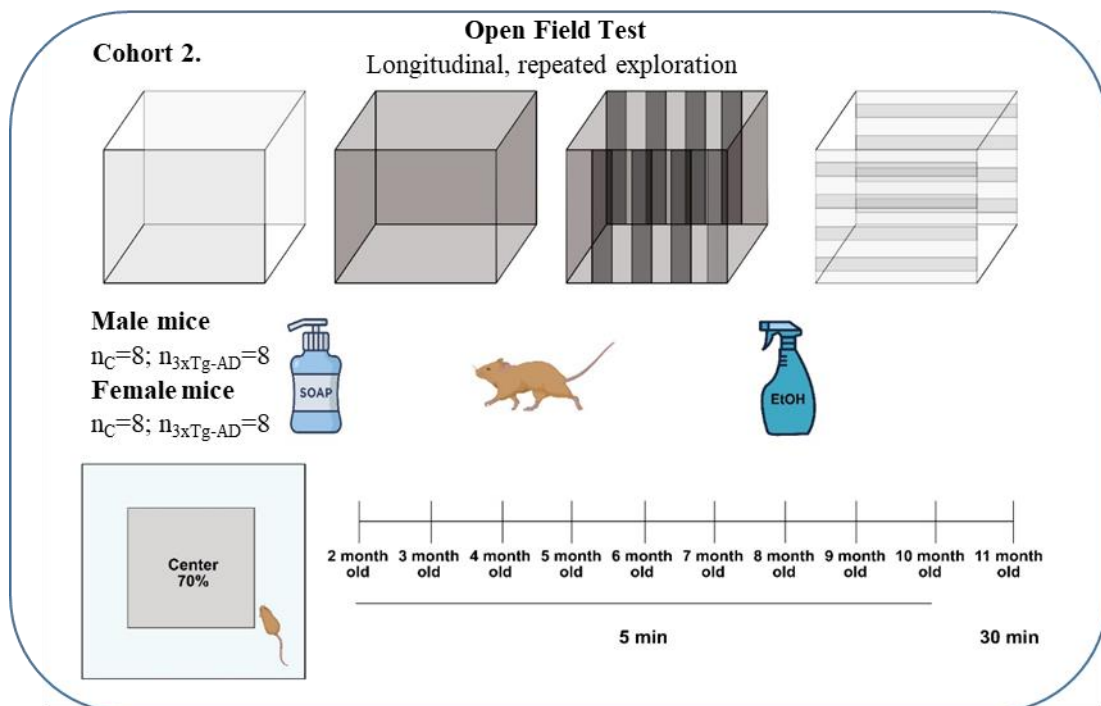
Figure 9. Schematic representation of Cohort 2 in Experimental Series 1. Longitudinal, repeated (between 2 and 11 months of age) exploration of OFT behaviour in male and female mice (n = 8/group at the beginning).

Hypolocomotion was found repeatedly during 5 min testing. Thus, the question arose whether it is an initial anxiety in a new environment (which will be released after a

while) or more a sign of innate anxiety from open, bright spaces, which do not diminish over time. To test this hypothesis, at the termination of our experiment (in 11-month-old mice), we conducted a more prolonged observation (30 min).

Cohort 3. Immunohistochemical confirmation of Aβ accumulation and p-tau appearance in 2- and 12-month-old animals (i.e., before and after the presumable transient period (294); female, n = 3; 3xTg-AD) in the olfactory bulb (OB), motor and somatosensory cortex, hippocampus, and basolateral amygdala (BLA) regions as relevant regions for cognitive impairment (cortex, hippocampus), emotions (BLA), or smell loss (OB).

III.2.2. Musculoskeletal and Cerebellar Changes in the Context of Motor Alterations

First detailed behavioural characterization was conducted along different aspects of locomotion (muscle strength (grip test), motor-coordination (rotarod), general locomotion in a box (OFT) as well as in a highly motivating water environment (MWM)). Moreover, fine motoric was examined using food-motivated test, where the animals had to collect pellets. The animals were 6-month-old at the start of experiments and around 8-months-old at end of tests. We used males throughout, and the number of the animals can be found on the Figure 10 representing Cohorts 1-4.

Cohort 1. The muscle strength was measured by grip test (5 trials on a single day) followed by a 5-day rotarod test (3 trial/day) 2 days later to test motor-coordination (n = 9-10/group).

Cohort 2. In the "gold standard" of spatial memory measurement, MWM, we focused on locomotor abilities (n = 6/group).

Cohort 3. (Training, Experimental Animal) Mice were first subjected to an OFT followed by food-motivated learning tests (radial arm maze (RAM), single pellet reaching test (SPRT), staircase) at restricted diet (n = 10/group). Animals were sacrificed after 2 months at the end of extensive behavioural testing referred to later as trained. The blood glucose and lipid parameters were measured immediately after sacrifice, while the serum, muscle and brain samples were collected and later analysed by qPCR and Western blot technics (for in vitro measurements: n = 7/group).

Cohort 4. A separate group of mice was kept in an enriched environment from 2.5-month of age consisting of repeated handling, occasional running wheel in the cage,

changes in cage size and hiding elements referred later as handling group (n = 5-6/group).
Locomotion was detected in these animals at 6-month-old age in an OFT.
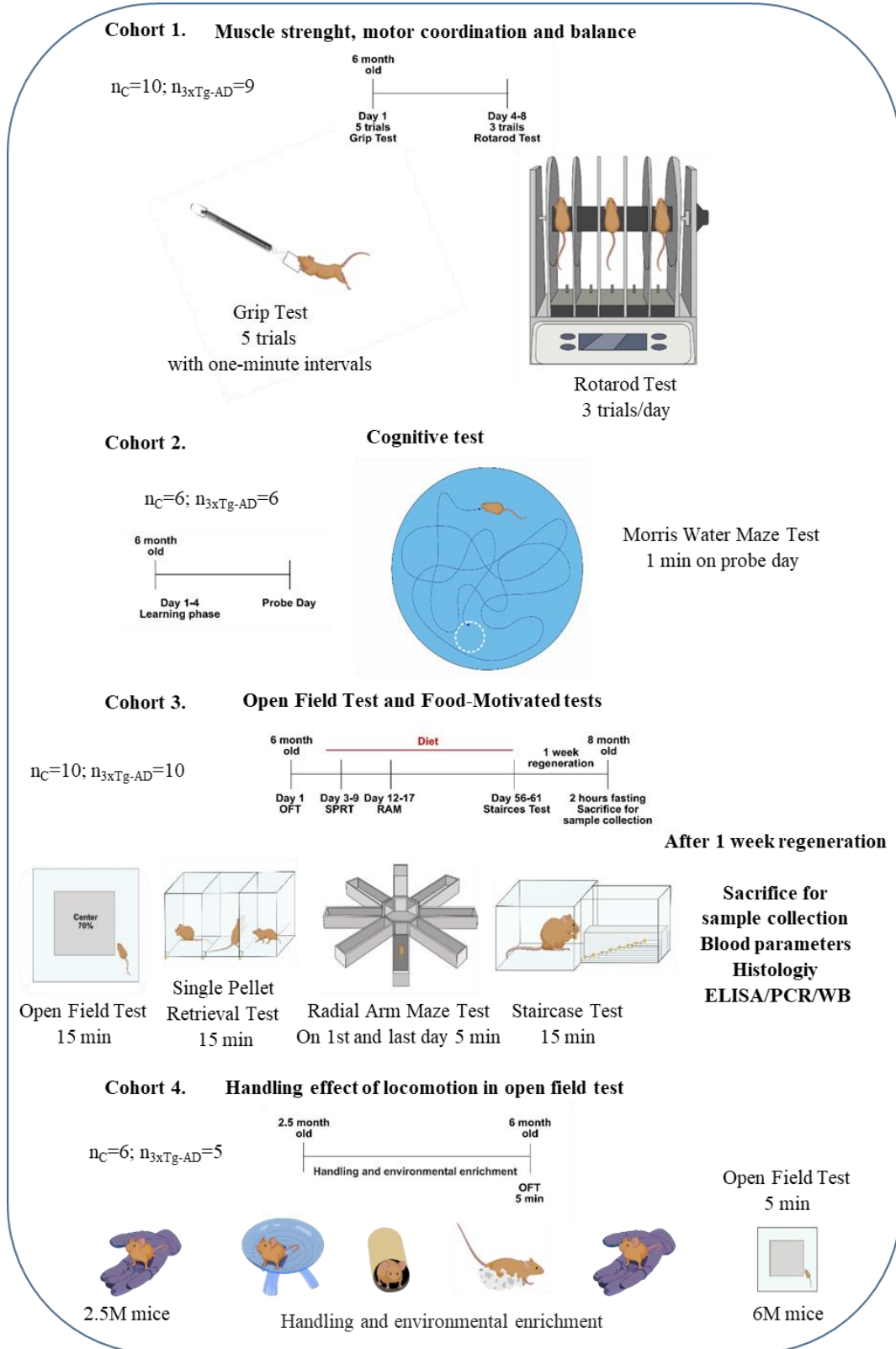
Figure 10. Shematic representation of teh conducted behavioral test and interventiones. The number of animals per groups is given for each Cohort separately. Abbreviation: M: age in month

Cohort 5. (Naïve Animal) For in vitro measurement a test-free group was also involved as they can also influence the outcome. Thus, in this Cohort animals were sacrificed without testing (n = 4/group). The muscle and brain samples were used in qPCR and Western blot experiments.

III. 2.3. Disrupted HPT Axis and Imbalance in MBH Neuropeptides as a Possible Underlying Mechanism of Metabolic Shifts

As during the previous experimental series in **Cohort 3.** we found „food craving" in 3xTg-AD mice, here we intended to study the energy homeostasis of these animals.

Cohort 1. First, we further confirmed previous results in a food-motivated test specifically designed to study cognitive capability (operant condition test, OCT Figure 11), as those could have been confounded by repeated testing.
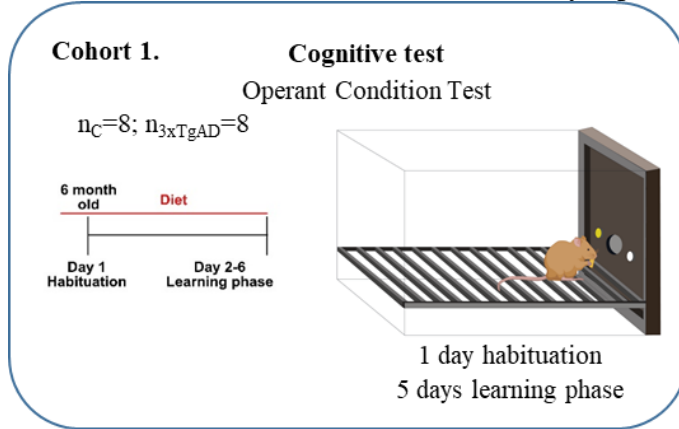
Figure 11. Schematic representation of Cohort 1 in Experimental Series 3. The cognitive abilities of 6-month-old male mice (n = 8/group) were examined in a food-motivated test. The classic OCT was preceded by 1 day habituation. The learning phase consisted of 5 days.

Cohort 2. Next, in a new series metabolic phenotyping was conducted comparing 4 and 8-month-old male mice (before and after a transient period) (Figure 12).
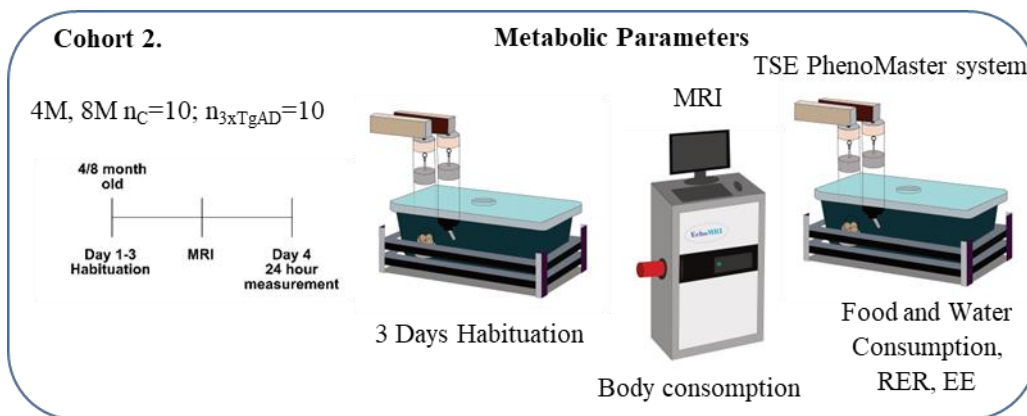
Figure 12. Schematic representation of Cohort 2 in Experimental Series 3. The body composition of male mice (4- (n = 10/group) and 8-month-old (n = 5-7/group)) was determined by EchoMRI than the animals were transferred to metabolic (calo) cages of the Phenomaster Metabolic Phenotyping where the metabolic parameters were recorded. Abbreviation: M: age in month

III.3. Behavioural Testing

Tests were carried out during the dark, active phase of the day in a separate room under red light or in semi-darkness and recorded by ceiling-mounted camera (Samsung SNB 7000) for fox odour, MWM, OFT, RAM and staircase test. The experiments were performed with randomization of the animals. Data were analysed later by computer–based event recorders Noldus EthoVision (Noldus, Wageningen, the Netherlands) or manually with Solomon Coder (https://solomoncoder.com/). Each test apparatus was cleaned with 20% ethanol and water and dried prior to the next animal being introduced (except MWM where water was not changes between animals).

III.3.1. Temporal Appearance of Enhanced Innate Anxiety

III.3.1.1. Predator Odor Test Using 2-methyl-thiazoline (2MT) (Experimental Series 1., Cohort 1.)

We assessed the avoidance response to an ecologically relevant aversive stimulus (i.e., predator odour) by means of a synthetic analogue of a fox anogenital product (2-methyl-2-thiazoline; 2MT; Merck, Sigma Aldrich, St. Louis, MO, USA, #M83406), in a transparent Plexiglas arena (43 × 27 × 19 cm) (254). Testing was carried out in a fume hood with medium-light intensity (120 lux) in covered arenas to equalize odour exposure across subjects. During testing, 2MT (Merck, Sigma Aldrich; St. Louis, MO, USA, #M83406, 40 μl in 1 ml distilled water, 50 μl/animal) was presented on a filter paper placed in a plastic vial cap affixed to the corner. One eighth of the box containing 2MT was defined as approach zone, while the distant quarter as avoidance zone. At start, animals were placed in the corner opposing the odour zone and were left to freely explore the covered arena for 10 min. Filter papers were immediately removed at the end of the test, then the testing arena was cleaned with 20% ethanol, wiped dry, and left ventilated for an additional 2 min before the next test. The following parameters were analysed by EthoVision XT 15 software (Noldus, Wageningen, the Netherlands):

(1) locomotor/horizontal exploratory activity (total distance moved in cm)

(2) the time spent in the approach zone (corrected by locomotion: (duration spent in the approach zone)/(distance travelled), s/m);

(3) the number of entries into the approach zone;

(4) the time spent in the avoidance zone (corrected by locomotion: (duration spent in the avoidance zone)/ (distance travelled), s/m);

(5) the number of entries into the avoidance zone; and

(6) time spent with immobility (not moving; s).

Male mice were used throughout. However, 2- and 15-month females were also additionally involved. In these 2- and 15-month age-groups, additional behavioural variables were quantified, namely hand-scored by an experimenter blind to treatment groups (Solomon Coder, version beta 19.08.02, Budapest, Hungary). During manual analysis, animal behaviour in the arena can be separated more finely; freezing behaviour can be identified with greater precision, as well as behaviours such as sniffing and rearing on two legs. These variables were the following (time spent with the given behaviour expressed as % of 10 min observation period):

(1) freezing: no apparent movement;

(2) sniffing the odour container;

(3) rearing: vertical movement.

The number of animals is on Figure 8.

III. 3.1.2. Open Field Test (OFT) (Experimental Series 1., Cohort 2.)

Exploratory activity and anxiety-like behaviour without predator stimuli was assessed in an open field arena under medium-light intensity (120 lux). The exact size (50 × 45 × 15 cm or 40 × 40 × 30 cm) as well as the colour (white or black) and smell (ethanol or soap) of the arena was changed from month to month to avoid loss of interest. Nevertheless, the plastic walls were always cleaned between animals and 4 animals were tested at a time. Mice were placed in the centre and were allowed to explore the arena for 5 min (295). At 11 months of age (last occasion), the 30 min test was conducted. The distance travelled was considered as a main parameter of locomotion. The inner 70% zone was considered as centre, and time spent here was an index of anxiety. Here we did not calculate corrected duration spent in the centre, while the animals were placed there and not moving animals stayed there, leading to a misleading reduced anxiety. The number of animals is on Figure 9.

All behavioural variables were quantified using EthoVision XT 15 software (Noldus, Wageningen, the Netherlands).

III.3.2. Musculoskeletal and Cerebellar Changes in the Context of Motor Alterations

III.3.2.1. Muscle strength: Grip Test (Experimental Series 2., Cohort 1.)

An analog Grip Strength Meter (Pesola Medio-Line 40300) was used to measure forelimb grip strength. The 6-month-old male mouse was allowed to grasp the bar mounted on the force spring scales. The scale was reset to 0 g after stabilization and the tail of mouse was slowly pulled back by the trained experimenter (296). The peak pull force (g) was recorded by the drag pointer at the time the mouse released its forepaws from the bar. Trials in which only one forepaw, or the hind limbs were used and in which the mouse turned during the pull or leaves the bar without resistance were excluded. Given that the speed of the tail pull can influence the measurement, we conducted the procedure at a constant speed sufficiently slow to permit mice to build up a resistance against it. We performed 5 consecutive measurements on a single day at one-minute intervals. The number of animals is on Figure 10.

III.3.2.2. Motor-coordination: Rotarod Test (Experimental Series 2., Cohort 1.)

Motor coordination and balance were measured using a rotarod treadmill with automatic timers and falling sensors (IITC Rotarod Series 8, IITC Life Science, North America Headquarters, USA). The mouse was placed on a 3 cm diameter drum, whose surface was textured to avoid slipping. The rotarod started to rotate with 5 round per minute (rpm) and accelerated continuously to 25 rpm during 300 s (297). When the mice fell onto the individual sensing platforms the results were recorded. The experiment was repeated three times a day for 5 days. The machine automatically measured the falling latency, the speed at the time of the fall and the distance travelled till the fall. The number of animals is on Figure 10.

III. 3.2.3. General locomotion: Open Field Test (OFT) (Experimental Series 2., Cohort 3 and 4.)

The test was conducted and analysed similarly as described in II.3.1.2. Here, only 6-month-old male mice were examined, and the dimension of the test box was 40 cm x 36 cm x 19 cm and animals were left there for 15 min.

To reduce anxious behaviour, a separate group of male mice was kept in enriched environment from 2.5-month of age consisting of repeated handling, occasional running wheel in the cage, changes in cage size and hiding elements referred later as handling

group (Cohort 4.). Locomotion was detected in these animals at 6-month-old age in an OFT. The number of animals is on Figure 9 and 10.

III.3.2.4. Motivation-Induced Locomotion in Cognitive Tests

III.3.2.4.1. Morris Water Maze (MWM; Experimental Series 2., Cohort 2.)

A circular pool made of bright grey plastic (90 cm in diameter and 40 cm in height) was filled with tap water (24 ± 2 °C), made opaque by white wall paint, and the level of the water was 1 cm higher than the platform (6 cm in diameter) except for learning day 1, when the platform was above the water (294) (Figure 10). The apparatus was divided into 4 quadrants and the platform was installed in the middle of one quadrant. Mice were released into the water from different points across trials and were allowed to swim freely for 1 min to find the platform. If they did not find the platform in time, they were helped to find it and allowed to stay there for 10 secundum. The learning phase (day 1-4) consisted of 5 trials with 30-minute intertrial interval (when the animals were returned to their home cages) and was repeated for 4 consecutive days. On day 5 the platform was removed from the water and the mice had 1 minute to search for the missing platform. As a measure of punishment-induced locomotion, on day 5, on the "probe" day the total distance moved was automatically detected. The number of animals is on Figure 10.

III.3.2.4.2. Radial Arm Maze (RAM; Experimental Series 2., Cohort 3.)

Mice were put in the well-defined central region of the eight arms maze (each arm was 25 cm long, 7.5 cm wide, and 6 cm tall, the central part had 20 cm diameter) (Figure 10) for 10 min and were allowed to freely explore the equipment and collect 45mg pellet (Dustless Precision Pellets® Rodent, Purified, 45mg, Bio-Serv, Bilaney Consultants GmbH, Germany, #F0021-J). The habituation phase lasted for 2 days, the mice were placed in the empty maze on the first day and one pellet was hidden at the end of each arm on the second day (294). The learning phase lasted for 5 days with the same three arms baited. Subsequently, on "probe" day 6, during a 5 min test no pellets were provided. Our focus was on the distance travelled on" probe" day as a measure of reward-induced locomotion. The number of animals is on Figure 10.

III.3.2.5. Fine Motor Skills Tests

III.3.2.5.1. Single Pellet Reaching Test (also known as single-pellet skilled reaching test (Experimental Series 2., Cohort 3.)

Mice were tested in a three-lane single pellet reaching box constructed of clear Plexiglas with each lane consisting of 5 mm slots positioned against the front-right wall of the box (Figure 10). On the first day pellets were put inside the box close to the lanes, on the next day in the lane, while for the next 5 days outside, 5 mm from the lane (298). The mouse had to reach out on the 3 mm lane and pull in the pellet. The mouse can collect a maximum of 15 pellets (Dustless Precision Pellets® Rodent, Purified, 45mg, Bio-Serv, Bilaney Consultants GmbH, Germany, #F0021-J) per day for 15 minutes. If the 15 pellets were successfully collected, the experiment was terminated. Pellets successfully pulled into the lane during the experiment were counted. The videos of the last day were analysed manually with Solomon coder, from which the spent time of trying and feeding (s) were extracted. The number of animals is on Figure 10.

III.3.2.5.2. Staircase Test (Experimental Series 2., Cohort 3.)

The staircase test was performed in an apparatus validated on mice (299). The test apparatus comprises a wider start compartment and a narrow corridor. A central plinth runs the full length of the corridor with a narrow trough on either side, into which a removable double staircase can be inserted with eight steps on each side. There is a recess on each step where the 45mg reward pellets (see III.3.3.5.1.) are placed. The mouse can climb onto the central plinth using its right and left paws to collect reward pellets. The mouse had 15 minutes to collect the pellets. On the first day we also placed pellets on the central plinth, but on the next 5 days the mice could only collect reward pellets from the steps. During the days the consumed pellets were counted, from which the learning curve was obtained. Trying (frequency, duration (s)), eating (duration), successful and unsuccessful trying were analysed with Solomon coder from videos of all 6 days. Reward preference and duration of trying (DT) and eating were analysed. The number of animals is on Figure 10.

$$\text{reward preference (\%)} = \frac{\text{successful trying}}{\text{trying} + \text{succesful trying} + \text{failed trying}} * 100$$

III. 3.3. Disrupted HPT Axis and Imbalance in MBH Neuropeptides as a Possible Underlying Mechanism of Metabolic Shifts

III.3.3.1. Operant Condition Test (Experimental Series 3., Cohort 1.)

The test was performed in an automated operant chamber (Med Associates, St. Albans, VT, USA) with two nose holes (300). As a reward, 45 mg of food pellets (see III.3.3.5.1.) was used. Animals were placed inside a test chamber for 30 min to freely explore the environment. A nose poke into one of the nose holes was immediately associated with a reward followed by a 25-secundum-long time out with the chamber light switched on (time-out period), while the other nose hole was not baited (incorrect). During the time-out period, responses were not rewarded but were registered. The test was divided into two phases: habituation (days 1) and learning (days 2–5), and data only from the learning phase was shown. Reward preference (RP) (ratio of responses on the rewarded nose hole) was calculated. The number of rewarded responses and time-out reward hole nose pokes were also recorded. The number of animals is on Figure 11.

$$\text{reward preference (\%)} = \frac{\text{correct nose poke}}{\text{correct nose poke} + \text{incorect nose poke}} * 100$$

III.3.3.2. In vivo metabolic measurements (Experimental Series 3., Cohort 2)

First, the animals were transferred to training boxes (one/cage) for 3-day acclimatization. Before the measurement started, the body composition was measured by EchoMRI-700 (700 Whole Body Composition Analyzer; E26-233RM, Echo Medical Systems, Houston, TX, USA). This Magnetic Resonance Analyzer allows very quick and precise analyses of body composition without the need of sedation or anaesthesia. During the scanning mice were placed in a specially sized, clear plastic holder. The system determines the total body fat content, the lean body mass, and the free and total water content of the animals (300).

$$\text{hydration ratio} = \frac{\text{total water} - \text{free water}}{\text{lean}} * 100$$

After acclimatization to training boxes and EchoMRI measurement, mice were transferred to metabolic (calo) cages. In the Phenomaster Metabolic Phenotyping system (TSE Systems Gmbh, Berlin, Germany) metabolic variables were measured for 24 hours. Data of metabolic variables (food- and O_2 consumption and CO_2 production) were automatically collected in every 9 minutes (301). The respiratory exchange ratio (RER) was calculated with the following formula: V_{CO2}/V_{O2}. The program automatically

integrates and analyses CO_2 production (V_{CO_2}) and O_2 consumption (V_{O_2}), both adjusted for body weight. Heat production (H), calculated per cage, does not directly account for body weight; however, normalizing EE to lean mass provides a more accurate assessment of metabolic activity, as fat tissue has negligible energy requirements.

The program calculated the following values:

$V_{O2} = Flow(ml) * (V_1 + V_2) / (N_2Ref * 100.0)$, representing O_2 consumption.

$V_{CO2} = Flow(ml) * d_{CO2} / 100.0$, representing CO_2 production.

$H = (CV_{O2} * V_{O2} + CV_{CO2} * V_{CO2}) / 1000$, expressed as Kcal/h.

To get H in Watt, we multiplied the Kcal/h data with 1.16306.

Finally, energy expenditure (EE) was calculated by dividing heat production (H) by lean mass (kg):

$EE = H(Kcal/h) / lean\ mass(kg)$

It is more accurate to report EE relative to lean body mass (measured by EchoMRI; kcal/h/kg lean). For better transparency, the data were aggregated in a 3-hour resolution, as well as the changes in both the dark and the light cycle were examined separately.

The number of animals is on Figure 12.

III.4. Immunohistochemistry (Experimental Series 1., Cohort 3.)

Mice were anesthetized intraperitoneally (i.p.) with a ketamine-xylazine solution (16.6 mg/ml and 0.6 mg/ml, respectively) at a dose of 125 mg/kg ketamine and 25 mg/kg xylazine, in 0.9% saline at a concentration of 10 ml/kg. They were then transcardially perfused with ice-cold phosphate-buffered saline (PBS), followed by ice-cold paraformaldehyde (4% PFA VWR International, Leuven, Belgium, #28794.295, in TRIS VWR International, Leuven, Belgium, #103154M). Brains were rapidly removed and post-fixed overnight in 4% PFA at 4 °C, then incubated in a solution containing 30% sucrose (D-(+) saccharose puriss, Lach-Ner, Neratovice, Czech Republic, #57-50-1) in TRIS before slicing. Thirty μm coronal sections were collected on a sliding microtome and stored in a cryoprotectant solution (containing 20% glycerine, Molar Chemicals, Halásztelek, Hungary, #03490-101-340, 30% ethylene glycol, Molar Chemicals, Halásztelek, Hungary, #03010-203-340) at −20 °C until immunohistochemically staining.

To investigate the amyloid plaques and hyperphosphorylated tau (Experimental Series I., Cohort 3.), we used peroxidase-based immunohistochemistry, with nickel-

diaminobenzidine tetrahydrochloride (Ni-DAB; 3,3'-Diaminobenzidine tetrahydrochloride hydrate, Merck, Sigma Aldrich, St. Louis, MO, USA, #D5637-1G, nickel (II) sulphate hexahydrate, Merck, Sigma Aldrich, St. Louis, MO, USA, #227676-500G) visualization. Before staining for amyloid, a 95%, 10 min formic acid (Merck, Sigma- Aldrich, St. Louis, MO, USA, #F0507) pretreatment was performed. Slices were incubated for 72 h, at 4°C in primary antibodies: anti-Aβ1–42 (1:500, polyclonal anti-rabbit, Invitrogen, Waltham, MA USA, #71–5800) and anti-phospho-Tau (1:500, monoclonal anti-mouse AT8, Invitrogen, Waltham, MA USA, #MN1020). As secondary, biotinylated anti-rabbit (1:200, Jackson ImmunoResearch, West Grove, PA, #111–065-003) and anti-mouse (1:200, Jackson ImmunoResearch, West Grove, PA, #715–065-151) antibodies were used, followed by an avidin-biotin treatment (VECTASTAIN Elite ABC-Peroxidase Kits, Vector Laboratories, Newark, CA, USA, #PK-6100) at room temperature for 2 h. Visualization was performed with a Ni-DAB and glucose oxidase (Merck, Sigma Aldrich, St. Louis, MO USA, #G7141-10KU) solution.

Sections containing the appropriate brain regions were selected using the Paxinos atlas (302) (OB: Bregma (Br) +3.56 mm to +2.34 mm; motor and somatosensory cortex Br +0.6 mm to +1.2mm; hippocampus Br -1.58 mm to -2.46 mm; CA1 region of the hippocampus: Br -2.80 mm to -3.39; CA3 region of the hippocampus: Br -2.79 mm to -3.39 mm; BLA: Br -2.69 mm to -3.39 mm).

The labelling was imaged using Nikon Eclipse Ei microscope with a Digital Sight 1000 camera at 4× magnification and representative images are presented.

III.5. Histological Evaluation of Joints (Experimental Series 2., Cohort 3.)

Hind limbs were dissected and after additional tissues were removed, joint samples were washed in PBS three times and fixed in a 4:1 mixture of absolute ethanol and 40% formaldehyde. Limbs were decalcified in 4% EDTA for four weeks until bones became soft. Then samples were dehydrated in ascending alcohol row and embedded in paraffin. 7 µm thick serial sections were made and dimethyl-methylene-blue (DMMB) staining (Merck, Sigma Aldrich, St. Louis, MO USA, #931418-92-7) was performed for morphological analysis. Staining protocol was carried out according to the manufacturer's instructions.

Photomicrographs were taken using a DP74 camera (Olympus Corporation, Tokyo, Japan) on an Olympus Bx53 microscope (Olympus Corporation, Tokyo, Japan).

For the measurement of articular cartilage 10× magnification photomicrographs of DMMB staining were investigated and a customized mathematical formula was used as described before (303).

For the examination of thick and thinner collagen fibre ratio in articular cartilage Picrosirius red (Merck, Sigma Aldrich, St. Louis, MO USA, #14726-29-5) staining was used. In polarized light turning the light plane with $\lambda/4$ thick collagen fibres appeared in red, thinner collagen fibre in green colour. Samples were investigated in an Olympus Bx53 polarization microscope (Olympus Corporation, Tokyo, Japan) with constant settings and exposure time. In 20× magnification photomicrographs of red and green pixels of articular cartilage were determined with ImageJ 1.40g freeware (http://rsb.info.nih.gov/ij/ Wayne Rasband, developer, National Institutes of Health, Bethesda, MD).

Due to technical reasons the number of animals was different for each joint.

DMMB

knee joints $n_C=8$, $n_{3xTg-AD}=8$;

intertarsal joint $n_C=7$, $n_{3xTg-AD}=7$;

tarsometatarsal joint $n_C=7$, $n_{3xTg-AD}=6$;

interphalangeal joint $n_C=3$, $n_{3xTg-AD}=4$

Picrosirius red staining

knee joints $n_C=6$, $n_{3xTg-AD}=6$;

intertarsal joint $n_C=7$, $n_{3xTg-AD}=7$;

tarsometatarsal joint $n_C=6$, $n_{3xTg-AD}=7$;

interphalangeal joint $n_C=4$, $n_{3xTg-AD}=4$

III.6. Blood and Serum Parameters

III.6.1. Blood glucose and other blood parameters (Experimental Series 2., Cohort 3.

Blood glucose, cholesterol, triglyceride, and uric acid levels were determined from one drop of blood during decapitation. Blood glucose (mmol/l) and triglyceride (mmol/l) levels were measured by MultiCarein (BSI Biochemical Systems International, Arezzo, Italy, #I 00078284) while cholesterol (mmol/l) and uric acid (μM) levels were detected by Wellmed Easy Touch GCU (Bioptik Technology, Inc., Miaoli County, Taiwan, #ET 301). The number of animals is on Figure 10.

III.6.2. Enzyme-Linked Immunosorbent Assay (ELISA; Experimental Series 2., Cohort 3.)

During decapitation the blood samples were collected and immediately placed on ice until centrifugation was performed. The samples were centrifuged at 4°C 2500g for 30 min and serum were collected in Eppendorf tubes. Samples were stored at -20°C until used. For determination of free T4 (fT4) and free T3 (fT3) levels, AccuLite ELISA fT3 and fT4 CLIA kits (Monobind Inc., Lake Forest, CA USA, #1275-300) were used according to manufacturer's protocol using iMARKTM Microplate Absorbance Reader (Bio-Rad Hungary Ltd., Budapest, Hungary). Duplicates of the samples and 6 standards of known concentration were measured on the 96-well plate and the values were given in ng/dl. The number of animals is on Figure 10.

III.7. Quantitative PCR (qPCR)

Mice were sacrificed by decapitation and their brain and gastrocnemius muscle were snap-frozen on dry ice and stored at -80°C until use (Experimental Series 2., Cohort 3 and 5) On dry ice the cerebellum was cut in half. Total RNA was extracted from gastrocnemius muscle and one half of the cerebellum using RNAzol® RT (Merck, Sigma Aldrich, St. Louis, MO USA, Sigma #R4533-50ML).

From a separate set of animals (Experimental Series 2., Cohort 3 and 5) the PVN and MBH were dissected by micro punch technique. These areas and the pituitary gland were snap-frozen on dry ice and stored at -80°C until use.

Total RNA was extracted using RNeasy Mini Kit (QIAGEN, Hilden, Germany, #74106). Reverse transcription of the RNA samples was made by High-Capacity RNA-to-cDNA™ Kit (Thermo Fisher Scientific, Waltham, MA, USA, # 4387406). Total RNA purity and quantity were assessed using a NanoPhotometer NP80 (IMPLEN GmbH, München, Germany). cDNA synthesis was confirmed using One Step PCR and analysed by electrophoresis on a 1.5% agarose gel with DreamTaq Green PCR (Thermo Fisher Scientific, Waltham, MA, USA, #2772182). This allowed for an evaluation of RNA integrity and the efficiency of the reverse transcription process. SensiFAST SYBR Lo-ROX Kit (Izinta Trade Ltd., Budapest, Hungary, # BIO-94005) was used for qPCR. Quantitative PCR was performed in an Applied Biosystems QuantStudio 5 Real-Time PCR System (Thermo Fisher Scientific, Waltham, MA, USA). Quantification reactions were performed in duplicate for each sample using the 'delta-delta Ct' method,

normalized to the average of the control group data, and linearized by $2^{-\Delta\Delta Ct}$ (304). Glyceraldehyde 3-phosphate dehydrogenase (GAPDH) was chosen as a reference (housekeeping) gene. Primers used for qPCR are listed in Table 1. Primers were designed using Primer-BLAST (NCBI) and were acquired from the Bio-Science Kft (Budapest, Hungary). The number of animals is on Figure 10.

Table 1. Primer sequences used in qPCR analysis of gene expression.

Gene	Forward primer sequence	Reverse primer sequence
GAPDH	CCC TGT TGC TGT AGC CGT AT	AGA ACA TCA TCC CTG CAT CC
Myostatin	ATT GGC TCA AAC AGC CTG AA	AAG GCT TCA AAA TCG ACC GT
Follistatin	GAA TGT GCC GTC ACA GAG AA	CTC ATC GCG GTT AGC TTG A
COX4	GTC TTC CGG TTG CGG G	CAC TCT TCA CAA CAC TCC CAT
BCL2	GAG CTT TGA GCA GGT AGT GA	TGA AGA CAG ATC TGA GGG GTG
BAX	CTG ACA TGT TTG CTG ATG GC	CCA GCC ACC CTG GTC TT
TRH	GCT CTG GCT TTG ATC TTC GT	TTG TGA TCC AGG AAT CTA AGG C
TRβ2	GTG AAT CAG CCT TAT ACC TG	ACA GGT GAT GCA GCG ATA GT
TSHβ	TCA ACA CCA CCA TCT GTG CT	TTG CCA CAC TTG CAG CTT AC
DIO1	CTG GGA TTT CAT TCA AGG CAG	CCA CGT TGT TCT TAA AAG CCC
DIO2	GAT GCT CCC AAT TCC AGT GT	AGT GAA AGG TGG TCA GGT GG
DIO3	ATG CGT ATC AGA CGA CAA CC	CAA AAT TGA GCA CCA ACG GG
MCT8	GCT GAG CCA GTG CAA GAA	GCT GCT TGG AAC TCC ACT T
CART	CGC TAT GTT GCA GAT CGA AG	GTC CCT TCA CAA GCA CTT CA
POMC	CAT CTT TGT CCC CAG AGA GC	TTT TCA GTC AGG GGC TGT TC
AgRP	TTT CTG CTC CCT TGG TTT CC	GGC AGT AGC AAA AGG CAT TG
NPY	GCC ACG ATG CTA GGT AAC AA	TTG ATG TAG TGT CGC AGA GC
MCHR	ATC TCC GAT GGC CAG GAT AA	TGG TAC CAA ACA CTG AAG GC

III.8. Western Blot Analysis (WB, Experimental Series 2., Cohort 3 and 5)

Proteins were isolated from the other half of the cerebellum. Protein lysates were prepared with 500µl RIPA buffer (10mM Tris-HCl, 1mM EDTA, 0.5mM EGTA, 150mM NaCl, 0.1% SDS, 1%TritonX) containing Protease and Phosphatase Inhibitor Cocktail (Sigma #PPC1010). Protein extract was mixed with 2x Laemmli buffer (4% SDS, 20% glycerol, 0.004% Bromophenol blue, 0.125M Tris HCl, 10% β-mercaptoethanol) and denaturized for 10 min at 95°C. The protein samples were then separated on a 15% polyacrylamide gel with electrophoresis and transferred to a nitrocellulose membrane (Bio-Rad Hungary Ltd., Budapest, Hungary, #1620115). The membranes were blocked by 5% skim milk in TBS buffer containing 0.02% Tween20 and then incubated with

rabbit polyclonal anti-caspase3 antibody (1:1000, Abcam, Cambridge, UK, #ab13847), rabbit monoclonal anti-cytochrome C IV subunits (COX IV, a mitochondrial marker) (D6I4K) (1:500, Cell Signaling Technology Europe, B.V., Leiden, The Netherlands, #38563), mouse monoclonal anti-BAX antibody (1:500, Santa Cruz Biotechnology, Heidelberg, Germany, #sc-7480), mouse monoclonal anti-Bcl-2 antibody (1:500, Santa Cruz Biotechnology, Heidelberg, Germany, #sc-7382) and rabbit recombinant-GAPDH (1:5000, Abcam, Cambridge, UK, #ab181603) at 4°C overnight. After washing with TBS buffer containing 0.02% Tween20, the membranes were incubated for 2 hours with horse radish peroxidase-conjugated anti-rabbit IgG secondary antibodies (1:2500, Sigma #SAB3700853). The protein bands were detected using the ECL chemiluminescence reagent (Bio-Rad Hungary Ltd., Budapest, Hungary, #170-5061) by Li-COR Imaging system (Li-COR, C-DiGit™ Blot Scanner 3600). The images were analysed directly by the Image Studio™ software (LI-COR Biosciences), where optical densities (pixel/area) were measured. The number of animals is on Figure 10.

III.9. Statistical Analysis

Data are presented as means ± SEM and were analysed using GraphPad Prism (version 6.0). Statistical analyses included two-way ANOVA and repeated-measures ANOVA for various comparisons, as detailed below:

Three-way or Mixed-effects analysis:

- ✓ Fox odour: genotype and sex and age

Two-way ANOVA or Mixed-effects analysis:

- ✓ Fox odour: genotype and sex
- ✓ Collagen thickness: genotype and red/green ratio
- ✓ qPCR: genotype and training
- ✓ Western Blot (WB): genotype and training
- ✓ MRI: genotype and age
- ✓ TSE PhenoMaster: genotype and age

Repeated-measures ANOVA or Mixed-effects analysis:

- ✓ Fox odour: genotype and age
- ✓ Open Field Test (OFT): genotype and age; genotype, sex, and 5 min intervals
- ✓ Grip test: genotype and trial
- ✓ Rotarod test: genotype and day

- ✓ Single Pellet Reaching Test (SPRT): genotype and day
- ✓ Staircase test: genotype and day
- ✓ TSE PhenoMaster: genotype, age, and 3-hour intervals
- ✓ Optical Coherence Tomography (OCT): genotype and day
- ✓ Radial Arm Maze (RAM): genotype and day

Post-hoc analyses were performed using Tukey HSD or Sidak tests.

For pairwise comparisons, **Student's t-test** or **Mann-Whitney U test** was applied

- ✓ grip test - average grip strength,
- ✓ rotarod test – average latency,
- ✓ OFT,
- ✓ RAM,
- ✓ MWM,
- ✓ cartilage thickness in pixels,
- ✓ TSE PhenoMaster – food- and water consumption 24h,
- ✓ blood parameters,
- ✓ ELISA – ft3, ft4.

Statistical significance was set at $p < 0.05$. Figures indicate post hoc comparison results, while main ANOVA effects are presented in the tables.

Figures were created using BioRender (https://biorender.com/), Adobe Affinity Design Software 1.10.5, and Vectornator Designer Software (https://www.vectornator.io/).

IV. Results

IV. 1. Temporal Emergence of Increased Innate Anxiety

IV.1.1. Fox Odour Avoidance Behaviour

The 3xTg-AD animals moved significantly less than their age-matched controls (Figure 13A; for statistics see Table 2.). Interestingly, the controls, but not the 3xTg-AD mice moved more with age. Despite this main genotype effect, during the post-hoc test the genotype difference reaches significancy only in some cases (2-, 4-, 18-month-old animals).

Coherent with the less movement, the 3xTg-AD animals spent more time in immobile, not moving position (Figure 13B; Table 2.). The animals tended to freeze less with age. However, once again, significant post hoc difference was detectable only in the same age groups that showed locomotor impairment.
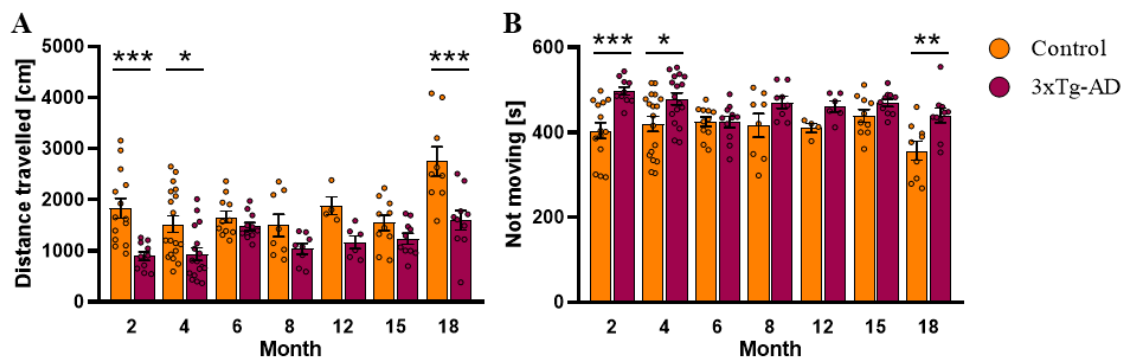
Figure 13. Age-Related Changes in Mobility During Fox Odour Avoidance in Male Mice. A. Distance Travelled in Centimetres for 10 Minutes. **B.** Time Spent without Movement.
Two-way ANOVA, Sidak's multiple comparisons test *$p<0.05$; **<0.01; ***$p<0.001$ vs control.
Male mice 2- $n_C=14$; $n_{3xTg-AD}=10$; 4- $n_C=18$; $n_{3xTg-AD}=17$; 6- $n_C=11$; $n_{3xTg-AD}=11$; 8- $n_C=8$; $n_{3xTg-AD}=8$; 12- $n_C=4$; $n_{3xTg-AD}=6$; 15- $n_C=10$; $n_{3xTg-AD}=10$; 18-month-old $n_C=9$; $n_{3xTg-AD}=10$

Table 2. Fox Odour Test Behaviour in Male Mice

Parameters	Genotype		Age		Genotype × Age	
	F	p	F	p	F	p
Distance [cm]	$42.84_{(1,132)}$	<0.001	$7.446_{(6,132)}$	<0.001	$2.098_{(6,132)}$	0.058
Not moving [s]	$23.95_{(1,33)}$	<0.001	$2.795_{(6,99)}$	0.015	$1.867_{(6,99)}$	0.094
Duration difference	$4.832_{(1,33)}$	0.035	$4.069_{(4.180,68.28)}$	0.005	$0.730_{(6,98)}$	0.627
Corrected approach time [s/m]	$1.431_{(1,132)}$	0.234	$2.599_{(6.132)}$	0.021	$0.559_{(6,132)}$	0.762
Approach frequency [#]	$23.08_{(1,132)}$	<0.001	$2.662_{(6,132)}$	0.018	$1.052_{(6,132)}$	0.395

Corrected avoidance duration [s/m]	$11.81_{(1,33)}$	0.002	$7.863_{(6,99)}$	<0.001	$1.833_{(6,99)}$	0.100
Avoidance frequency [#]	$42.24_{(1,132)}$	<0.001	$16.71_{(6,132)}$	<0.001	$2.605_{(6,132)}$	0.020

Several age-groups were studied (2, 4, 6, 8, 12, 15 and 18 months). This table contains the statistical data to Figure 13, 14, 15. Degree of freedom is in brackets. Significant differences are marked as red.

All animals were afraid of the fox odour reflected by the 200–500 sec more time spent in the avoidance than in approach zone despite only a double multiplier in their size. In fact, the 3xTg-AD mice in general avoided the 2MT smell more than their age matched controls (Figure 14, Table 2.).
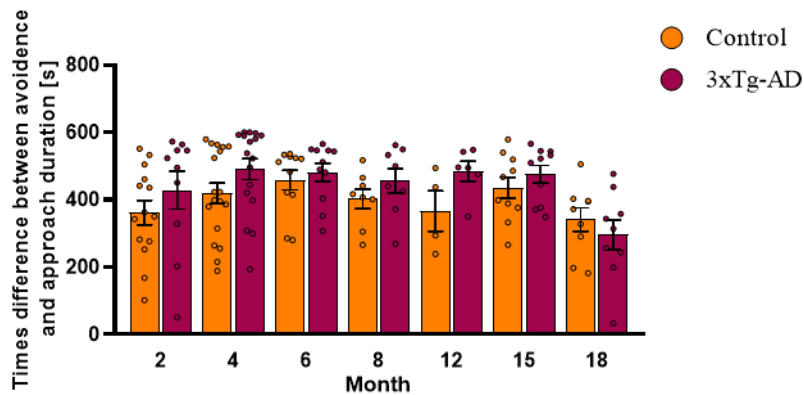
Figure 14.: Age-Dependent Zone Duration Difference in Fox Odor Avoidance. The time spent in the avoidance and approach zones were subtracted from each other.
Two-way ANOVA, Sidak's multiple comparisons test
Male mice 2- n_C=14; $n_{3xTg-AD}$=10; 4- n_C=18; $n_{3xTg-AD}$=17; 6- n_C=11; $n_{3xTg-AD}$=11; 8- n_C=8; $n_{3xTg-AD}$=8; 12- n_C=4; $n_{3xTg-AD}$=6; 15- n_C=10; $n_{3xTg-AD}$=10; 18-month-old n_C=9; $n_{3xTg-AD}$=10

Due to differences in locomotion, we corrected the time spent in different compartments with it (s/m) (Figure 15A, Table 2.). After correction, the previously significant genotype difference in approach time became non-significant. However, the age effect remained detectable. Namely, older animals spent significantly more time near the 2MT container than the younger animals. As expected, the approach frequency was lower in 3xTg-AD mice, but this also increased with age (Figure 15B). Although one might think that the avoidance time is a pure reverse of the approach time, there is a middle zone in between them (Figure 8). Thus, avoidance requires activity. Indeed, 3xTg-AD animals were more afraid of the 2MT smell, spending more time in the avoidance zone than their age-matched controls, and this effect became significant after correction (Figure 15C). Interestingly, a longer amount of time was accompanied by fewer entries

of 3xTg-AD mice into this avoidance zone (Figure 15D). The number of entries increased with age in control, but not in 3xTg-AD animals.
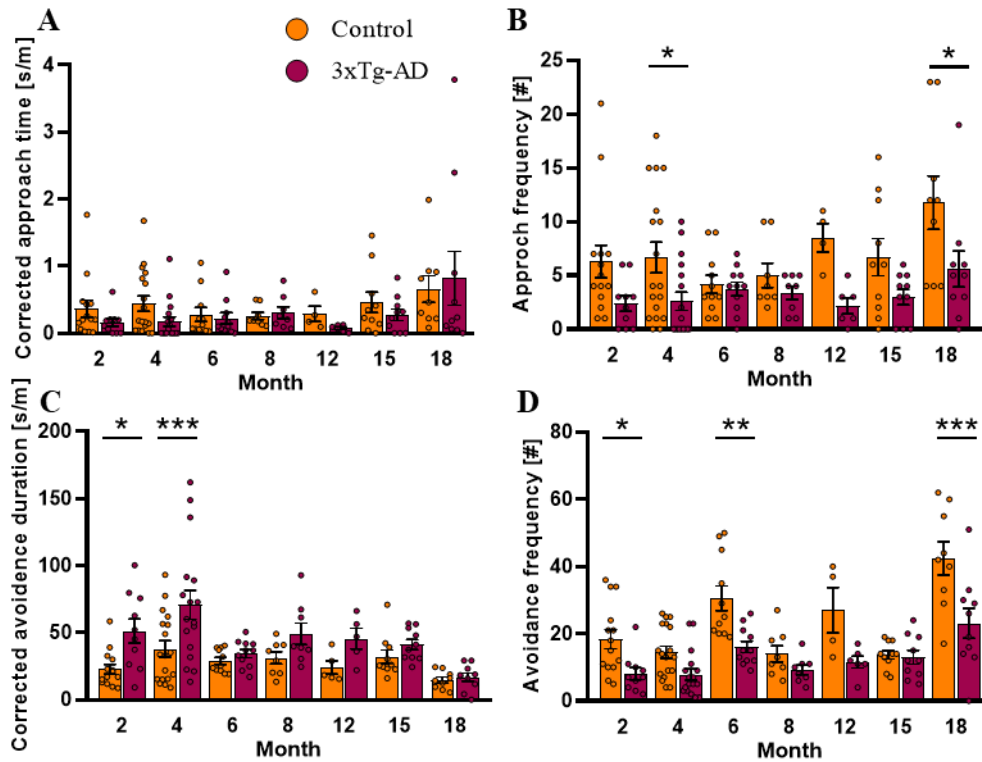
Figure 15. Fox Odour Test in Male Mice Across Different Age Groups. A. Corrected approach time to fox odour zone (sec/m). **B.** Frequency of approaching the odour zone. **C.** Locomotion corrected time spent in the avoidance zone (sec/m). **D.** Number of entries into the avoidance zone.
Two-way ANOVA, Mixed effects analysis, Sidak's multiple comparisons test *$p<0.05$; **$p<0.01$; ***$p<0.001$ vs control.
Male mice 2- $n_C=14$; $n_{3xTg-AD}=10$; 4- $n_C=18$; $n_{3xTg-AD}=17$; 6- $n_C=11$; $n_{3xTg-AD}=11$; 8- $n_C=8$; $n_{3xTg-AD}=8$; 12- $n_C=4$; $n_{3xTg-AD}=6$; 15- $n_C=10$; $n_{3xTg-AD}=10$; 18-month-old $n_C=9$; $n_{3xTg-AD}=10$

In selected age-groups we examined possible sex differences. First young, 2-month-old mice were studied. Similarly to previous tests, the 3xTg-AD animals moved significantly less than the controls (Figure 16A, Table 3.). The tendency for lower approach frequency, as well as significant genotype difference in corrected avoidance duration, avoidance frequency, as well as freezing time and frequency, and frequency of sniffing the 2MT container all suggested enhanced anxiety of 3xTg-AD animals (Figure 16B–H). Nevertheless, there was no difference between the two sexes. However, during post-hoc comparisons, 3xTg-AD males showed more significant changes than respective females.
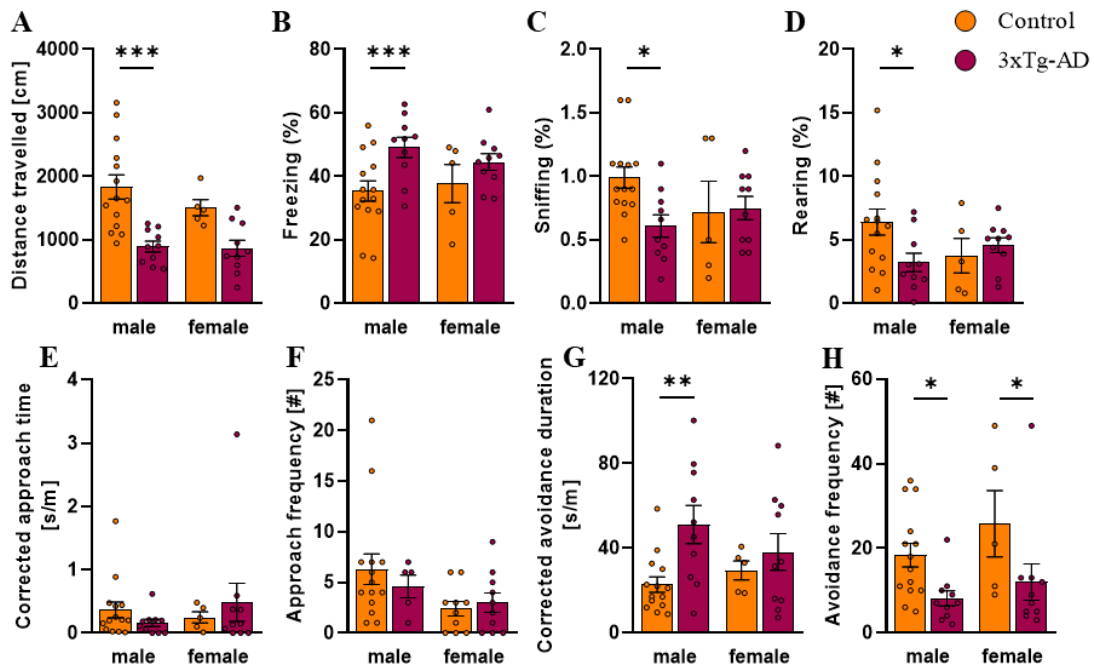
Figure 16. Fox Odour Test in 2-Month-Old Male and Female Animals. A. Distance travelled in centimetres during 10 min. **B.** Time spent freezing as a percentage of 10 min observation period. **C.** Time spent sniffing the 2MT container as a percentage of 10 min observation period. **D.** Time spent rearing as a percentage of 10 min observation period. **E.** Corrected approach time to fox odour zone. **F.** Frequency of approaching the odour zone. **G.** Corrected avoidance duration. **H.** Number of entries into the avoidance zone.

Two-way ANOVA, Mixed effects analysis, Sidak's multiple comparisons test $*p<0.05$; $**p<0.01$, $***p<0.001$ vs control.

2-month-old male mice $n_C=14$; $n_{3xTg-AD}=10$; **2-month-old female mice** $n_C=5$; $n_{3xTg-AD}=10$

Table 3. Fox Odour Test in 2-month-old Male and Female Animals.

Parameters	Genotype		Sex		Genotype × Sex	
	F	p	F	p	F	p
Distance [cm]	$22.99_{(1,13)}$	<0.001	$0.775_{(1,22)}$	0.388	$0.762_{(1,13)}$	0.399
Freezing (%)	$21.18_{(1,13)}$	<0.001	$0.491_{(1,22)}$	0.491	$1.615_{(1,13)}$	0.226
Sniffing (%)	$2.403_{(1,13)}$	0.145	$0.311_{(1,22)}$	0.583	$3.311_{(1,13)}$	0.092
Rearing (%)	$1.355_{(1,35)}$	0.252	$0.41_{(1,35)}$	0.526	$3.95_{(1,35)}$	0.055
Corrected approach time [sec/m]	$0.833_{(1,13)}$	0.378	$0.561_{(1,22)}$	0.462	$0.02_{(1,13)}$	0.891
Approach frequency [#]	$0.154_{(1,35)}$	0.697	$3.93_{(1,35)}$	0.055	$0.682_{(1,35)}$	0.414
Corrected avoidance duration [sec/m]	$7.104_{(1,13)}$	0.019	$0.129_{(1,22)}$	0.723	$2.039_{(1,13)}$	0.177
Avoidance frequency [#]	$17.69_{(1,13)}$	0.001	$2.771_{(1,22)}$	0.110	$0.434_{(1,13)}$	0.522

This table contains the statistical data to Figure 16. Degree of freedom is in brackets. Significant differences are marked as red.

In 15-month-old animals, in accordance with previous results, the 3xTg-AD animals moved less than controls both horizontally and vertically (Figure 17A, 17D, respectively, Table 4.). They also approach the fox odour container less (Figure 17F) and spent more time far from it (Figure 17G). Moreover, the 3xTg-AD animals sniffed the 2MT container less and for shorter periods (Figure 17C) and spent more time freezing (Fig. 17B) than their controls. At this age, the sex difference was more pronounced. The females moved less (both horizontally (Figure 17A) and vertically (Figure 17D)) and spent more time near the 2MT container compared to males (Figure 17E), irrespective of their genotype. In contrast to 2-month-old animals, here, in post-hoc comparisons, 3xTg-AD females showed a more significant change than matched males.
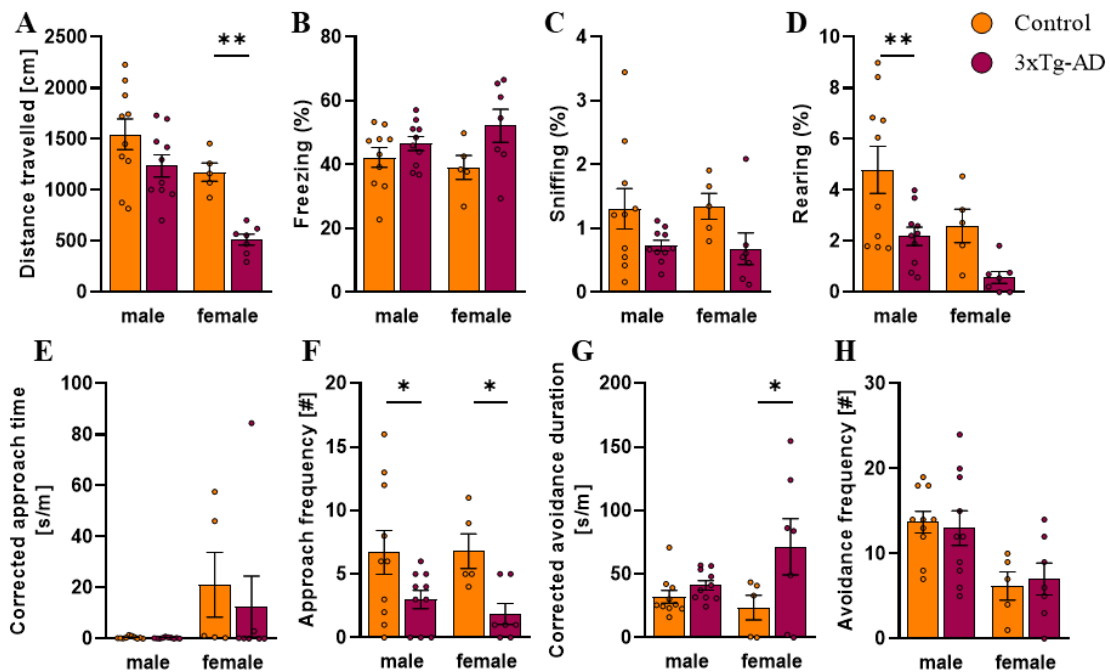
Figure 17. Fox Odour Test in 15-Month-Old Male and Female Animals. A. Distance travelled in centimetres during 10 min. **B.** Time spent freezing as a percentage of 10 min observation period. **C.** Time spent sniffing the 2MT container as a percentage of 10 min observation period. **D.** Time spent rearing as a percentage of 10 min observation period. **E.** Corrected approach time to fox odour zone. **F.** Number of approaches to the odour zone. **G.** Corrected time spent in the avoidance zone. **H.** Number of entries into the avoidance zone.
Two-way ANOVA, Mixed effects analysis, Sidak's multiple comparisons test *$p<0.05$; **$p<0.01$, ***$p<0.001$ vs control.
15-month-ol male mice $n_C=10$; $n_{3xTg-AD}=10$ **15-month-old female mice** $n_C=5$; $n_{3xTg-AD}=7$

Table 4. Fox Odour Test in 15-month-old Male and Female Animals

Parameters	Genotype		Sex		Genotype × Sex	
	F	**p**	**F**	**p**	**F**	**p**
Distance [cm]	$14.35_{(1,28)}$	<0.001	$18.20_{(1,28)}$	<0.001	$1.890_{(1,28)}$	0.180

Freezing (%)	$5.804_{(1,13)}$	0.032	$0.118_{(1,15)}$	0.736	$1.433_{(1,13)}$	0.253
Sniffing (%)	$6.307_{(1,13)}$	0.026	$0.001_{(1,15)}$	0.974	$0.03_{(1,13)}$	0.865
Rearing (%)	$14.76_{(1,13)}$	0.002	$6.226_{(1,15)}$	0.025	$0.288_{(1,13)}$	0.600
Corrected approach time [s/m]	$2.661_{(1,13)}$	0.127	$4.973_{(1,15)}$	0.042	$2.539_{(1,13)}$	0.135
Approach frequency [#]	$13.15_{(1,13)}$	0.003	$0.1_{(1,15)}$	0.757	$0.312_{(1,13)}$	0.586
Corrected avoidance duration [s/m]	$6.479_{(1,28)}$	0.017	$0.944_{(1,28)}$	0.340	$2.996_{(1,28)}$	0.095
Avoidance frequency [#]	$0.001_{(1,13)}$	0.978	$12.300_{(1,15)}$	0.003	$0.174_{(1,13)}$	0.683

This table contains the statistical data to Figure 17. Degree of freedom is in brackets. Significant differences are marked as red.

To gain better insight into the relationships between age and various parameters, the combined statistical analysis of the male and female data is shown in Table 5 (figure not shown). The analysis reveals significant genotype effects across most measured variables, indicating distinct behavioural differences between 3xTg-AD and control mice. Notably, female animals move less than expected, irrespective of genotype. The effect of age is evident primarily in rearing behaviour, corrected approach time, and avoidance zone entry frequency, where older animals display a significant decline. Furthermore, interactions between sex, age, and genotype, while generally non-significant, suggest the importance of considering these factors together to fully understand their combined effects. (Only the part of the table indicating the effect of age is shown here.)

Table 5. Fox Odour Test in 2 and 15-month-old Male and Female Animals, Combined Sex and Age and Genotype Analysis

	Distance [cm]		Freezing (%)	
	F	**p**	**F**	**p**
Age	$2.019_{(1, 63)}$	0.160	$1.291_{(1, 40)}$	0.262
Sex x Age	$2.748_{(1, 63)}$	0.102	$0.148_{(1, 23)}$	0.704
Age x Genotype	$1.844_{(1, 63)}$	0.179	$0.044_{(1, 40)}$	0.836
Sex x Age x Genotype	$2.137_{(1, 63)}$	0.149	$2.678_{(1, 23)}$	0.115
	Sniffing (%)		Rearing (%)	
	F	**p**	**F**	**p**
Age	$3.687_{(1, 40)}$	0.062	$7.548_{(1, 40)}$	0.009
Sex x Age	$0.047_{(1, 23)}$	0.830	$0.838_{(1, 23)}$	0.370
Age x Genotype	$2.861_{(1, 40)}$	0.099	$0.828_{(1, 40)}$	0.368
Sex x Age x Genotype	$0.917_{(1, 23)}$	0.348	$2.406_{(1, 23)}$	0.135

	Corrected approach time [s/m]		Approach frequency [#]	
	F	**p**	**F**	**p**
Age	$7.332_{(1, 40)}$	0.010	$0.281_{(1, 63)}$	0.598
Sex x Age	$7.181_{(1, 23)}$	0.013	$1.290_{(1, 63)}$	0.260
Age x Genotype	$0.517_{(1, 40)}$	0.477	$3.733_{(1, 63)}$	0.058
Sex x Age x Genotype	$0.525_{(1, 23)}$	0.476	$0.814_{(1, 63)}$	0.370
	Corrected avoidance duration [s/m]		Avoidance frequency [#]	
	F	**p**	**F**	**p**
Age	$1.036_{(1, 63)}$	0.312	$26.26_{(1, 63)}$	<0.001
Sex x Age	$1.150_{(1, 63)}$	0.288	$1.912_{(1, 63)}$	0.172
Age x Genotype	$0.5727_{(1, 63)}$	0.452	$2.962_{(1, 63)}$	0.090
Sex x Age x Genotype	$4.966_{(1, 63)}$	0.029	$0.066_{(1, 63)}$	0.798

This table contains the statistical data to 2- and 15-month-old male and females behaviour parameters. Degree of freedom is in brackets. Significant differences are marked as red.

IV.1.2. Open Field Test

During repeated testing, the 3xTg-AD animals generally moved less (Figure 18, Table 6.). Although there was no overall difference between sexes, there was a tendency with more pronounced difference between genotypes in females than in males. In females, all post-hoc comparisons between genotypes were significant, while males did not show genotype difference from the age of 4 months.
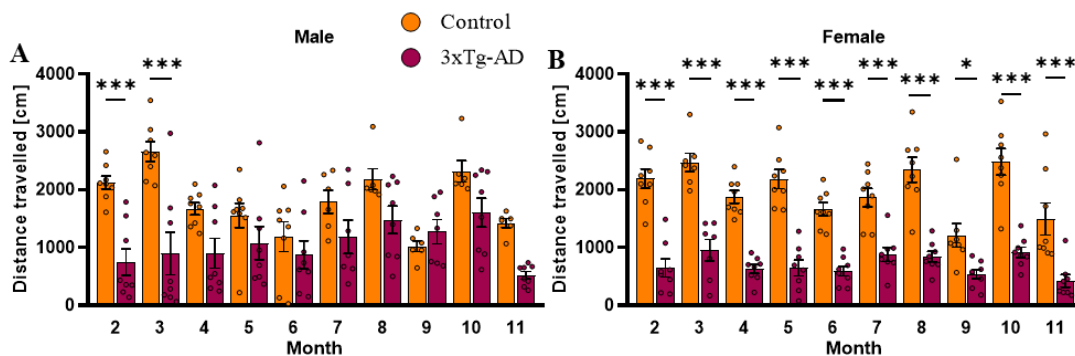
Figure 18. Open Field Test from 2 to 11 Months. A. Males**, B.** Females. Distance travelled in centimetres during 5 min observation period.
Repeated measures ANOVA, Sidak's multiple comparisons test *p<0.05; ***p<0.001 vs control.
Male mice n_C=8; $n_{3xTg-AD}$=8; **Female mice** n_C=8; $n_{3xTg-AD}$=8

Table 6. Open Field Test between 2- and 11-month.

Parameters	Genotype		Age		Genotype × Age	
	F	p	F	p	F	p
Male						
Distance [cm]	$7.087_{(1,14)}$	0.019	$10.76_{(9,114)}$	<0.001	$7.804_{(9,114)}$	<0.001
Time spent in centre (%)	$0.091_{(1,14)}$	0.767	$7.899_{(9,115)}$	<0.001	$1.271_{(9,115)}$	0.260
Female						
Distance [cm]	$86.89_{(1,14)}$	<0.001	$9.837_{(9,124)}$	<0.001	$2.889_{(9,124)}$	0.004
Time spent in centre (%)	$38.92_{(1,14)}$	<0.001	$8.110_{(9.123)}$	<0.001	$2.223_{(9,123)}$	0.025

This table contains the statistical data to Figure 18 and 19. Degree of freedom is in brackets. Significant differences are marked as red.

The 3xTg-AD spent significantly less time in the centre of the arena than control animals (Figure 19A, B; Table 6.). However, females spent less time in the centre than males (p<0.01), with a more pronounced difference between genotypes in females than males. In fact, post-hoc testing found genotype differences only in females from the age of 7 months.
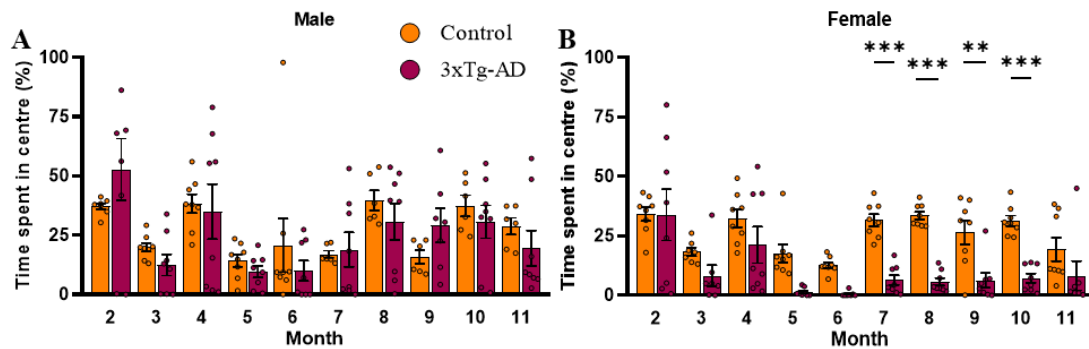
Figure 19. Open Field Test from 2 to 11 Months. A. Males**, B.** Females. Percentage of time spent in the centre of the open field during 5 min observation period.
Repeated-measures ANOVA, Sidak's multiple comparisons test **p<0.01; ***p<0.001 vs control.
Male mice n_C=8; $n_{3xTg-AD}$=8; **Female mice** n_C=8; $n_{3xTg-AD}$=8

Despite no clear correlation between body weight and emotionality (305), we cannot rule out the possibility that changes in body weight influenced the above-mentioned parameters. In our hands, the initial body weight at two months was higher, as expected, in males than in females (Figure 20, Table 7.). As anticipated, body weight exhibited a significant increase with age in all groups, with this increase gradually slowing down and stabilizing around 8 months of age. Throughout the study period, control males consistently displayed the highest body weight, while control females consistently exhibited the lowest. Notably, the body weight of both 3xTg-AD and control females followed a similar developmental pattern up to 6 months of age. However, starting from 6 months, the 3xTg-AD females displayed a notably higher body weight. In contrast, among males, the divergence in body weight became evident at around 7 months of age, with control male mice surpassing the transgenic males.

Figure 20. Body Weight Changes with Age in Both Sexes.
Repeated measures ANOVA
Male mice n_C=8; $n_{3xTg-AD}$=8;
Female mice n_C=8; $n_{3xTg-AD}$=8
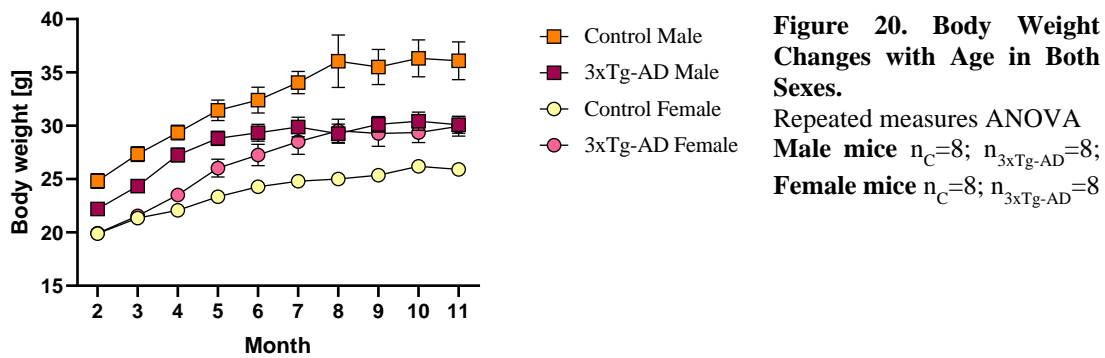
Table 7. Body Weight Changes with Age in Both Sexes.

	Body weight [g]	
	F	**p**
Age	$144.8_{(1.759,47.11)}$	<0.001
Sex	$46.83_{(1,28)}$	<0.001
Genotype	$0.588_{(1,28)}$	0.450
Age x Sex	$1.290_{(9,241)}$	0.243
Age x Genotype	$1.240_{(9,241)}$	0.271
Sex x Genotype	$20.15_{(1,28)}$	<0.001
Age x Sex x Genotype	$7.340_{(9,241)}$	<0.001

This table contains the statistical data to Figure 20. Degree of freedom is in brackets. Significant differences are marked as red.

When analysed using Pearson correlation, no significant correlations were found between the rate of body weight gain and the distance travelled during the OFTs or the time spent in the centre for male mice. This lack of correlation was observed in both the

control group (distance travelled: r= 0.056, p = 0.0503, time spent in centre (%): r = <0.001, p = 0.848) and the transgenic group (distance travelled: r = 0.042, p = 0.071, time spent in centre (%): r = < 0.001, p = 0.813).

In contrast, for female mice, body weight gain showed correlations with the observed behaviour. Control females exhibited a correlation with the distance travelled (distance travelled: r = 0.089, p = 0.007, time spent in centre (%): r = 0.009, p = 0.400), while 3xTg-AD females showed a correlation with the time spent in the centre (distance travelled: r = 0.013, p = 0.315, time spent in centre (%): r = 0.110, p = 0.003).

At the end of the monthly observation period, in 11-month-old animals, we examined the temporal development of behaviour as well. The 3xTgAD animals moved significantly less during the whole 30 min observation period (Figure 21A, Table 8.). The sex as well as the time had no influence on this parameter (i.e., no habituation was observed). Regarding the time spent in the centre (Figure 21B, Table 8.), the control animals spent more and more time in the centre as a sign of reduced anxiety over time, while the 3xTg-AD animals spent significantly less time in the centre. Females were more anxious, spending less time in the central compartment.
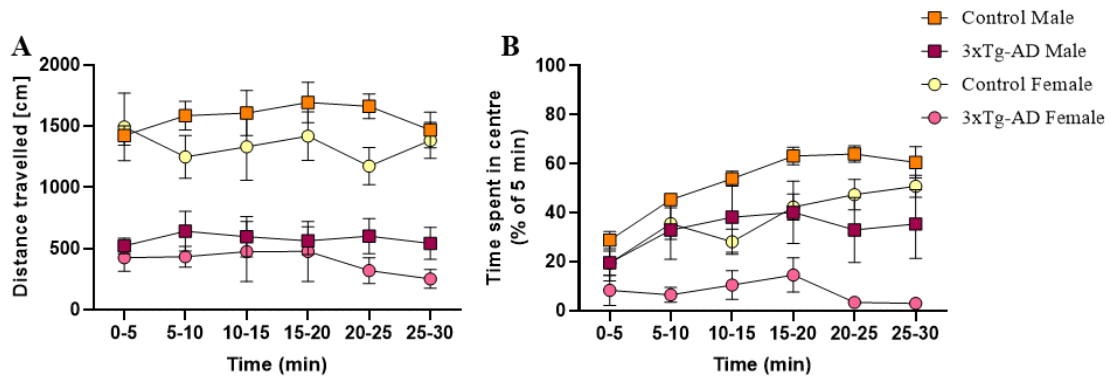
Figure 21. Open Field Test during a 30-Minute Observation Period in 11-Month-Old Animals. A. Distance travelled in centimetres given in 5 min time bins throughout the entire 30 min observation period. **B**. Percentage of time spent in the centre in 5 min time bins.
Repeated measures ANOVA
Male mice n_C=8; $n_{3xTg-AD}$=8; **Female mice** n_C=8; $n_{3xTg-AD}$=8

Table 8. Open Field Test during a 30-Minute Observation Period in 11-Month-Old Animals

	Distance travelled [cm]		Time spent in centre (%)	
	F	**p**	**F**	**p**
Time	$0.963_{(5,130)}$	0.443	$13.64_{(3.08,75.14)}$	<0.001
Sex	$1.940_{(1,26)}$	0.176	$8.768_{(1,26)}$	0.007

Genotype	$43.00_{(1,26)}$	<0.001	$14.05_{(1,26)}$	0.001
Time x Sex	$1.781_{(5,130)}$	0.121	$1.674_{(5,122)}$	0.146
Time x Genotype	$0.425_{(5,130)}$	0.831	$7.177_{(5,122)}$	<0.001
Sex x Genotype	$0.030_{(1,26)}$	0.865	$0.483_{(1,26)}$	0.493
Time x Sex x Genotype	$1.031_{(5,130)}$	0.402	$1.351_{(5,122)}$	0.247

This table contains the statistical data to Figure 21. Degree of freedom is in brackets. Significant differences are marked as red.

IV.1.3. Immunohistochemical Confirmation of Temporal Appearance of the Histological Hallmarks

Using Ni-DAB immunohistochemistry we were able to confirm the progressive appearance of the classical hallmark of AD (Aβ and p-tau) in brain areas important for memory formation (e.g., hippocampus; Figure 22F, G, J-M) as well as in the amygdala, an important centre of emotions including anxiety (Figure 22H, I, N, O). Moreover, the deposits were detectable in the OB (Figure 22A–C) and piriform cortex (Figure 22N, O), brain areas participating in olfaction (306). Interestingly, Aβ was only minimally present in two-month-old animals, while the signal intensity for p-tau was already high in this age group. Nevertheless, the number of positively stained cells (both for Aβ as well as p-tau) was higher in the brain of one-year-old animals than in two-month-old ones. These deposits were not detectable in the brain of control mice (data not shown).

Amyloid-β$_{1-42}$ Plaques

2-month-old 3xTg-AD   1-year-old 3xTg-AD   2-month-old 3xTg-AD   1-year-old 3xTg-AD

Hyperphosphorylated Tau

2-month-old 3xTg-AD | 1-year-old 3xTg-AD
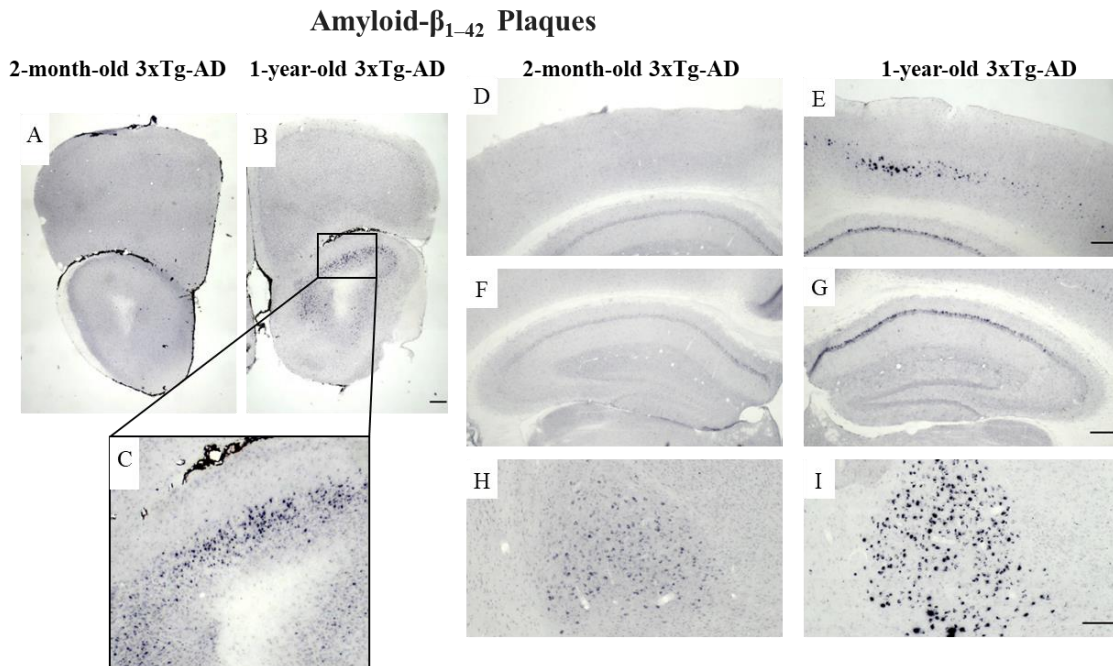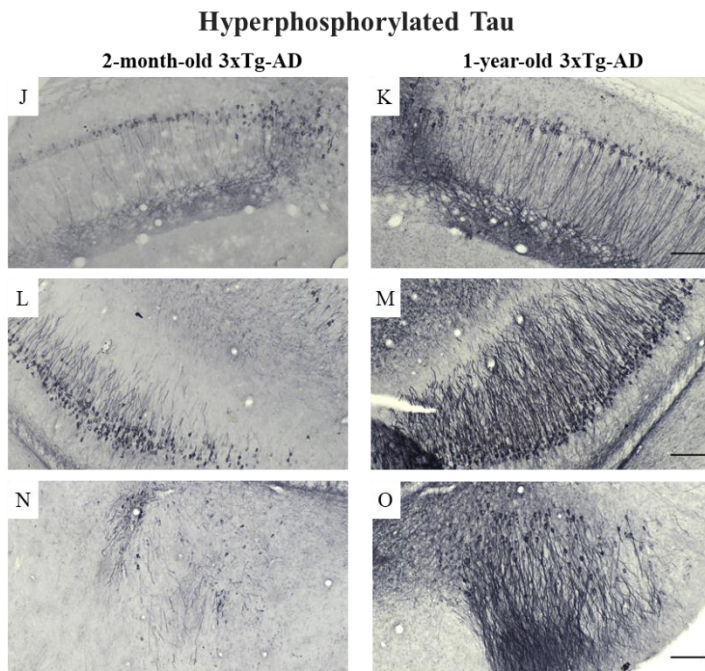
Figure 22. Ni-DAB Immunohistochemistry in 2-month-old and 1-year-old 3xTg-AD Mice. A-I: Amyloid-β_{1-42}; **J-O:** Phospho-Tau. The images depict various brain regions: A-C: the olfactory bulb, D,E: motor- and somatosensory-cortex, F,G: hippocampus, H.,I: basolateral and basomedial amygdala; J,K: pyramidal cell layer in the CA1 region of the hippocampus, L,M: pyramidal cell layer in the CA3 region of the hippocampus, N,O: basolateral amygdaloid nucleus, amygdalopiriform area, and entorhinal cortex. Scale bars: B, E, G: 200 µm, I, K, M, O: 100 µm. n=3/group

IV.2. Musculoskeletal and Cerebellar Changes in the Context of Motor Alterations

IV.2.1. Motor Alterations During Different Behavioural Test

The grip test, which assesses muscle strength in mice, revealed a significant loss of muscle strength in 6-month-old, male 3xTg-AD animals compared to controls (Figure 23B, Table 10.). The AD mice performed significantly worse during all trials without any changes between trials (Figure 23A; Table 9.).
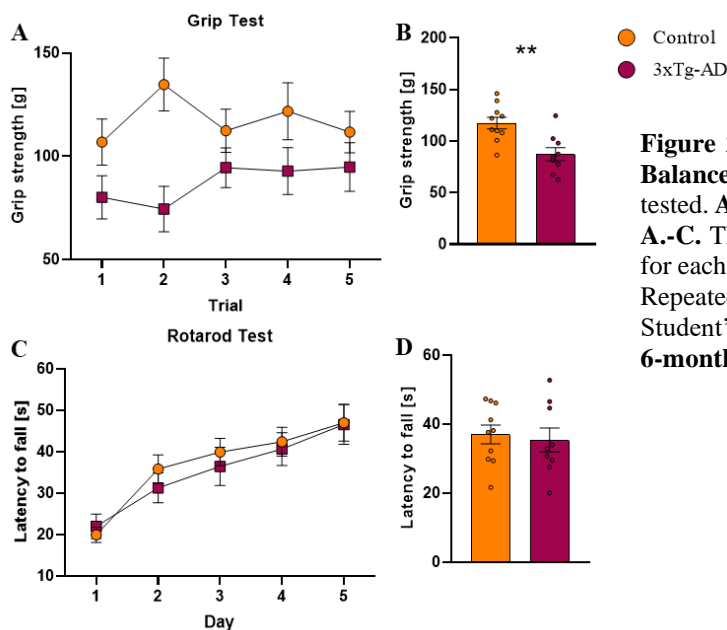
Figure 23. Muscle Strength and Motor Balance. 6-month-old male mice were tested. **A.-B**. Grip Test **C.-D.** Rotarod Test. **A.-C.** The falling time is given separately for each trial. **B.D.:** Average of the 5 trials. Repeated measures ANOVA Student's t-test, **p<0.01 vs control. **6-month-old male mice** n_C=10; $n_{3xTg-AD}$=9

Table 9. Motor Alterations during Different Behavioural Tests. Temporal resolution

Parameters	Genotype		Trial/Day/Min		Genotype × Trial/Day	
	F	**p**	**F**	**p**	**F**	**p**
Grip test (5 trials)	$17.610_{(1,85)}$	<0.001	$0.423_{(4,85)}$	0.792	$1.201_{(4,85)}$	0.317
Rotarod test (5day)	$0.811_{(1,40)}$	0.373	$11.140_{(4,45)}$	<0.001	$0.342_{(4,40)}$	0.848
Open Field 15min	$148_{(1,135)}$	<0.001	$9.589_{(14,135)}$	<0.001	$0.375_{(14,135)}$	0.980
SPRT	$19.990_{(1,105)}$	<0.001	$19.180_{(6,105)}$	<0.001	$0.764_{(6,105)}$	0.600
Staircase test DT	$62.580_{(1,54)}$	<0.001	$4.206_{(5,54)}$	0.003	$3.444_{(5,54)}$	0.009
Staircase test SR	$17.320_{(1,54)}$	<0.001	$4.615_{(5,54)}$	0.001	$1.204_{(5,54)}$	0.320

This table contains the statistical data to the averages on Figure 23-24 and 26. Degree of freedom is in brackets. Significant differences are marked as red. Abbreviations: DT: distance travelled; SR: success rate; SPRT: single pellet reaching task.

Table 10. Motor Alterations during Different Behavioural Tests.

Parameters	Genotype	
	$t_{(df)}$	**p**
Grip test average	$3.576_{(17)}$	0.002
Rotarod test average	$0.373_{(17)}$	0.714
Open Field	$3.083_{(18)}$	0.006
Open Field (handling)	$1.049_{(12)}$	0.315
RAM first day	$0.95_{(18)}$	0.355
RAM last day	$3.711_{(18)}$	0.002
MWM	$0.051_{(10)}$	0.961

This table contains the statistical data to the averages on Figure 23-25. Degree of freedom is in brackets. Significant differences are marked as red. Abbreviations: MWM: Morris water maze; RAM: radial arm maze test.

No significant difference was observed between the two genotypes during the rotarod test, which measures motor coordination (Figure 23D, Table 10.). All mice improved their performance over time as they remained on the continuously accelerating rotating rod for longer durations from day to day (Figure 23C, Table 9.).

During this experimental series we repeated the previous OFT (see IV.1.2.) in 6-month-old animals with a higher temporal resolution (using 1-min bins). We could confirm our previous data that the 3xTg-AD mice exhibited reduced movement both in the first 5 minutes (Figure 24B, Table 10.) and during a prolonged 15-minute observation period (Figure 24A. Table 9.). After an initial period of freezing, the mice began to explore the environment, as reflected by the high level of distance travelled during the second minute of observation. Although the interest gradually decreased, the difference between the genotypes remained constant throughout the 15 minutes. Furthermore, when the animals were kept in an enriched environment and handled repeatedly, the locomotor difference disappeared (Figure 24C, Table 10.).
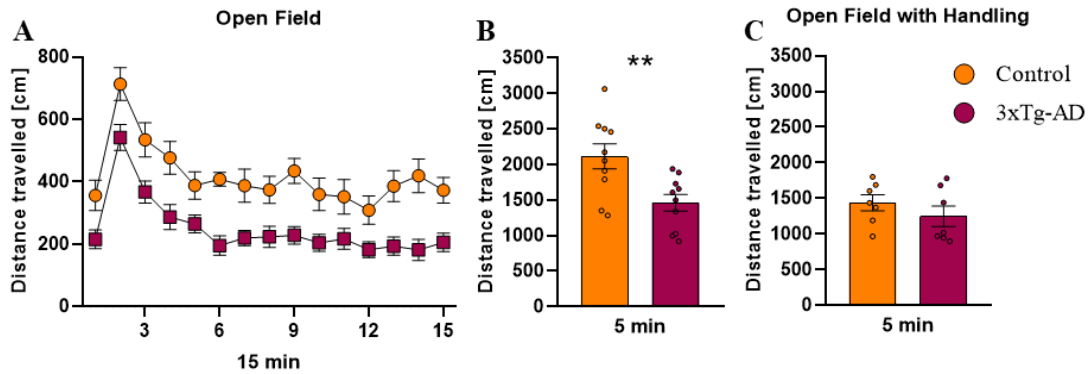
Figure 24. General Locomotion in Open Field Test. A-B. Distance travelled in centimetres in 1-min bins (A.) or in average (B.). **C.** Average values during 5 min observation in animals kept in enriched environment and were repeatedly handled.
Repeated measures ANOVA
Student's t-test **$p < 0.01$ vs control.
6-month-old male mice $n_C = 10$; $n_{3xTg-AD} = 10$

Given the significantly lower muscle strength and locomotor activity detected in the transgenic mice, we investigated whether positive (food) or negative (escape from water) reinforcements could act as appropriate motivators for normal locomotion. While these tests aimed to assess cognition, here we focused solely on locomotion in the test boxes.

On the first day of the RAM test, when there was no food in the arena, no difference was observed between the groups (Figure 25A, Table 10.), like when the animals were handled repeatedly before the OFT. However, when we compared the "probe" on the last day, when food motivation had developed, we found that transgenic mice moved significantly more in the RAM compared to the control group (Figure 25B,

Table 10.). This indicated that food motivation encouraged transgenic mice to be more active.
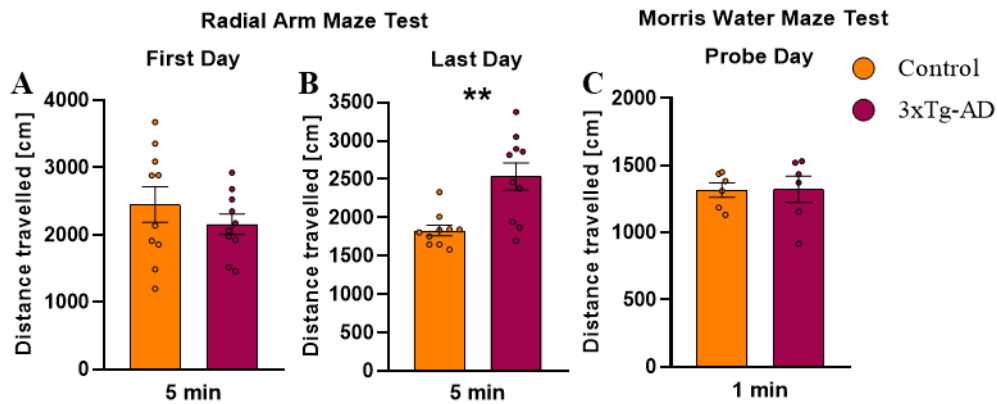
Figure 25. Motivation-Induced Locomotion in Cognitive Tests. A-B. Radial arm maze (RAM) test without pellets. **C**. Morris water maze (MWM) test.
Student's t-test **p<0.01 vs control.
MWM 6-month-old male mice n_C=6; $n_{3xTg-AD}$=6; **RAM 6-month-old male mice** n_C=10; $n_{3xTg-AD}$=10

During the MWM test, we compared the "probe" day between genotypes, as only on this day did the animals spend equal time in the pool, similar to the RAM test. Our results clearly showed that both the transgenic and control groups covered an equal distance during the 1-minute observation period (Figure 25C, Table 10.).

Based on clinical observation and considering the problems in muscle strength and movement, we expected early fine motor problems in the 3xTg-AD animals.

In the SPRT, where mice were trained for 7 days to collect pellets using their paws through a 5 mm wide lane, the transgenic mice paradoxically collected significantly more rewards (Figure 26A, Table 9.). Moreover, as the days progressed, both groups showed a significant increase in reward acquisition, suggesting that they learned the task.

Figure 26. Fine Motoric Tests. A. Single pellet reaching test (SPRT). **B-C.** Staircase test. Repeated measures ANOVA
6-month-old male mice $n_C=10$; $n_{3xTg-AD}=10$
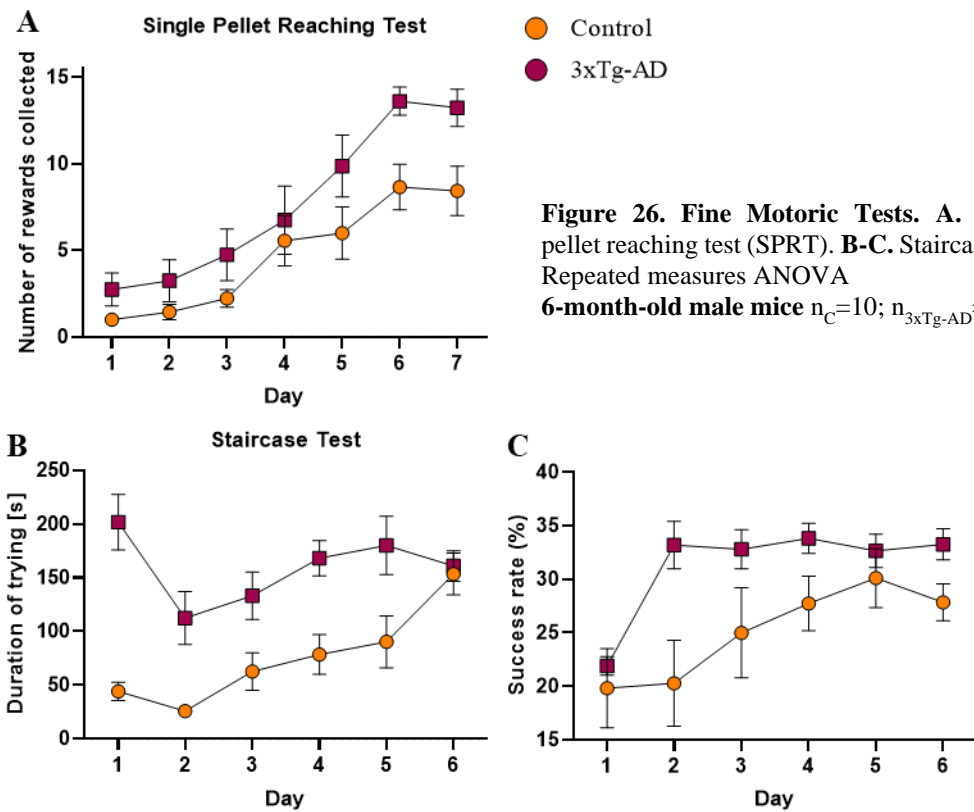
In the Staircase test, transgenic mice initially spent significantly more time attempting to reach the pellet (Figure 26B, Table 9.). However, this disparity gradually diminished, as evidenced by a significant genotype x time interaction. The success rate on the first day was approximately 20% for both groups (Figure 26C, Table 9.). Nevertheless, a notable increase in the success rate was observed in the transgenic mice on the second day, and this improved performance was consistently maintained in the following days. Conversely, the control group exhibited a gradual increase in their success rate over time. By the fifth day, both groups of animals had achieved a similar success rate in collecting the pellet (Figure 26C, Table 9.). It appears that the transgenic mice, after initially dedicating more time to their attempts during the early stages of the experiment, adjusted both their time allocation and success rate from the second day onwards. In contrast, the control group displayed a steady increase in both parameters throughout the experiment.

IV.2.2. Histological evaluation of joints

Collagen fibres orientation and thickness can be examined with Picrosirius staining. In polarized light collagen - independently from its type - appeared in red colour, which showed normal morphology of articular cartilage both in control and in 3xTg-AD

mice knee joints (Figure 27A, B, Table 11.). No morphological differences were identified in intertarsal, tarsometatarsal and interphalangeal joints (Figure 27C-H). In polarized light turned with $\lambda/4$ collagen fibres can be visualized – depending on their thickness - in red (thicker) or green (thinner) colour. In articular cartilage of all examined joints articular (knee: Figure 27A,B; intertarsal: Figure 27C,F; tarsometatarsal: Figure 27D,G; interphalangeal: Figure 27E,H) thicker collagen fibres were normally oriented forming maltan crosses and significantly lower thinner than thicker collagen fibres was present independently from the genotype (307) (Figure 27A, B).
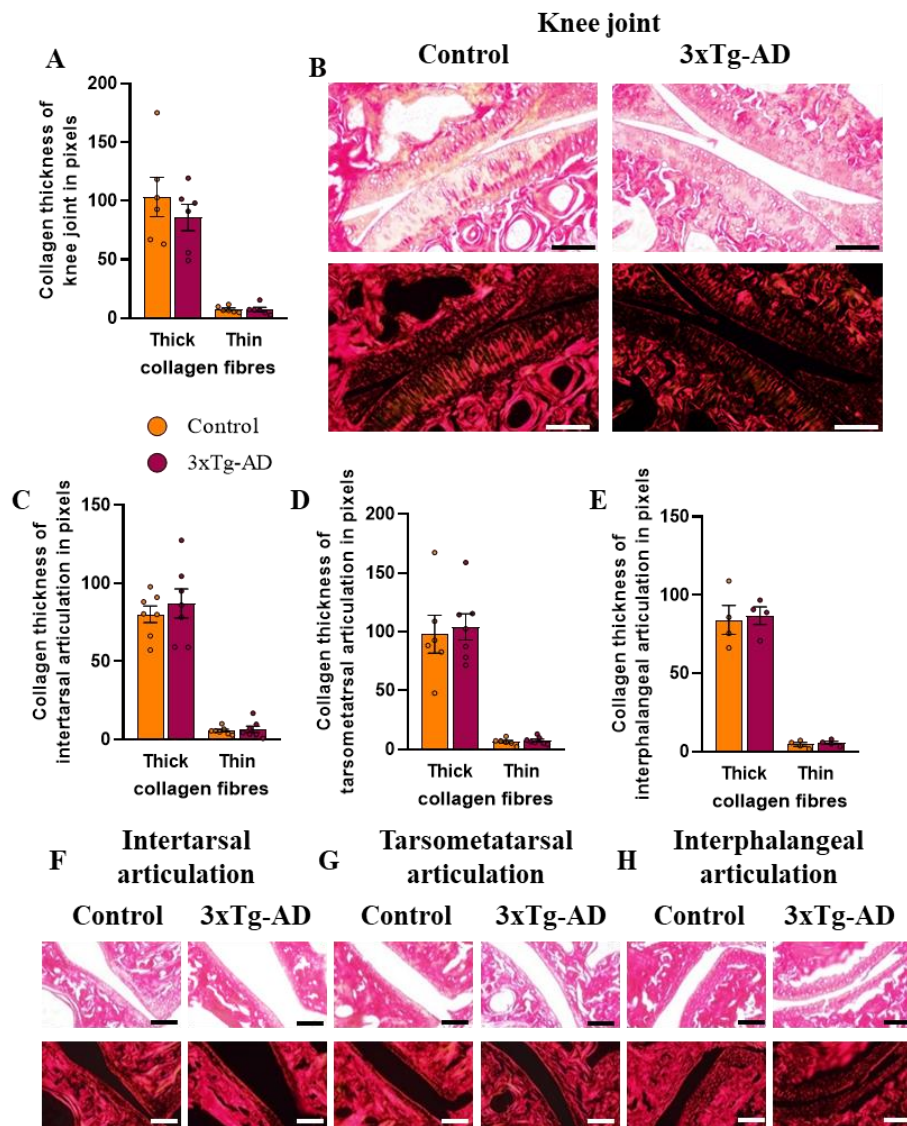
Figure 27. Collagen Fiber Thickness Analysis of Knee, Intertarsal, Tarsometatarsal, and Interphalangeal Joints. B, F-H. Picrosirius red staining was used in normal and in $\lambda/4$ polarized light to investigate collagen fibre thickness. The images were captured at an original magnification of 20×, with a scale bar of 50 μm. **A, C-E.** Thick and thin collagen fibres / red and green pixel density of the articular cartilage was analysed.

Two-way ANOVA, Mixed effects analysis, Sidak's multiple comparisons test

8-month-old male mice 8M knee joints $n_C=6$, $n_{3xTg-AD}=6$; intertarsal joint $n_C=7$, $n_{3xTg-AD}=7$; tarsometatarsal joint $n_C=6$, $n_{3xTg-AD}=7$; interphalangeal joint $n_C=4$, $n_{3xTg-AD}=4$

Table 11. Collagen Fiber Thickness Analysis of Knee, Intertarsal, Tarsometatarsal, and Interphalangeal Joints.

Parameters	Genotype		Thick and Thin Collagen Fibres		Genotype × Thick/Thin	
Collagen thickness of	**F**	**p**	**F**	**p**	**F**	**p**
knee joint	$0.514_{(1,10)}$	0.490	$133.700_{(1,10)}$	<0.001	$0.496_{(1,10)}$	0.498
intertarsal articulation	$0.551_{(1,12)}$	0.472	$184.600_{(1,12)}$	<0.001	$0.334_{(1,12)}$	0.574

65

tarsometatarsal articulation	$0.138_{(1,10)}$	0.719	$95.550(1,12)$	<0.001	$0.070_{(1,10)}$	0.797
interphalangeal articulation	$0.092_{(1,6)}$	0.772	$264.200_{(1,6)}$	<0.001	$0.020_{(1,6)}$	0.891

This table contains the statistical data to the Figure 27. Degree of freedom is in brackets. Significant differences are marked as red.

Glycosaminoglycan content of hyaline cartilage, visualized with DMMB staining, showed normal metachromasia in knee, intertarsal, and interphalangeal articular cartilage in both genotypes (Figure 28A-E, Table 12.). There was a tendency toward thinner metatarsal cartilage in 3xTg-AD compared to controls.
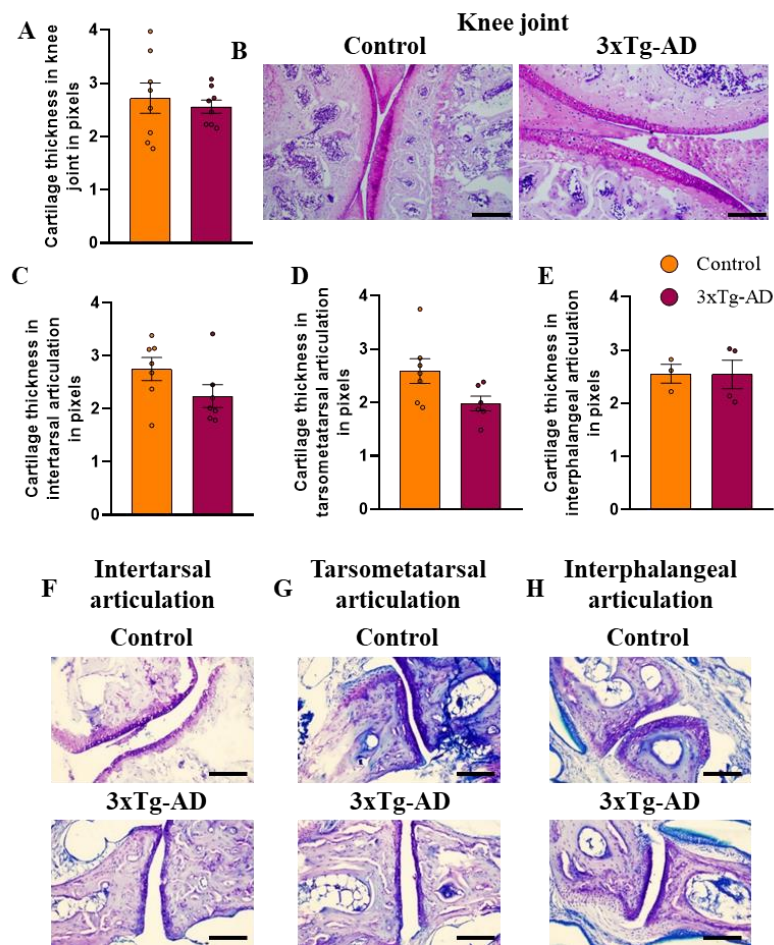
Figure 28. Morphological Analysis of Knee, Intertarsal, Tarsometatarsal, and Interphalangeal Joints. B, F-H. Histological differences were visualized using Dimethyl methylene blue (DMMB) staining. Images were taken at an original magnification of 10×, with a scale bar of 100 μm. **A, C-E.** Geometric analysis of mouse articular cartilage was performed.
Student's t-test, Mann-Whitney U test
8-month-old male mice knee joints n_C=8, $n_{3xTg-AD}$=8; intertarsal joint n_C=7, $n_{3xTg-AD}$=7; tarsometatarsal joint n_C=n=7, $n_{3xTg-AD}$=6; interphalangeal joint n_C==3, $n_{3xTg-AD}$=4

Table 12. Morphological Analysis of Knee, Intertarsal, Tarsometatarsal, and Interphalangeal Joints

Parameters	Genotype	
Thickness of joint in pixels	$t_{(df)}$	**p**
knee joint	$0.505_{(14)}$	0.622
intertarsal articulation	$1.672_{(12)}$	0.120
tarsometatarsal articulation	$2.156_{(11)}$	0.054
interphalangeal articulation	$0.034_{(5)}$	0.974

This table contains the statistical data to the Figure 28. Degree of freedom is in brackets. The tendency is marked as blue.

IV.2.3. Changes at molecular levels

To examine the possible beneficial effect of a restricted diet plus repeated testing (referred to as training), the molecular changes detected after extensive behavioural testing were compared to an absolute control group.

IV.2.3.1. mRNA expression levels in the gastrocnemius muscle

In the RT-qPCR analysis of the gastrocnemius muscle of 6-month-old male 3xTg-AD and control mice, no significant differences were detected in the mRNA expression levels of myostatin and follistatin (Figure 29A-B, Table 13.). However, following the training, follistatin levels decreased (Figure 29B), leading to an increased myostatin/follistatin ratio (Figure 29C). The genotype had no effect of the observed parameters.
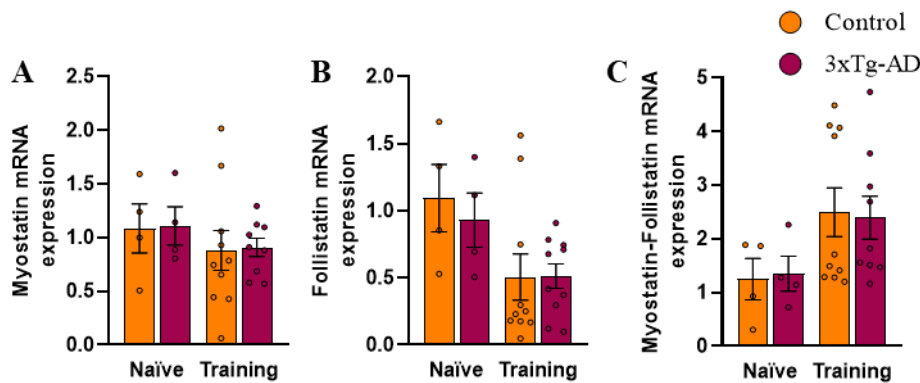
Figure 29. The Myostatin and Follistatin System in the Gastrocnemius Muscle. The mRNA values were calculated by the $2^{-\Delta\Delta Ct}$ method using glyceraldehyde-3-phosphate dehydrogenase (GAPDH) as housekeeping gene and normalized to the values in the average of control group. **A.** Myostatin mRNA expression. **B.** Follistatin mRNA expression. **C.** Myostatin / follistatin ratio.
Two-way ANOVA, Mixed effects analysis, Sidak's multiple comparisons test
Animals were sacrificed without testing (Naïve) n_C=4, $n_{3xTg-AD}$=4; **8-month-old male mice (Experimental Animal, Training)** n_C=10, $n_{3xTg-AD}$=10

67

Table 13. mRNA Changes in Musculus Gastrocnemius Measured by qPCR.

	Genotype		Training		Genotype x Training interaction	
	F	**p**	**F**	**p**	**F**	**p**
Myostatin	$0.012_{(1,11)}$	0.914	$1.076_{(1,12)}$	0.320	$0.001_{(1,11)}$	0.975
Follistatin	$0.349_{(1,12)}$	0.566	$5.019_{(1,12)}$	0.045	$0.423_{(1,12)}$	0.528
Myostatin-Follistatin ratio	$<0.001_{(1,23)}$	0.999	$5.132_{(1,23)}$	0.033	$0.043_{(1,23)}$	0.838
COX4	$0.594_{(1,11)}$	0.457	$0.6771_{(1,12)}$	0.427	$0.669_{(1,11)}$	0.431
BAX	$1.609_{(1,11)}$	0.231	$1.901_{(1,12)}$	0.193	$0.002_{(1,11)}$	0.967
BCL2	$1.853_{(1,10)}$	0.203	$1.282_{(1,12)}$	0.280	$0.460_{(1,10)}$	0.513
BCL2 – BAX ratio	$1.101_{(1,10)}$	0.319	$7.088_{(1,12)}$	0.021	$1.427_{(1,10)}$	0.260

This table contains the statistical data to the Figures 29, 30. Degree of freedom is in brackets. Significant difference is marked as red. Abbreviations: BAX: gene of Bcl-2 associated X protein; BCL2: gene of B-cell leukaemia/lymphoma 2; COX4: gene of cytochrome c oxidase subunit 4

We also compared the mRNA expression of the mitochondrial marker COX4 (Figure 30A, Table 13.), the pro-apoptotic BAX (Figure 30B, Table 13.), and the anti-apoptotic BCL2 (Figure 30C, Table 13.). No differences were found between animals in these mRNA expression levels (neither the genotype, not the training well as their interaction was significant). However, the training increased the BCL2/BAX ratio (Fig. 29D).

Figure 30. Mitochondrial System in the Gastrocnemius Muscle. The mRNA values were calculated by the $2^{-\Delta\Delta Ct}$ method using GAPDH as housekeeping gene and normalized to the values in the average of control group. **A.** The mitochondrial marker, COX4 mRNA expression. **B.** The expression level of the pro-apoptotic BAX mRNA. **C**. The anti-apoptotic BCL2 mRNA expression. **D.** The BCL2 and BAX mRNA ratio. Abbreviations: BAX: gene of Bcl-2 associated X protein; BCL2: gene of B-cell leukaemia/lymphoma 2; COX4: gene of cytochrome c oxidase subunit 4.
Two-way ANOVA, Mixed effects analysis, Sidak's multiple comparisons test
Animals were sacrificed without testing (Naïve) $n_C=4$, $n_{3xTg-AD}=4$; **8-month-old male mice (Experimental Animal, Training)** $n_C=10$, $n_{3xTg-AD}=10$

IV.2.3.2. mRNA expression and protein levels in the cerebellum

In the cerebellum, we examined the previously mentioned mitochondrial and apoptotic genes. COX4 mRNA level was significantly higher in transgenic mice compared to control mice (Figure 31A, Table 14.). However, after the training, BAX mRNA levels decreased by approximately 20% (Figure 31B), BCL2 mRNA levels increased (Figure 31C), leading to a significant cumulative increase in the BCL2/BAX ratio (Figure 31D). No genotype difference was observed in the latest parameters.

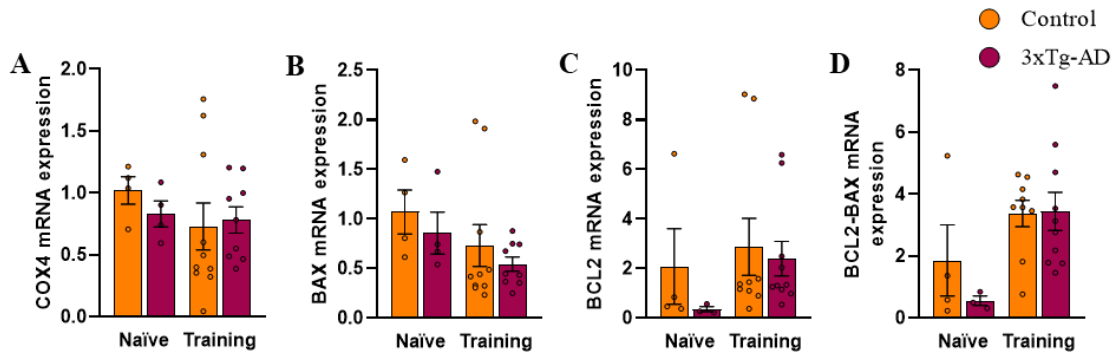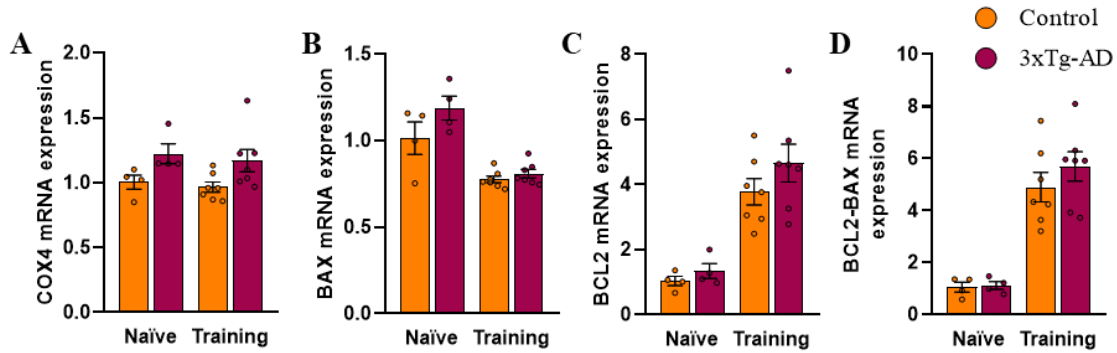**Figure 31. mRNA Expression Level Changes in the Mitochondrial Systems in the Cerebellum** The mRNA values were calculated by the $2^{-\Delta\Delta Ct}$ method using GAPDH as housekeeping gene and normalized to the values in the average of control group. **A.** The mitochondrial marker, COX4 mRNA expression. **B.** The expression level of the pro-apoptotic BAX mRNA. **C**. The anti-apoptotic BCL2 mRNA expression. **D.** The anti-apoptotic BCL2 mRNA expression. **D.** The BCL2 and BAX mRNA ratio. Abbreviations: BAX: gene of Bcl-2 associated X protein; BCL2: gene of B-cell leukaemia/lymphoma 2; COX4: gene of cytochrome c oxidase subunit 4.
Two-way ANOVA, Mixed effects analysis, Sidak's multiple comparisons test
Animals were sacrificed without testing (Naïve) n_C=4, $n_{3xTg-AD}$=4; **8-month-old male mice (Experimental Animal, Training)** n_C=10, $n_{3xTg-AD}$=10

Table 14. Apoptotic and Mitochondrial Markers in the Cerebellum.

		Genotype		Training		Genotype x Training interaction	
		F	p	F	p	F	p
mRNA by qPCR	**COX4**	$10.98_{(1,9)}$	0.009	$0.325_{(1,9)}$	0.582	$0.011_{(1,9)}$	0.918
	BAX	$4.306_{(1,9)}$	0.068	$50.32_{(1,9)}$	<0.001	$2.001_{(1,9)}$	0.191
	BCL2	$2.285_{(1,9)}$	0.165	$28.95_{(1,9)}$	<0.001	$0.532_{(1,9)}$	0.484
	BCL2-BAX	$1.163_{(1,9)}$	0.309	$40.11_{(1,9)}$	<0.001	$0.850_{(1,9)}$	0.381
Protein by Western blot	**COXIV**	$31.72_{(1,9)}$	<0.001	$1.089_{(1,9)}$	0.324	$3.632_{(1,9)}$	0.089
	BAX	$9.980_{(1,9)}$	0.012	$4.523_{(1,9)}$	0.0623	$1.120_{(1,9)}$	0.318
	cleaved Cas3	$4.266_{(1,9)}$	0.069	$21.67_{(1,9)}$	0.001	$2.577_{(1,9)}$	0.143
	proCas3	$18.95_{(1,9)}$	0.002	$0.357_{(1,9)}$	0.565	$0.865_{(1,9)}$	0.377
	Bcl-2	$0.453_{(1,9)}$	0.518	$0.857_{(1,9)}$	0.379	$0.378_{(1,9)}$	0.554

| | Bcl-2/BAX | $5.835_{(1,9)}$ | 0.039 | $8.710_{(1,9)}$ | 0.016 | $0.047_{(1,9)}$ | 0.833 |

This table contains the statistical data to the Figures 31,32. Degree of freedom is in brackets. Significant difference is marked as red. Abbreviations: COX4: gene of cytochrome c oxidase subunit 4 isoform 1; BAX: gene of Bcl-2 Associated X protein; BCL2: gene of B-cell leukaemia/lymphoma 2; COXIV: protein of cytochrome c oxidase subunit 4; BAX: Bcl-2 Associated X protein; cleaved Cas3: cleaved Caspase 3; proCas3: Procaspase 3; Bcl-2: B-cell leukaemia/lymphoma 2 protein.

As the mRNA levels might not necessarily reflect the produced protein amount, therefore we examined by Western blot the protein content as well. Similarly to the mRNA levels, the COXIV protein content in the cerebellum was notably higher in transgenic mice compared to control mice, and this disparity was unaffected by training (Figure 32B, Table 13.). Similar trends were observed in the levels of BAX protein, with higher levels in 3xTg-AD mice, and no discernible influence from training, which contrasted with the observation at mRNA level (Figure 32C, Table 14.). However, another pro-apoptotic protein, cleaved caspase-3, did not exhibit significant differences between genotypes, but was influenced by training (Figure 32E, Table 14.). Paradoxically, the level of the pro-caspase-3 enzyme protein was reduced in 3xTg-AD mice compared to control animals, with no observable training effect (Figure 32F, Table 14.). No alterations in the expression of the anti-apoptotic protein Bcl-2 were detected (Figure 32D, Table 14.). In the pro- and anti-apoptotic BAX/BCl-2 ratio the training has similar, increasing effect as at mRNA level (Figure 32G, Table 14.). However, at protein level, the 3xTg-AD mice had lower ratios than controls.
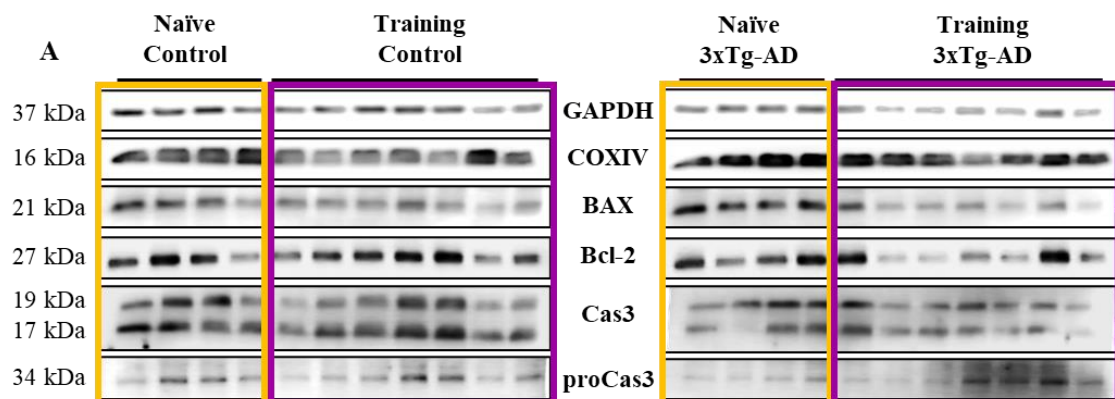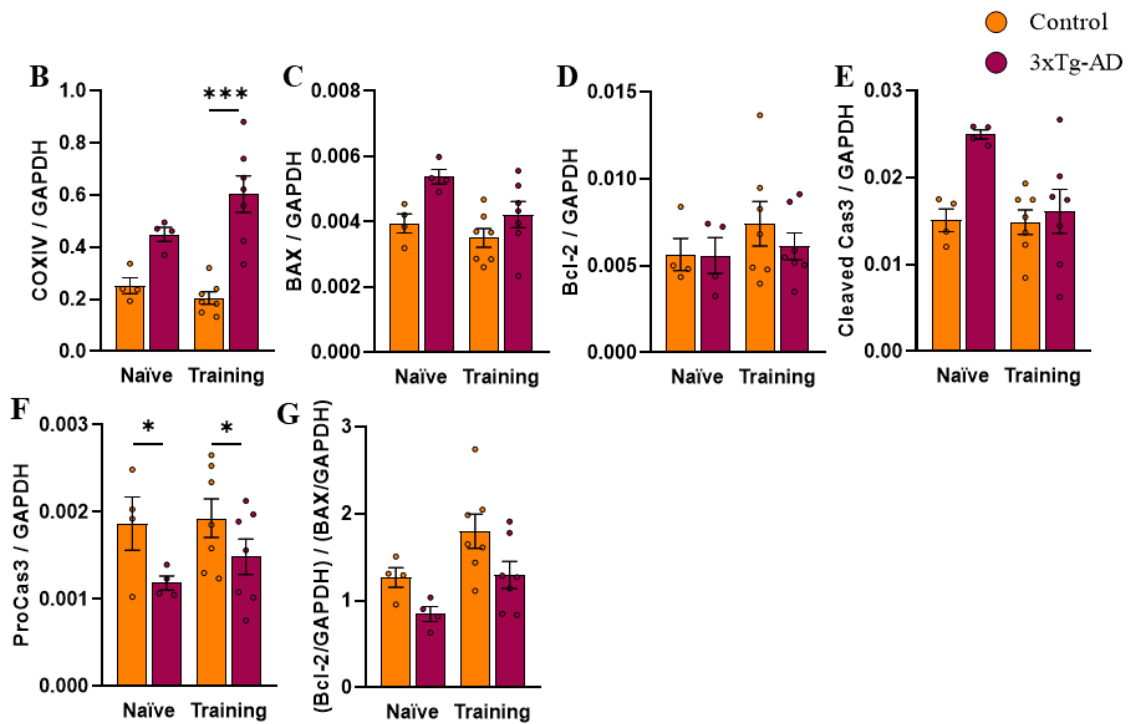
Figure 32. Protein Level Changes in the Mitochondrial Systems of the Cerebellum A. Representative Western blot analyses. The first column displays samples from control (Bl6) mice, while the second column shows samples from 3xTg-AD mice. Within each block, the first 4 bands represent samples from mice without training (naïve), and the last 7 bands represent samples from mice with training. The blots show the following proteins from top to bottom: GAPDH (37 kDa) as the housekeeping protein, COXIV (16 kDa), BAX (21 kDa), Bcl-2 (27 kDa), cleaved Cas3 (19 and 17 kDa) and proCas3 (34 kDa). The protein levels were expressed in comparison to the GAPDH. **B.** COXIV protein level. **C.** BAX protein levels. **D.** Bcl-2 protein level. **F.** proCas3 protein level. **G.** Bcl-2/BAX ratio. Abbreviations: GAPDH: glyceraldehyde-3-phosphate dehydrogenase protein; COXIV: protein of cytochrome c oxidase subunit 4; BAX: Bcl-2 Associated X protein; cleaved Cas3: cleaved Caspase-3; proCas3: Procaspase-3; Bcl-2: B-cell leukaemia/lymphoma 2 protein

Two-way ANOVA, Sidak's multiple comparisons test $*<0.5$, $**p<0.01$, $***p<0.001$ vs control.

Animals were sacrificed without testing (Naïve) $n_C=4$, $n_{3xTg-AD}=4$; **8-month-old male mice (Experimental Animal, Training)** $n_C=10$, $n_{3xTg-AD}=10$

IV. 3. Disrupted HPT Axis and Imbalance in MBH Neuropeptides as a Possible Underlying Mechanism of Metabolic Shifts

IV.3.1. Changes in body composition measured with MRI and Metabolic parameters in TSE PhenoMaster Metabolic Unit

Although we previously followed the body weight changes of one set of animals (see Figure 20), in this cohort we made a more detailed body composition analysis comparing not only the genotype, but also two age-groups, the 4- and 8-month-old male mice. In this series no differences were detected in body weight between 3xTg-AD and control mice, regardless of age (Figure 33A, Table 15.). However, a body weight increase was observed in both groups as they aged. However, although at 4-month there was no genotype effect in body fat or lean weight percentage, but at 8-month the 3xTg-AD animals had less fat and more lean mass than controls (Figure 33B, C, Table 15.). There was no genotypic difference in the hydration ratio, while, unsurprisingly, it increased with age, consistent with other examined parameters (Figure 33D, Table 15.).
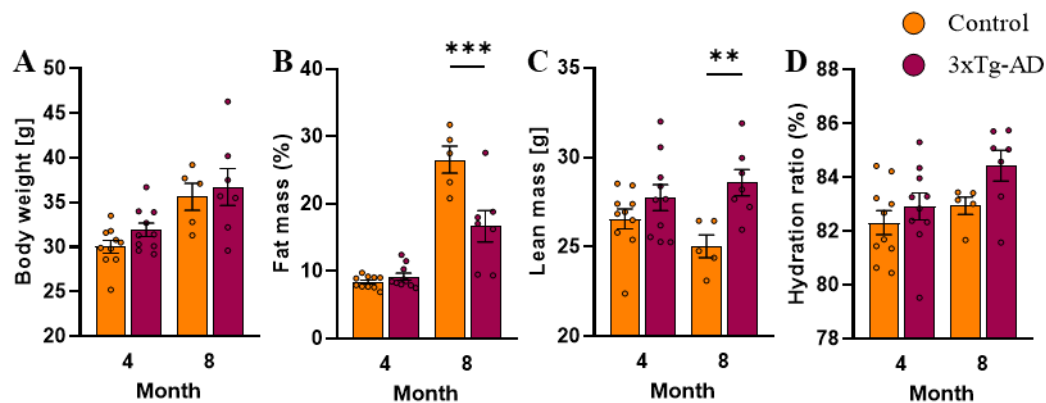
Figure 33. Body Composition by MRI. Body weight (A), Fat mass in percentage (B), lean mass (in g) as well as hydration ratio was measured in 4- and 8-month-old mice of both genotypes.
Two-way ANAOVA, Sidak's multiple comparisons test **p<0.01, ***p<0.001 vs control.
4-month-old male mice n_C=10; $n_{3xTg-AD}$=10, **8-month-old male mice** n_C=5; $n_{3xTg-AD}$=7

Table 15. Body Composition by MRI. Figure 33

Parameters	Genotype		Age		Genotype × Age	
	F	p	F	p	F	p
Bodyweight	$1.500_{(1,13)}$	0.242	$15.940_{(1,15)}$	0.001	$0.147_{(1,13)}$	0.707
Fat mass [%]	$12.44_{(1,28)}$	0.002	$98.68_{(1,28)}$	<0.001	$17.14_{(1,28)}$	<0.001
Lean mass [g]	$11.32_{(1,13)}$	0.005	$0.204_{(1,15)}$	0.658	$2.801_{(1,13)}$	0.118
Hydration ratio [%]	$4.038_{(1,28)}$	0.054	$4.23_{(1,28)}$	0.049	$0.728_{(1,28)}$	0.401

This table contains the statistical data to the Figures 33. Degree of freedom is in brackets. Significant differences are marked as red.

In the assessment of metabolic activity within the metabolic chambers, a characteristic diurnal pattern akin to that observed in rodents becomes apparent in both genotypes (Figure 34A-D; Table 16.). Rodents typically exhibit heightened activity during the dark phase of the night, juxtaposed with restfulness during the light phase of the day. Consequently, food intake decreases upon entering the light phase, coupled with augmentation upon entering the dark phase (Figure 34A). This temporal pattern is also mirrored by the corresponding water consumption (Figure 34B) as well as the RER (Figure 34C) and EE (Figure 34D). Nonetheless, it is worth noting that age-related and genotypic disparities have also been ascertained. Notably, substantial differentials have been discerned in the 3-hour resolution of food and water consumption and the RER values, both as a function of genotype and age, with a noteworthy interplay between the two factors (Figure 34A-C). The genotypic divergence becomes more pronounced with advancing age. This observation distinctly illustrates that 8-month-old transgenic mice evince a considerable augmentation in food and water consumption compared to age-matched control counterparts over a 24-hour period (Figure 34E, F). Paradoxically, this heightened consumption does not correspondingly translate to a significant influence on EE (Figure 34D). Rather, a discernible impact is observed solely in the confluence of temporal variation, age-related dynamics, and genotypic distinctions.

Legend: Control 4-month-old (orange square), Contol 8-month-old (yellow circle), 3xTg-AD 4-month-old (dark red square), 3xTg-AD 8-month-old (purple circle), Control (orange circle), 3xTg-AD (dark red circle)

A Food consumption — [g] vs 3 hours resolution

B Water consumption — [ml] vs 3 hours resolution

C Respiration Exchange Rate — vs 3 hours resolution

D Energy expenditure — [kCal/h/kg lean] vs 3 hours resolution

E Food consumption in 24 hours — [g] vs Month, ***

F Water consumption in 24 hours — [ml] vs Month, ***

Figure 34. Metabolic Parameters of 4- and 8-month-old Mice in PhenoMastre System Calo Cage. A-D. Both food and water intake, along with respiratory exchange ratio (RER) and energy expenditure values, exhibited the circadian rhythm characteristic of rodents, as showed in the 3-hour resolution monitoring. **E-F.** The same values were given for 24h as well. **C.** The RER values expressed in 3h bins.

Repeated measures ANOVA, Mixed effects analysis, Two-way ANOVA, Sidak's multiple comparisons test ***$p<0.001$ vs control.
4-month-old male mice $n_C=10$; $n_{3xTg-AD}=10$, **8-month-old male mice** $n_C=5$; $n_{3xTg-AD}=7$

Table 16. Metabolic Parameters of 4- and 8-month-old mice in PhenoMaster calo cage.

	Food consumption		Water consumption		RER		EE	
	F	**p**	**F**	**p**	**F**	**p**	**F**	**p**
Time	$15.29_{(7, 189)}$	<0.001	$20.89_{(7, 195)}$	<0.001	$29.60_{(7, 196)}$	<0.001	$64.08_{(7, 196)}$	<0.001
Age	$13.39_{(1, 27)}$	0.001	$5.044_{(1, 28)}$	0.033	$16.06_{(1, 28)}$	<0.001	$3.108_{(1, 28)}$	0.089
Genotype	$25.55_{(1, 27)}$	<0.001	$12.77_{(1, 28)}$	0.001	$6.031_{(1, 28)}$	0.021	$0.801_{(1, 28)}$	0.379
Time x Age	$0.872_{(7, 189)}$	0.530	$2.561_{(7, 195)}$	0.015	$2.617_{(7, 196)}$	0.013	$2.32_{(7, 196)}$	0.027

Time x Genotype	$1.298_{(7, 189)}$	0.253	$0.78_{(7, 195)}$	0.605	$0.778_{(7, 196)}$	0.607	$1.417_{(7, 196)}$	0.200
Age x Genotype	$7.837_{(1, 27)}$	0.009	$9.309_{(1, 28)}$	0.005	$10.65_{(1, 28)}$	0.003	$0.014_{(1, 28)}$	0.907
Time x Age x Genotype	$2.251_{(7, 189)}$	0.032	$2.35_{(7, 195)}$	0.025	$0.606_{(7, 196)}$	0.750	$2.476_{(7, 196)}$	0.019

This table contains the statistical data to the Figures 34. Degree of freedom is in brackets. Significant differences are marked as red. Abbreviations: RER: Respiratory Exchange Ratio; EE: Energy Expenditure

IV.3.2. Food-Motivated Behavioural Tests

As previous tests aimed to examine food motivated cognitive performance showed an even superior ability of 3xTg-AD mice to collect food (see Figure 25), we made a more detailed examination of food motivated behaviour. During the 5-day learning phase of the OCT, the total responses of the two groups showed no significant difference (Figure 35A, Table 17.). However, there were significant differences in values between the individual days. Interestingly, we not only found variations in reward preference between days but also observed that transgenic mice performed better during this cognitive test (Figure 35B, Table 17.).
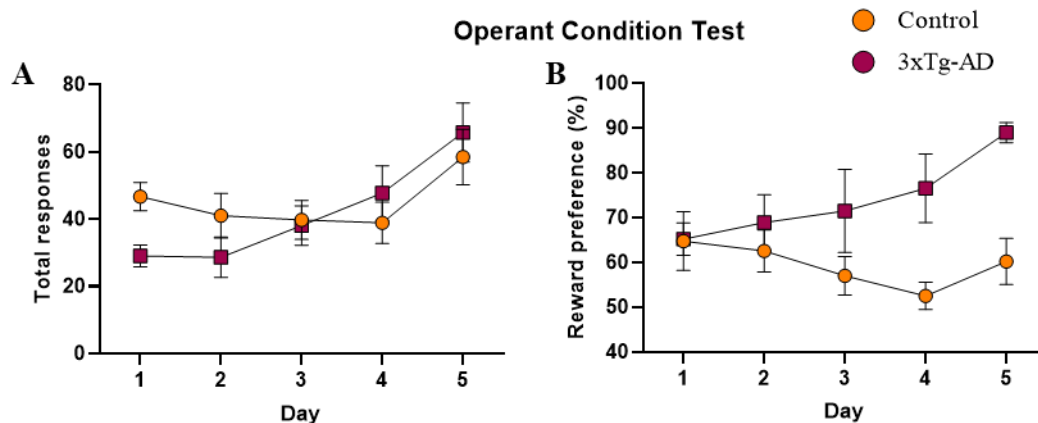
Figure 35. Food-Motivated Cognitive, Test Operant Condition Test. A. Total responses during 5 consecutive days in food restricted mice. **B.** Reward preferences.
Repeated measures ANOVA
6-month-old male mice $n_C=8$; $n_{3xTg-AD}=8$

Table 17. Food-Motivated Behavioural Tests.

Parameters	Genotype		Time		Genotype x Time	
	F	**p**	**F**	**p**	**F**	**p**
OCT Total response	$0.907_{(1,35)}$	0.348	$4.294_{(4,35)}$	0.006	$2.392_{(4,35)}$	0.069
OCT Reward preference	$16.13_{(1,35)}$	<0.001	$1.56_{(4,35)}$	0.206	$1.536_{(4,35)}$	0.213

Staircase test Duration of feeding (%)	$4.561_{(1,18)}$	0.047	$29.03_{(5,90)}$	<0.001	$4.999_{(5,90)}$	<0.001
Staircase test Number of collected rewards	$31.65_{(1,18)}$	0.001	$38.53_{(5,90)}$	0.001	$2.224_{(5,90)}$	0.059
RAM Number of collected rewards	$8.892_{(1,16)}$	0.008	$4.401_{(5,80)}$	0.001	$4.758_{(5,80)}$	<0.001

This table contains the statistical data to the Figures 35-37. Degree of freedom is in brackets. Significant differences are marked as red. Abbreviations: OCT: Operant Condition Test, SPRT: Single Pellet Reaching Test, RAM: Radial Arm Maze Test

We obtained more paradoxical results during the cognitive fine motor tests, particularly those presented in the "Motor Alterations During Different Behavioural Tests" section, specifically in the SPRT. (Figure 26A Table 8.) and the staircase test (Figure 36B, C, Table 17.). In the SPRT, the 7-day learning curves showed that both groups of animals increased the number of collected rewards as the days went by, with the 3xTg-AD mice demonstrating a significantly higher number of rewards collected (Figure 26A). On the last day, we also evaluated the time spent eating, which showed that the transgenic mice spent significantly more time eating during the test than the control group (Figure 36A, $t_{(16)}=3.923$; p=0.0012.). A similar pattern can be observed in the learning curve emerging during the staircase test (Figure 36B). With time, the number of
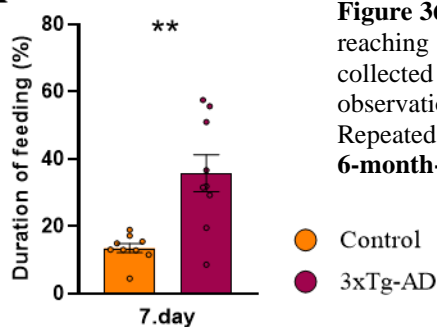
Figure 36. Food-Motivated Fine Motoric Tests. A. Single pellet reaching test (SPRT). **B.C.** Staircase test. **B**. The number of collected rewards. **A.C.** Duration of feeding in percent of the observation period.
Repeated measures ANOVA, Student's t-test **p<0.01 vs control.
6-month-old male mice $n_C=10$; $n_{3xTg-AD}=10$
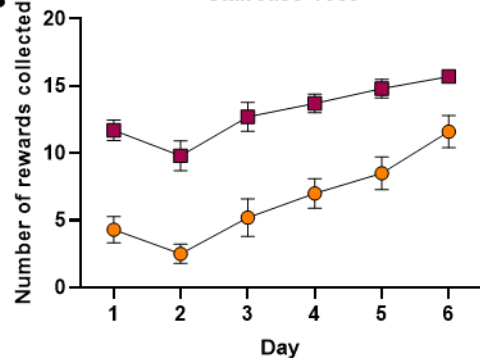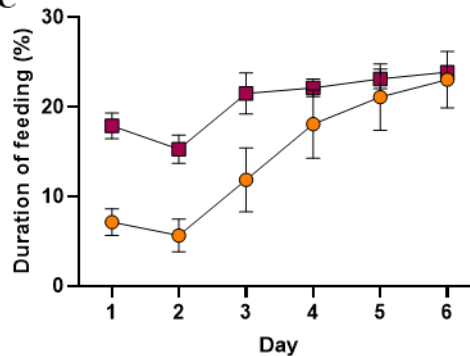
collected rewards increases in both groups, which was significantly higher in the case of transgenic mice. During the 6-day test, the time spent feeding also developed similarly, so it is not surprising that the 3xTg-AD mice spent more time eating (Figure 36C).

In the last food-motivated test, the RAM, the transgenic mice consumed all the pellets within 10 minutes on all 6 days, in contrast to the control group (Figure 37A, Table 17.). On the probe day, in the maze without pellets, there was no difference in the reward preference between the genotypes calculated from the frequency of visits to the previously rewarded / all arms (Figure 37B, $t_{(18)}=0.857$; $p=0.403$).
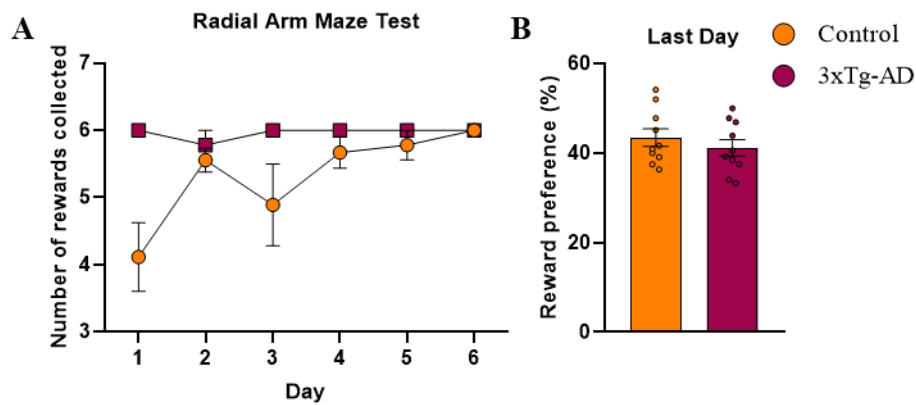
Figure 37. Food-Motivated Radial Arm Maze Test. A. The number of collected rewards and well as the **B.** reward preference on last, probe day is presented.
Repeated measures ANOVA, Student's t-test
6-month-old male mice $n_C=10$; $n_{3xTg-AD}=10$

IV.3.3. Blood Sugar and Other Parameters in the Blood

One week after the behavioural tests, there were no significant genotypic differences in the body weight of the 8-month-old animals (Figure 38A, Table 18.). However, the blood sugar level of the transgenic mice after 2 hours of starvation was lower compared to the control mice (Figure 38B, Table 18.), while there was no difference in the other parameters. Similar values were detected in the blood cholesterol (Figure 38C, Table 18.), triglyceride (Figure 38D, Table 18.), and uric acid levels (Figure 38E, Table 18.) in the two groups of animals.

Figure 38. Blood Sugar and Other Blood Parameters. These parameters measured by commercially available equipment and test strip after 2 hours of food deprivation, among rest.
Student's t-test ***p<0.001 vs control
8-month-old male mice Body weight, glucose, triglyceride $n_C=10$; $n_{3xTg-AD}=10$; cholesterol $n_C=7$; $n_{3xTg-AD}=10$; uric acid $n_C=10$; $n_{3xTg-AD}=7$
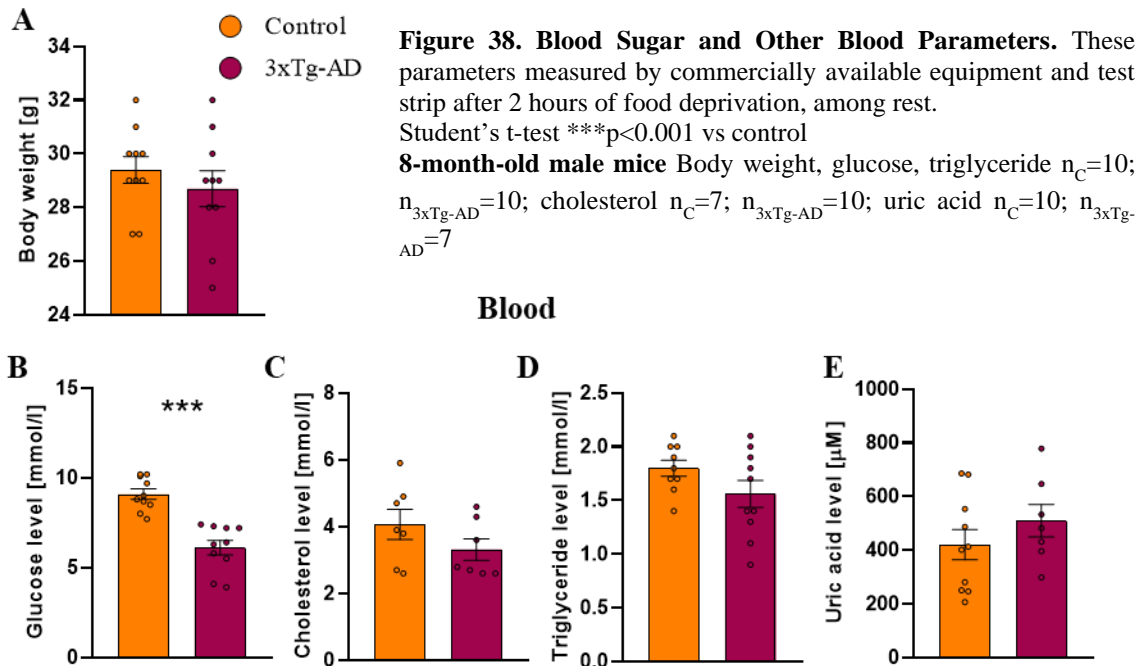
Table 18. Blood Sugar and Other Blood Parameters.

Parameters	Genotype	
	$t_{(df)}$	p
Body weight [g]	$0.840_{(18)}$	0.412
Glucose [mmol/l]	$5.955_{(18)}$	<0.001
Cholesterol [mmol/l]	$1.364_{(12)}$	0.198
Triglyceride [mmol/l]	$1.586_{(17)}$	0.131
Uric acid [µM]	$1.052_{(15)}$	0.310

This table contains the statistical data to the Figure 38. Degree of freedom is in brackets. Significant differences are marked as red.

IV.3.4. Main Factors of the Hypothalamic-Pituitary-Thyroid Axis

The level of fT4 measured in the serum was higher in the 3xTg-AD mice compared to the control group (Figure 39A, Table 19.), while there was no difference in the level of fT3 between the two groups (Figure 39B, Table 19.).

In the PVN, there was a significant increase in the expression of TRH mRNA (Figure 39C, Table 19.) and a significant decrease in the thyroid hormone receptor-β2 (TRβ2) mRNA level in the transgenic mice compared to the control group (Figure 39D, Table 19.).

On the other hand, in the pituitary, the TSHβ mRNA expression level did not change in the 3xTg-AD mice compared to the control mice (Figure 39E, Table 19.), while the expression of the TRβ2 receptor mRNA showed a significant decrease (Figure 39F, Table 19.), like the result obtained in the PVN.

In the MBH, where hypophysiotropic TRH-containing axons terminate, a decrease in TSH mRNA expression level can also be observed in transgenic mice compared to controls (Figure 39G, Table 19.). Additionally, the mRNA expression level of the thyroid transporter monocarboxylate transporter 8 (MCT8) was significantly reduced in the MBH area (Figure 39H, Table 19.).

Serum

Paraventricular Nucleus of the Hypothalamus

Pituitary Gland

Mediobasal hypothalamus

Figure 39. Main Factors in Hypothalamic-Pituitary-Thyroid Axis. A.-B. Serum content of fT4/fT3 measured by ELISA. **C.-H.** The mRNA values were calculated by the $2^{-\Delta\Delta Ct}$ method using GAPDH as housekeeping gene and normalized to the values in the average of control group. In the PVN, the TRH (**C.**) and TRβ2 receptor (**D**.) similarly in the pituitary gland TSHβ (**E.**) and TRβ2 receptor (**F**.) mRNA expression, while in the MBH beside the TSHβ (**G.**) level the thyroid transporter MCT8 were also measured. Abbreviations: AgRP: agouti-related peptide; fT4/fT3: serum free thyroxine/ triiodothyronine; MCT8: monocarboxylate transporter 8; TRH: thyrotropin-stimulating hormone, TRβ2 receptor: thyroid hormone β2 receptor; TSHβ: thyrotropin-stimulating hormone. Student's t-test, Mann-Whitney U test *p<0.05, **p<0.01, ***p<0.001 vs control.
8-month-old male mice fT4 n_C=10; $n_{3xTg-AD}$=10; fT3 n_C=9; $n_{3xTg-AD}$=8; **PVN** TRH n_C=6; $n_{3xTg-AD}$=6, TRβ2 n_C=7; $n_{3xTg-AD}$=7, **pituitary gland** TSHβ, TRβ2 n_C=10; $n_{3xTg-AD}$=10, **MBH** TSHβ, MCT8 n_C=7; $n_{3xTg-AD}$=7

Table 19. Main Factors of the Hypothalamic-Pituitary-Thyroid Axis and Food Intake Regulation

Parameters	Genotype	
	$t_{(df)}$	p
Serum		
fT4	$2.363_{(18)}$	0.030
fT3	$0.562_{(15)}$	0.583
Paraventricular Nucleus of Hypothalamus		
TRH	$4.787_{(10)}$	<0.001
TRβ2 receptor	$2.521_{(12)}$	0.027
Pituitary Gland		
TSHβ	$1.117_{(20)}$	0.277

TRβ2 receptor	$6.217_{(20)}$	<0.001
DIO1	$2.569_{(10)}$	0.028
DIO2	$3.320_{(10)}$	0.008
DIO3	$1.454_{(10)}$	0.177
Mediobasal hypothalamus		
DIO1	$1.393_{(10)}$	0.194
DIO2	$5.389_{(12)}$	<0.001
DIO3	$0.468_{(10)}$	0.650
TSHβ	$3.474_{(11)}$	0.005
MCT8	$4.198_{(10)}$	0.002
CART	$4.249_{(12)}$	0.001
POMC	$6.302_{(10)}$	<0.001
AgRP	$4.442_{(12)}$	<0.001
NPY	$6.622_{(11)}$	<0.001
(POMC+CART)-(AgRP+NPY)	$2.242_{(12)}$	0.045
MCHR	$0.158_{(12)}$	0.878

This table contains the statistical data to the Figure 39-41. The first two values represent the result of an ELISA measurement, while all other values are from a qPCR examination. Degree of freedom is in brackets. Significant differences are marked as red. Abbreviations: fT4: serum free thyroxine, fT3: serum free triiodothyronine, TRH: thyrotropin-stimulating hormone, TRβ2 receptor: thyroid hormone β2 receptor, TSHβ: thyrotropin-stimulating hormone, DIO1: deiodinase enzyme type 1, DIO2: deiodinase enzyme type 2, DIO3: deiodinase enzyme type 3, MCT8: monocarboxylate transporter 8, CART: cocaine and amphetamine-regulated transcript, POMC: proopiomelanocortin, AgRP: agouti-related peptide, NPY: neuropeptide Y, MCHR: melanin-concentrating hormone receptor

IV.3.5. Deiodinase System in the Pituitary and Mediobasal Hypothalamus

The mRNA expression levels of DIO enzymes, which play a fundamental role in the formation of local thyroid hormone levels, exhibited variations in the pituitary gland and MBH (Figure 40, Table 19.). In the pituitary gland, the levels of DIO mRNA expression for both type 1 and type 2 deiodinases were increased in the transgenic mice (Figure 40A, B). Although D1 has the capability to convert T4 to T3, this is not its primary function. Under normal physiological conditions, D2 predominates in the regulation of the HPT axis. However, in the MBH, we only found a significant difference in the type 2 DIO mRNA expression level without changes DIO1 (Figure 40D); surprisingly, in the AD mouse model, the expression of DIO2 gene was lower compared to the mRNA expression level of the control group (Figure 40E) In the case of type 3, the inactivating

DIO enzyme, similar mRNA expression levels were detected in the two genotypes (Figure 40C, F).
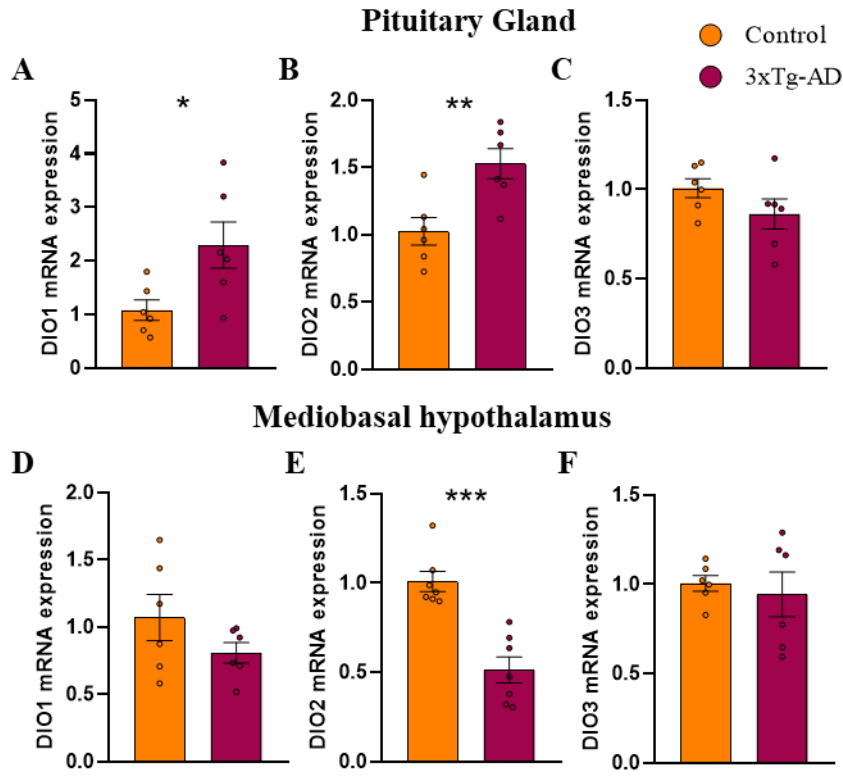

Figure 40. mRNA Expression Levels of Deiodinase Enzymes. The mRNA values were calculated by the $2^{-\Delta\Delta Ct}$ method using GAPDH as housekeeping gene and normalized to the values in the average of control group. **A-C.** In the pituitary gland, the DIO1, DIO2, and DIO3 **D-F.** similarly in the mediobasal hypothalamus the DIO1, DIO2 and DIO3 mRNA expression also measured. Abbreviation: DIO: deiodinase enzyme type 1, 2 and 3.
Student's t-test, Mann-Whitney U test $*p<0.05$, $**p<0.01$, $***p<0.001$ vs control.
8-month-old male mice $n_C=6\text{-}7$; $n_{3xTg\text{-}AD}=6\text{-}7$

IV.3.6. Development of Genes Regulating Nutrient Uptake in the MBH

After studying the HPT axis, we also mapped the mRNA expression pattern of genes regulating food intake (POMC; CART; NPY; AgRP) in the MBH (Figure 41A-E, Table 18.). The mRNA expression level of each tested gene was significantly lower in the AD mouse model than in the controls (Figure 41A-D). When we tried to summarize the actual effect extracting the sum of the orexigenic AgRP-NPY levels from the anorexigenic POMC-CART gene expression levels, however, it becomes evident that the ratio of food intake inhibiting hormones is lower in transgenic than control mice (Figure 41E, Table 19.).

The melanin-concentrating hormone receptor (MCHR) is another key player in regulating food intake. The mRNA expression level of these genes did not differ between the two groups (Figure 41F).
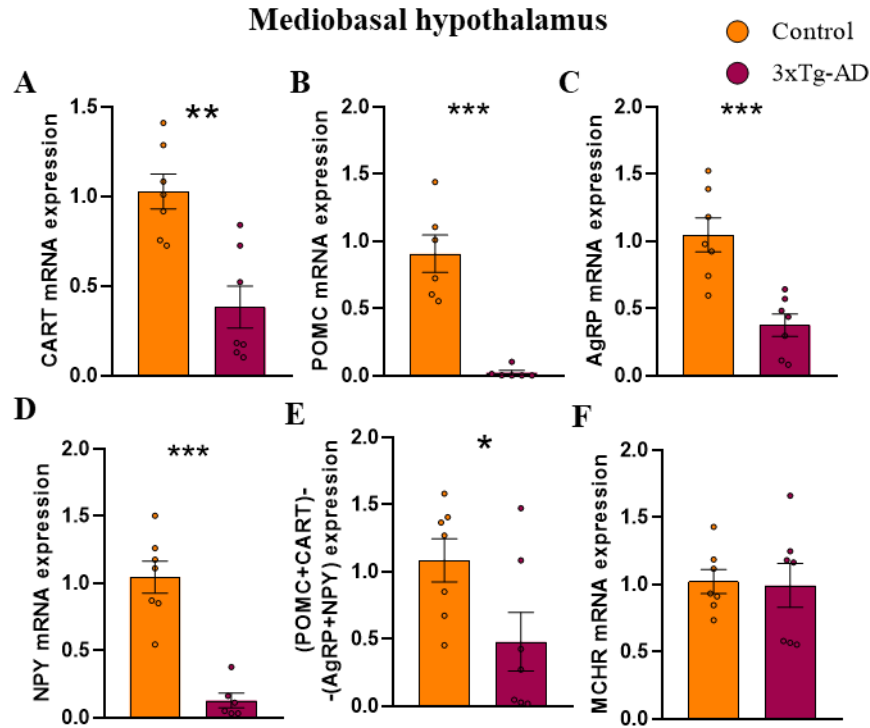

Figure 41. Genes Regulating Nutrient Uptake in the Mediobasal Hypothalamus. The mRNA values were calculated by the $2^{-\Delta\Delta Ct}$ method using GAPDH as housekeeping gene and normalized to the values in the average of control group. The anorexigenic CART (**A.**) and POMC (**B**.) as well as the orexigenic AgRP (**C**.) and NPY (**D.**) were measured by qPCR, similarly to the MCHR (**F**.), while a difference between food intake inhibitory and stimulatory factors were calculated (**E**.). Abbreviations: CART: cocaine and amphetamine-regulated transcript, POMC: proopiomelanocortin, AgRP: agouti-related peptide, NPY: neuropeptide Y, MCHR: melanin-concentrating hormone receptor.
Student's t-test, Mann-Whitney U test *p<0.05, **p<0.01, ***p<0.001 vs control.
Male mice 8M n_C=6-7; $n_{3xTg-AD}$=6-7

The interactions between the orexigenic and anorexigenic outputs of the ARC and the HPT axis are strong (73). Therefore, we examined the correlation between the mRNA levels of TRH and the measured peptides using Pearson correlation analysis. However, significant correlation was found only between TRH mRNA and AgRP mRNA levels in 3xTg-AD mice (r = 0.982, p < 0.001); the other results are not presented. Thus, mRNA expression levels did not provide insight into the strength of this interaction. This indicates that mRNA expression alone does not fully capture the complexity of the regulatory mechanisms involving hypophysiotropic TRH neurons and their orexigenic and anorexigenic inputs.

V. Discussion

V.1. Temporal Emergence of Increased Innate Anxiety

Our data shed light on the intricate relationship between anxiety-like behaviours, AD-related pathological changes, and olfaction in 3xTg-AD mice. Notably, increased innate anxiety emerged as early as two months of age in these mice (Figure 16), aligning with human studies that propose anxiety as a potential prodromal symptom for symptomatic AD. This early onset of anxiety coincided with the appearance of Aβ and p-tau pathology in brain regions associated with emotional processing, particularly the amygdala (Figure 22H, N). This pathological accumulation of misfolded proteins could contribute to early synaptic disturbances, potentially leading to anxiety-like symptoms in these mice. Conversely, early anxiety might also accelerate the development of AD pathology leading to a vicious circle. Therefore, it was not surprising that at 12 months of age we detected a higher prevalence of deposits, both Aβ and p-tau, compared to two-month-old mice (Figure 22). Nevertheless, the precise nature of the relationship between Aβ, p-tau and anxiety require further investigation.

In line with our hypothesis, there was a transient period with reduced anxiety-like behaviour in 3xTg-AD mice, occurring approximately around six months of age (Figure 13, 14, 15). This could be attributed to an early increase in synaptic transmission in 3xTg-AD mice (260-262), followed by a subsequent decline in older age (260, 263). These changes might lead to a temporal alleviation of symptoms during this intermediate phase.

It is evident that the influence of fox odour on mouse behaviour is mediated primarily through the olfactory system, as demonstrated by studies involving transient receptor potential ankyrin 1 knockout mice lacking this receptor in their olfactory system, which did not exhibit avoidance of the fox odour (306). Notably, human studies have suggested that olfactory loss may predict the onset of subsequent dementia (308, 309) and may contribute to cognitive decline (310). Similarly, various animal models of AD, including 3xTg-AD mice, have displayed olfactory deficits (311, 312). However, it is essential to consider that evaluating olfaction through tasks involving the finding of buried food can be confounded by metabolic and motivational factors, which are known to be altered in 3xTg-AD mice (313). Moreover, olfactory function can be influenced by sexual drive, leading to sex-related differences in olfactory performance (312). Interestingly, one study reported in 3xTg-AD mice an age-related decline in finding the

buried food, but this was observed solely in female mice (311). Furthermore, olfaction-related deficits in discriminating between different odours were only evident in 1.5-year-old 3xTg-AD females, but not in one-year-old ones (312). Remarkably, peanut butter seemed to be more attractive to 3xTg-AD animals than to their control counterparts, while their response to peppermint, a repellent odour, remained unchanged (314). Nevertheless, in one-year-old 3xTg-AD animals, PET scans detected hypometabolism in brain areas relevant to olfaction, such as the piriform cortex (315). Our immunohistochemical data supported these findings, confirming the presence of both Aβ and pTau (Figure 22) in these olfactory regions, including the olfactory bulb and piriform cortex. Furthermore, in another model involving double-transgenic AD mice, Aβ plaque burden in the olfactory bulb was detectable as early as four months of age. However, behavioural alterations, such as reduced avoidance of the trimethylthiazoline (TMT) component of fox odour, were only noticeable in 8-month-old mice, not in 4-month-old ones (316). Collectively, although pathological changes and altered olfactory behaviours are apparent in aged 3xTg-AD mice, it becomes evident that olfactory deficits alone cannot account for the increased avoidance response to predator odour, as we might expect reduced avoidance even in 18-month-old animals if olfactory loss were the sole explanatory factor. This intricate interplay between anxiety, AD pathology, and olfaction underscores the multifaceted nature of AD and the need for further research to unravel its complexities.

We consistently observed reduced mobility in these 3xTg-AD mice during both fox odor exposure and OFT, regardless of sexes (Figure 18, 19). This finding aligns with previous research, which documented significant decreases in movement at 3, 9, and 12 months of age in 3xTg-AD mice, while no notable differences were observed at 6 months (244). This pattern was further substantiated by additional studies, confirming the absence of genotype differences in 6-month-old animals (240, 317). One plausible explanation for this phenomenon is the potential temporary reduction in synaptic dysfunction within this specific age group. In line with our observations, a different AD model involving the conditional knockout of the membrane protein seizure 6-like (SEZ6L), a neuronal substrate of the AD protease BACE1, also exhibited decreased motor-coordination. While the loss of fine and even gross motor skills can potentially serve as early signs of AD (318, 319), we hypothesized that the diminished locomotion observed in our 3xTg-AD mice is primarily a consequence of increased innate anxiety, particularly in response to

bright, open environments (320). This is supported by our subsequent studies when the animals were more motivated to move for food (positive reinforcement on RAM) or to avoid water (in MWM) (Figure 25). Typically, a decline in locomotion occurs within the first minute of prolonged OFTs (321). Several factors could account for this initial drop, ranging from the novelty and surprise of the situation to the presence of an unfamiliar experimenter. Notably, our animals were repeatedly tested by the same experimenter, which likely reduced the initial discomfort associated with the test, thus preventing a significant decrease in distance travelled (Figure 18). Nevertheless, the genotype difference in mobility persisted throughout the entire 30-minute observation period, highlighting the intrinsic nature of anxiety induced by bright, open spaces in 3xTg-AD mice (Figure 21). During a 30-minute observation period the anxiety typically reduces as can be seen by the gradually increased time spent in the centrum for control mice (Figure 21). However, in 3xTg-AD mice such timely anxiolysis could not be observed, most probably masked by reduced locomotion.

As for sex difference after the 6-month transient period the 3xTg-AD females exhibited increased fear responses to both predator odour and open spaces compared to males. In humans, women typically exhibit higher levels of anxiety (322), and their emotional state can significantly influence cognitive capabilities (323). This female prone prevalence of anxiety was more pronounced in our older animals, suggesting that typical sex differences in anxiety-related behaviour may progressively develop over time.

Lastly, our analysis of the relationship between body weight changes and behaviour unveiled interesting sex-specific connections (Figure18, 19, 20). For males, we did not find any significant correlations between body weight changes and mobility or anxiety-related behaviours. In contrast, heavier control females moved less in OFT than the lighter ones. Additionally, heavier 3xTg-AD females spent less time in the central, exposed area of the arena than the lighter ones.

A consistent finding across these studies is the reduced mobility observed in 3xTg-AD mice, especially in response to anxiogenic situations and bright, open environments. This reduced mobility is not attributed to motor problems (see RAM and MWM), but is likely a consequence of increased innate anxiety, as it can be alleviated by positive or negative motivation and familiarization with the testing environment.

V.2. Musculoskeletal and Cerebellar Changes in the Context of Motor Alterations

As we repeatedly observed locomotor impairment in our 3xTg-AD mice strain we decided to make an in-depth analysis both at behavioural as well as at molecular level. Here we concentrated on the transient phase using involving 6-month-old 3xTg-AD mice with to hope to reveal early signs and examined only males to avoid any confounding factors due to cyclic changes.

First, in the OFT, we confirmed the clear motor impairment (Figure 24A, B) (324). However, as mentioned before, this impairment proved to be malleable when we introduced various forms of motivation. Positive motivation, like food rewards in the RAM (Figure 25B), and negative motivation, such as avoiding water in the MWM (Figure 25C), effectively mitigated this impairment. This supports the notion that this hypolocomotion is not due to motor problems but may be a sign of enhanced anxiety (294). Indeed, when the mice were habituated to the experimenter and the changing environment, the locomotor impairment disappeared (Figure 24C). It may seem contradictory that when the 3xTg-AD mice had to work for food (RAM, SPRT, Staircase), they performed better in learning tasks than the controls (RAM: more distance travelled representing more searching (Figure 25B), SPRT: more collected pellets (Figure 26A), staircase: more time spent trying (Figure 26B), higher success rate (Figure 26C)). Some studies have reported working memory deficits during RAM tests in 14 and 18-month-old 3xTg-AD mice when the animals had to work for water reward (325). Another study also reported working and reference memory errors related to food reward, but they used female mice (no report on age) and a prolonged examination period (not clear which day from the 10 is presented) (326). Injection of Aβ into the brain results in memory deficits in RAM (327-330). Moreover, the APP mutant 6-month-old male TgCRND8 mice also showed working and reference memory deficits in RAM, but they were also moving more than controls despite reduced locomotion in OFT, further supporting enhanced food drive (331, 332). However, another study using 4-month-old male Swedish APP mutant mice reported working and reference memory errors with more time needed for food consumption (333). Based on these results, we might assume that not the APP mutation but rather the tau (MAPT P301L) pathology or other functions of PSEN1, such as Notch signalling, β-cadherin processing, and calcium metabolism (334), might be

responsible for enhanced metabolism in our mice, which is undoubtedly an important part of AD pathology (see AD as type 3 diabetes mellitus (335)). To unravel the details of this metabolic connection we conducted a further experimental series (details see there).

Nevertheless, despite superior skills in food-motivated tests, 3xTg-AD mice spent more time trying to catch the food, suggesting some impairment in fine motor abilities as can be expected based upon human studies (336). Thus, our strain is suitable for testing this prodromal sign.

Picrosirius staining under polarized light was utilized to examine the orientation and thickness of collagen fibres, with thicker fibres appearing red and thinner fibres green. DMMB staining was employed to visualize the glycosaminoglycan content, displaying normal metachromasia. These staining techniques provided a detailed analysis of the joint structures. The normal, everyday home cage movement was further supported by the absence of differences in the collagen fibre orientation and thickness in the knee and foot joints between the two groups, indicating similar mechanical loading (Figures 27, 28).

However, muscle strength of 3xTg-AD mice was lower than the controls (Figure 23A, B), without motor-coordination problems observed in the rotarod test (Figure 23C). The impaired grip strength is consistent with previous findings in 6-month-old male and female 3xTg-AD mice (337), as well as with a recent study showing muscle atrophy and cognitive impairment in APP/PS1 mice, accompanied by decreased myostatin levels (98). Myostatin is a growth and differentiation factor that acts as a negative regulator of muscle mass (99) (Figure 3). Inhibition of myostatin is a potentially important mechanism in the treatment of diseases accompanied by muscular atrophy and degeneration, such as muscular dystrophy (338). One of the best-known endogenous inhibitory factors of myostatin is follistatin, the increase of which can increase muscle size and strength (339). However, in our model, the myostatin-follistatin system does not seem to be altered (Figure 29). Moreover, contrary to our expectation, training decreased, rather than increased follistatin levels, leading to an enhanced myostatin/follistatin ratio in the gastrocnemius muscle (Figure 29). Previous reports in humans showed that training might increase follistatin and decrease myostatin levels (340), but the molecules were measured in the blood, not directly in the muscle, and these changes were mostly found after resistance training (341). Interestingly, a stronger relationship was found between these proteins and muscle power, rather than muscle strength (342). Moreover, these proteins

are strongly associated with metabolism as well, as myostatin injection can induce cachexia (343), while follistatin may attenuate fat accumulation and improve insulin resistance (344). As our "training" included restricted diet, we might assume that the effect of lower calorie intake was more pronounced than the effect of repeated testing, which was far from being exhaustive resistance training. In support, in wrestlers, rapid weight loss decreased follistatin and increased myostatin-to-follistatin ratio, similar to our observation (345). All in all, the myostatin/follistatin ratio does not seem to explain the reduced muscle strength of 3xTg-AD mice; therefore, we focused on mitochondria and apoptosis.

Although in the gastrocnemius muscle the mRNA levels of the antiapoptotic BCL2 as well as pro-apoptotic BAX was not influenced by the genotype or training, their ratio, the BCL2/BAX, reflecting an antiapoptotic state, was increased by the training without genotype effect (Figure 30D). However, it still could not provide an explanation for the reduced muscle strength of the 3xTg-AD mice. In the cerebellum the antiapoptotic ration showed similar changes, but training had more profound effect as decreased pro- and increased anti-apoptotic levels were already detected when BAX and BCL2 were studied separately (Figure 31). Moreover, at protein levels not only the training had positive effect, but we also detected the negative impact of the AD-like genotype. Namely, the 3xTg-AD animals had lower Bcl-2/BAX ratio without an interaction with the training (Figure 32). In support, 6-month-old Thy-1 APP mice had also reduced anti- and pro-apoptotic factor ratios (Bcl-xL/BAX) in their cerebellum (152). Moreover, in our study, the downstream executioner apoptotic protein caspase-3 level was also elevated in the 3xTg-AD animals (Figure 32). Similarly, the hippocampus of 6- (346), 12- (347), as well as 15-month-old (348) 3xTg-AD mice showed higher BAX and caspase-3, while lower Bcl-2 levels. However, no such changes were detected in their cortex (349).

The anti-apoptotic shift in the Bcl-2/BAX ratio to training suggests that training may confer a degree of protection against apoptosis in the cerebellum. Indeed, training has been repeatedly confirmed to be beneficial in AD (350-352). Among other things, exercise can reduce the incidence of AD-related neuropathological burden and cognitive decline (353) and has even been reported to reduce plasma tau and Aβ levels (354). In a recently published study it was shown that long-term exercise has an effect on the development of fibrotic changes in the kidney, can restore the balance of renal function,

and induce increased clearance of systemic Aβ in AD (355). These results suggest that training exerts its protective effect not only in the central nervous system but also in the peripheral system during the progression of AD.

Nevertheless, cerebellar dysfunctions receive increasing attention in AD (273), as the cerebellum is important in organizing the motor functions (356). However, based upon molecular changes we have expected reduced performance of 3xTg-AD mice on the rotarod rather than grip test. As rotarod performance might be deeply influenced by the weight of the animals (see sex difference in (337)) we could have expected worse performance in our heavier 3xTg-AD animals solemnly based upon this fact (324). Indeed, in another AD model, the swe/PS1dE9 mice, high APP soluble Aβ oligomer levels were measured in the cerebellum, accompanied by balance and motor-coordination problems during the rotarod test already at 3 months of age, before the appearance of Aβ plaques (267). In contrast, several other AD mice models failed to show impaired motor-coordination in the rotarod test (see (356); M: month-old; 5M J20, 5-9-12M Tg2576, 2M APP23, 4-7-8-12M APP/PS1, 7-11-15-24M APP/PS1KI, 3-6-9M 5xFAD). Moreover, several other studies found even better rotarod performance of 3xTg-AD mice than their controls (2-6-9-12-15M (357), 6M (337), 12-14M (358), 16M (359)) in both sexes, suggested to be linked to the P301L transgene. Although the details of the rotarod test might be slightly different between laboratories, the previously mentioned studies suggest that there is no clear motor-coordination deficit in the 3xTg-AD animals. Indeed, the increase in the COXIV mitochondrial protein levels in the cerebellum of 3xTg-AD animals (Figure 32B), suggesting a better mitochondrial function, might have compensated for the enhanced apoptosis, leading to normal motor balance (Figure 23C, D). There is growing evidence that mitochondrial abnormalities are present in the early stages of AD (151, 360, 361), and that intervention at the mitochondrial level may improve AD-induced dysfunction and degeneration (362, 363). Already in 3-month-old Thy-1 APP mice, reduced mitochondrial membrane potential and ATP synthesis were detected in the cerebellum prior to plaque formation, while in 6-month-old mice, reduced mitochondrial complex IV activity was also detected by direct activity assay (152).

All in all, we could not detect major motor problems in the 3xTg-AD animals, confirming our hypothesis that their hypolocomotion might be linked to enhanced anxiety rather than inherent motor problems. Moreover, the intriguing performance of 3xTg-AD

mice in food-motivated tests, despite reduced muscle strength, hinted at complex connections between metabolism, memory, and motor abilities, which warrant further investigation.

V. 3. Disrupted HPT Axis and Imbalance in MBH Neuropeptides as a Possible Underlying Mechanism of Metabolic Shifts

As a general reflection of the metabolism, first we investigated the timely changes in body weight and composition comparing 4- and 8-month-old control and 3xTg-AD animals, before and after the transitory age (i.e. 6-month). Once again, we studied only males to reveal insights into the interplay of aging and genetic factors without confounding sex effects (364). While in this series no discernible differences were observed in body weight across genotypes, the observed increase in body weight with age underscores a common, natural physiological trend (Figure 33A). Notably, in our other studies on older male mice the 3xTg-AD mice were always heavier than the age-matched controls (10-month-old male mice n_C=37; $n_{3xTg-AD}$=36, $t_{(df)}$=8.490$_{(71)}$, $p<0.001***$). Nevertheless, the fat mass also increased with aging (Figure 33B) without changes in the lean mass (Figure 33C). This aligns with the anticipated age-related changes in adipose tissue accumulation (365). These observations are in line with the expected age-related shifts in hydration dynamics, as indicated by the consistent increment in hydration ratio with age (Figure 33D). However, at the 8-month transgenic mice had significantly lower body fat compared to control mice, highlighting the potential role of AD-related genetic factors in adipose tissue regulation. Moreover, the increased lean mass observed in transgenic mice at 8-month underscores the complexity of genotype-specific muscle mass regulation (Figure 33C).

Next, we elucidated the dynamics of the metabolic parameters measured in the metabolic cage (Figure 34). Importantly, the circadian rhythm of our mice were normal, because the relevant parameters showed the typical diurnal changes and the mice consumed two-thirds of their total food intake during the night (366). In line with the increased lean body mass of the 8-month-old 3xTg-AD animals they also showed increased food and water intake compared to the control group, which was not visible at 4-month (Figure 34E, F). Our findings align with a study showing a significant correlation between meal size, daily energy intake, and fat-free mass, highlighting the increased energy requirements of lean mass compared to adipose tissue (367, 368).

The RER is the ratio between the volume of CO_2 being produced by the body and the amount of O_2 being consumed. It gives us an indication as to whether the body is operating aerobically or anaerobically (Figure 34C) (369, 370). A ratio closer to 1 indicates predominantly glucose metabolism, whereas a ratio closer to 0.7 suggests reliance on fatty acid metabolism (371, 372). Both advancing age and the presence of AD-like genetic disorders amplify the variations in RER (Figure 34C), thereby exacerbating differences in body composition (Figure 33). While control animals transitioned from glucose to fatty acid metabolism with age, transgenic animals maintained a consistent glucose metabolism pattern. These genotype-related differences intensify with age, notably affecting body composition. Specifically, at 8 months, control mice exhibited higher body fat content and lower lean mass compared to transgenic counterparts, underscoring the impact of metabolic changes on physiological outcomes. In spite of the anticipated age-related reduction in EE (373, 374), our experiments did not reveal a significant genotype-related decrease in energy expenditure; rather, we observed a tendency for changes with age (Table 16.). This phenomenon might contribute to the observed increase in both the body weight and body fat percentage in 8-month-old animals compared to 4-month-old ones (Figure 33A, B) (375). Moreover, although the older 3xTg-AD mice continuously consumed more, their highest consumption values were reached during the dark, active phase, as well as at the beginning and end of the light phase, which may contribute to their food craving behaviour.

Indeed, paradoxically, the 6-month-old 3xTg-AD mice exhibited superior performance in food-motivated behavioural tests when compared to age-matched control mice (Figure 26, 35-37) as described before (see IV.2.1 fourth paragraph, IV.3.2. paragraphs). Notably, on the final day of SPRT and during all days of the staircase test, the transgenic mice spent significantly more time feeding, indicative of a substantial food drive (Figure 36A). Typically, these tests (lasting 14 days for SPRT (298) and 15 days for staircase test (299)) are conducted over extended periods, but due to the elevated motivational drive exhibited by the transgenic mice, our experiments were finished prematurely. This observation is further supported by the fact that during the RAM test the 3xTg-AD mice swiftly consumed all pellets on the initial day (Figure 37A), but there was no disparity in the superior preference of the correct arms visits between the two groups even not on the last day, suggesting that they did not learn the correct arms but

rather responded to the incentive of earning food (Figure 37B). The decline in blood sugar levels presents a potential contributing factor to the increased food demand observed in transgenic mice (Figure 38B) (376, 377).

This proposition gains further substantiation through the altered mRNA expression pattern detected within the HPT axis. Typically, an increase in serum fT4 concentrations (Figure 39A) would lead to a significant reduction in TRH mRNA levels in the PVN due to negative feedback (378). However, our observations deviate from this norm, as TRH mRNA levels were significantly higher in 3xTg-AD animals (Figure 39C). It is important to note that not all TRH neurons in the PVN are involved in HPT regulation (379). Using the microdissection technique, non-hypophysiotropic TRH neurons are also included in the sample. Assuming this error factor is uniform across individuals in each group, and that an active protein is formed, it could lead to higher TRH levels in transgenic mice. This anomaly might find its elucidation in the downregulation of TRβ2 mRNA levels (Figure 39D), ultimately resulting in a diminished thyroid hormone impact within the PVN. Notably, the higher TRH mRNA level does not manifest in the expression of pituitary TSH mRNA (Figure 39E). However, the increase in peripheral fT4 levels reduced the TRβ2 receptor expression in transgenic mice within this context as well (Figure 39F). The complex relationship between cognitive functions and the HPT axis is underlined by prior research where thyroxine treatment in a sporadic AD mouse model enhanced cognitive functions (282). Additionally, recent findings reported an amelioration of depression-like behaviour resulting from T3 treatment in the 3xTg-AD male mouse model we employed (283). Thus, the observed elevation in fT4 levels might even be compensatory and might mask the cognitive decline in our 3xTg-AD animals.

The picture is further clarified by considering the levels of DIO enzymes (380), which strengthen the T4-T3 conversion in the pituitary gland. Although changes in mRNA levels do not necessarily indicate changes in biological function, this is especially true for DIO2. The activity of DIO2 is primarily regulated by the ubiquitination-deubiquitination balance, a reversible post-translational mechanism. This poses a significant challenge for interpreting DIO2 mRNA measurements. One study has shown that there are tissue-specific differences in DIO2 ubiquitination, with relatively lower levels observed in the hypothalamus (381). However, DIO2 mRNA levels were elevated in our experiments (Figures 39A, B). If this increase translates to the active form of the

enzyme, it could enhance negative feedback and compensate for the elevated TRH mRNA levels (Figure 39C). The reduced DIO2 mRNA expression in the MBH (Figure 40E) further suggests a lower likelihood of it becoming an active enzyme. Despite these challenges, there are clear alterations in the HPT axis that might contribute to increased food cravings, particularly given the elevated fT4 levels.

Furthermore, the MBH, a pivotal brain region crucial for maintaining energy homeostasis, harbours genes responsible for regulating nutrient uptake and energy balance, often linked to metabolic irregularities (382, 383). In view of this, alongside our exploration of the HPT axis, we expanded our investigation to encompass the mRNA expression profile of genes governing the intricate regulation of food intake within the MBH (Figure 41). It is noteworthy to mention that the mRNA expression levels of each investigated gene were markedly diminished within the 3Tg-AD mouse model when compared to the control group (Figure 41A-D). The comprehensive evaluation of these gene expressions revealed that in transgenic mice the balance is shifted towards orexigenic peptides (Figure 41E). These changes might further strengthen the drive for food search in our animal model and may indicate that dysregulation of these genes in the MBH could contribute to AD pathology, although the exact mechanisms remain to be fully elucidated.

V. 4. Limitations of the Thesis

The mouse model, despite its widespread use in scientific research, does not always accurately represent human disorders. AD, particularly, is not characteristic of mice, making it necessary to use different models to study the disease. SAD cannot be tracked in mice, so researchers employ transgenic mouse strains carrying human gene mutations associated with fAD, which accounts for less than 5% of all AD cases (3, 4).

The commonly used control mouse, C57Bl6 (384), differs from the 3xTg-AD model because it lacks the same genetic cassette found in the transgenic mice. Recently, the Institute of Experimental Medicine (Budapest, Hungary) developed an improved control strain that incorporates the same genetic cassette as the transgenic mice, providing a more accurate comparison; however, testing of this new strain is still in progress.

Furthermore, the small sample size of mice limits the examination of the complex systems involved in AD progression.

Another significant challenge in this research is the reliance on qPCR for quantifying mRNA levels, which do not always correlate directly with protein abundance. This discrepancy arises from various post-translational modifications and regulatory mechanisms that influence protein function and stability (385). Factors such as the rate of translation, influenced by mRNA sequence features, the activity of regulatory elements like miRNAs and other non-coding RNAs, ribosome availability, and protein degradation rates all contribute to this complexity (386). These factors are highly dynamic and often specific to particular proteins, making it difficult to develop predictive models that accurately correlate transcript and protein levels. Therefore, while qPCR provides valuable insights into transcriptome dynamics, it is insufficient alone for capturing the organism's current physiological state.

VI. Conclusion

We have explored three interrelated topics that shed light on various aspects of AD progression in the 3xTg-AD mouse model. The following conclusions can be drawn:

1. 3xTg-AD mice exhibited **higher innate anxiety** (fear from fox odor and open spaces) than controls **at a young age**, without significant sex differences, indicating early signs of anxiety-related comorbidity.

2. Increased innate anxiety emerged as early as **two months, coinciding with Aβ and p-tau pathology** in emotional brain regions, suggesting a **link between early anxiety and AD progression.**

3. A **transient period of reduced anxiety-like behaviour** was noted around six months, possibly due to early increases in synaptic transmission followed by declines with age.

4. **Altered olfactory perception** in 3xTg-AD mice suggests that changes in smell perception may contribute to the progression of AD pathology in this model.

5. **Reduced locomotion** in 3xTg-AD mice indicates **enhanced anxiety**.

6. 3xTg-AD mice showed **reduced muscle strength** with no significant fine motor disturbances detected. Further investigations are necessary to fully elucidate the fine motor system.

7. **Physical exercise potentially reduces AD progression** in 3xTg-AD mice by shifting towards the anti-apoptotic pathway in the cerebellum, indicating neuroprotective effects.

8. The heightened food-motivated behaviour in older 3xTg-AD mice is likely linked to **changes in body composition**, as well as **disruptions in the HPT axis and the balance between orexigenic and anorexigenic pathways**.

VII. Summary

In this dissertation, we explored the intricate progression of AD using the 3xTg-AD mouse model, focusing on the interplay of anxiety, motor dysfunction, and metabolic changes. Our findings offer significant insights into the multifaceted nature of AD and underscore the value of the 3xTg-AD mouse model for studying this complex disorder.

Heightened Anxiety as an Early Indicator: The study revealed that 3xTg-AD mice exhibited higher innate anxiety compared to controls, with observable fear responses to fox odour and open spaces. This increased anxiety was detected as early as two months of age, coinciding with the appearance of Aβ and p-tau pathologies in brain regions associated with emotional processing, particularly the amygdala. These findings suggest that anxiety can be an early indicator of AD progression, highlighting the potential for early intervention.

Motor Dysfunction and Musculoskeletal Changes: We observed significant motor dysfunction in 3xTg-AD mice, characterized by reduced muscle strength without major motor-coordination problems. However, to fully understand fine motor problems, additional experiments are necessary due to the difference in motivation drive for food. In the joints and the gastrocnemius muscle, the transgenic animals measured normal parameters similar to the controls. An increased apoptotic pathway was observed in the cerebellum, possibly contributing to the development of motor problems. Our findings also suggest that physical exercise might mitigate some of these dysfunctions by promoting anti-apoptotic pathways in the cerebellum, emphasizing the potential neuroprotective effects of physical activity.

Metabolic Shifts and HPT Axis Disruption: The study confirmed that 3xTg-AD mice exhibit heightened food-motivated behaviour, increased food intake, and metabolic changes. These mice showed higher lean mass and lower fat mass, along with disturbances in the HPT axis and shifts towards orexigenic signals in the MBH. These metabolic alterations could be linked to the progression of AD, indicating a complex interaction between metabolic regulation and neurodegenerative processes.

This comprehensive assessment of the 3xTg-AD mouse model highlights the early and progressive behavioural and physiological changes associated with AD. The findings provide valuable insights into the role of anxiety, motor dysfunction, and metabolic changes in AD progression, offering potential avenues for therapeutic interventions.

VIII. References

List of Figures

All figures are original creations and have not been published previously.

1.   Blaszczyk JW. Pathogenesis of Dementia. Int J Mol Sci. 2022;24(1).

2.   Krasnovskaya O, Kononova A, Erofeev A, Gorelkin P, Majouga A, Beloglazkina E. Abeta-Targeting Bifunctional Chelators (BFCs) for Potential Therapeutic and PET Imaging Applications. Int J Mol Sci. 2022;24(1).

3.   Sleegers K, Van Duijn CM. Alzheimer's Disease: Genes, Pathogenesis and Risk Prediction. Community Genet. 2001;4(4):197-203.

4.   Selkoe DJ. Alzheimer's disease: genes, proteins, and therapy. Physiol Rev. 2001;81(2):741-766.

5.   R AA. Risk factors for Alzheimer's disease. Folia Neuropathol. 2019;57(2):87-105.

6.   Vicioso BA. Dementia: when is it not Alzheimer disease? Am J Med Sci. 2002;324(2):84-95.

7.   Dorszewska J, Prendecki M, Oczkowska A, Dezor M, Kozubski W. Molecular Basis of Familial and Sporadic Alzheimer's Disease. Curr Alzheimer Res. 2016;13(9):952-963.

8.   Scott KR, Barrett AM. Dementia syndromes: evaluation and treatment. Expert Rev Neurother. 2007;7(4):407-422.

9.   Elahi FM, Miller BL. A clinicopathological approach to the diagnosis of dementia. Nat Rev Neurol. 2017;13(8):457-476.

10.   2023 Alzheimer's disease facts and figures. Alzheimers Dement. 2023;19(4):1598-1695.

11.   Matthews FE, Brayne C, Lowe J, McKeith I, Wharton SB, Ince P. Epidemiological pathology of dementia: attributable-risks at death in the Medical Research Council Cognitive Function and Ageing Study. PLoS Med. 2009;6(11):e1000180.

12.   Sloane PD, Zimmerman S, Suchindran C, Reed P, Wang L, Boustani M, Sudha S. The public health impact of Alzheimer's disease, 2000-2050: potential implication of treatment advances. Annu Rev Public Health. 2002;23:213-231.

13. Qiu C, Kivipelto M, von Strauss E. Epidemiology of Alzheimer's disease: occurrence, determinants, and strategies toward intervention. Dialogues Clin Neurosci. 2009;11(2):111-128.

14. Roman GC. Facts, myths, and controversies in vascular dementia. J Neurol Sci. 2004;226(1-2):49-52.

15. Venkat P, Chopp M, Chen J. Models and mechanisms of vascular dementia. Exp Neurol. 2015;272:97-108.

16. Kane JPM, Surendranathan A, Bentley A, Barker SAH, Taylor JP, Thomas AJ, et al. Clinical prevalence of Lewy body dementia. Alzheimers Res Ther. 2018;10(1):19.

17. Prasad S, Katta MR, Abhishek S, Sridhar R, Valisekka SS, Hameed M, et al. Recent advances in Lewy body dementia: A comprehensive review. Dis Mon. 2023;69(5):101441.

18. Bang J, Spina S, Miller BL. Frontotemporal dementia. Lancet. 2015;386(10004):1672-1682.

19. Gouveia C, Morais LM, Guimaraes S, Camacho C, Jesus S. Creutzfeldt-Jakob Disease: A Rare Case of Dementia. Cureus. 2023;15(10):e47177.

20. Beam CR, Kaneshiro C, Jang JY, Reynolds CA, Pedersen NL, Gatz M. Differences Between Women and Men in Incidence Rates of Dementia and Alzheimer's Disease. J Alzheimers Dis. 2018;64(4):1077-1083.

21. Rettberg JR, Yao J, Brinton RD. Estrogen: a master regulator of bioenergetic systems in the brain and body. Front Neuroendocrinol. 2014;35(1):8-30.

22. Farkas S, Szabo A, Hegyi AE, Torok B, Fazekas CL, Ernszt D, et al. Estradiol and Estrogen-like Alternative Therapies in Use: The Importance of the Selective and Non-Classical Actions. Biomedicines. 2022;10(4).

23. Nelson HD, Humphrey LL, Nygren P, Teutsch SM, Allan JD. Postmenopausal hormone replacement therapy: scientific review. JAMA. 2002;288(7):872-881.

24. Horstman AM, Dillon EL, Urban RJ, Sheffield-Moore M. The role of androgens and estrogens on healthy aging and longevity. J Gerontol A Biol Sci Med Sci. 2012;67(11):1140-1152.

25. Inkster AM, Duarte-Guterman P, Albert AY, Barha CK, Galea LAM, Robinson WP, Alzheimer's Disease Neuroimaging I. Are sex differences in cognitive impairment reflected in epigenetic age acceleration metrics? Neurobiol Aging. 2022;109:192-194.

26.   Lopez-Lee C, Torres ERS, Carling G, Gan L. Mechanisms of sex differences in Alzheimer's disease. Neuron. 2024;112(8):1208-1221.

27.   Shang D, Wang L, Klionsky DJ, Cheng H, Zhou R. Sex differences in autophagy-mediated diseases: toward precision medicine. Autophagy. 2021;17(5):1065-1076.

28.   Congdon EE. Sex Differences in Autophagy Contribute to Female Vulnerability in Alzheimer's Disease. Front Neurosci. 2018;12:372.

29.   Weger BD, Gobet C, Yeung J, Martin E, Jimenez S, Betrisey B, et al. The Mouse Microbiome Is Required for Sex-Specific Diurnal Rhythms of Gene Expression and Metabolism. Cell Metab. 2019;29(2):362-82 e8.

30.   Dodiya HB, Lutz HL, Weigle IQ, Patel P, Michalkiewicz J, Roman-Santiago CJ, et al. Gut microbiota-driven brain Abeta amyloidosis in mice requires microglia. J Exp Med. 2022;219(1).

31.   Bixler EO, Vgontzas AN, Lin HM, Ten Have T, Rein J, Vela-Bueno A, Kales A. Prevalence of sleep-disordered breathing in women: effects of gender. Am J Respir Crit Care Med. 2001;163(3 Pt 1):608-613.

32.   Ju YS, Ooms SJ, Sutphen C, Macauley SL, Zangrilli MA, Jerome G, et al. Slow wave sleep disruption increases cerebrospinal fluid amyloid-beta levels. Brain. 2017;140(8):2104-2111.

33.   Perry DC, Sturm VE, Peterson MJ, Pieper CF, Bullock T, Boeve BF, et al. Association of traumatic brain injury with subsequent neurological and psychiatric disease: a meta-analysis. J Neurosurg. 2016;124(2):511-526.

34.   Cahill L. Why sex matters for neuroscience. Nat Rev Neurosci. 2006;7(6):477-484.

35.   Andreano JM, Cahill L. Sex influences on the neurobiology of learning and memory. Learn Mem. 2009;16(4):248-266.

36.   Bridel C, van Wieringen WN, Zetterberg H, Tijms BM, Teunissen CE, and the NFLG, et al. Diagnostic Value of Cerebrospinal Fluid Neurofilament Light Protein in Neurology: A Systematic Review and Meta-analysis. JAMA Neurol. 2019;76(9):1035-1048.

37.   Mielke MM, Syrjanen JA, Blennow K, Zetterberg H, Skoog I, Vemuri P, et al. Comparison of variables associated with cerebrospinal fluid neurofilament, total-tau, and neurogranin. Alzheimers Dement. 2019;15(11):1437-1447.

38.   Aggarwal NT, Mielke MM. Sex Differences in Alzheimer's Disease. Neurol Clin. 2023;41(2):343-358.

39.   Yokoi T. Alzheimer's Disease is a Disorder of Consciousness. Gerontol Geriatr Med. 2023;9:23337214231159759.

40.   Novais F, Starkstein S. Phenomenology of Depression in Alzheimer's Disease. J Alzheimers Dis. 2015;47(4):845-855.

41.   Tsuno N, Homma A. What is the association between depression and Alzheimer's disease? Expert Rev Neurother. 2009;9(11):1667-1676.

42.   Zhao QF, Tan L, Wang HF, Jiang T, Tan MS, Tan L, et al. The prevalence of neuropsychiatric symptoms in Alzheimer's disease: Systematic review and meta-analysis. J Affect Disord. 2016;190:264-271.

43.   Burke SL, Cadet T, Alcide A, O'Driscoll J, Maramaldi P. Psychosocial risk factors and Alzheimer's disease: the associative effect of depression, sleep disturbance, and anxiety. Aging Ment Health. 2018;22(12):1577-1584.

44.   Kwak YT, Yang Y, Koo MS. Anxiety in Dementia. Dement Neurocogn Disord. 2017;16(2):33-39.

45.   Nobis L, Husain M. Apathy in Alzheimer's disease. Curr Opin Behav Sci. 2018;22:7-13.

46.   Muhammad T, Meher T. Association of late-life depression with cognitive impairment: evidence from a cross-sectional study among older adults in India. BMC Geriatr. 2021;21(1):364.

47.   Vance DE, Moore BS, Farr KF, Struzick T. Procedural memory and emotional attachment in Alzheimer disease: implications for meaningful and engaging activities. J Neurosci Nurs. 2008;40(2):96-102.

48.   Halpin SN, Dillard RL, Puentes WJ. Socio-Emotional Adaptation Theory: Charting the Emotional Process of Alzheimer's Disease. Gerontologist. 2017;57(4):696-706.

49.   Mazzali G, Bissoli L, Gambina S, Residori L, Pagliari P, Guariento S, et al. Energy balance in Alzheimer's disease. J Nutr Health Aging. 2002;6(4):247-253.

50.   Poehlman ET, Dvorak RV. Energy expenditure, energy intake, and weight loss in Alzheimer disease. Am J Clin Nutr. 2000;71(2):650S-655S.

51.   Talbot K, Wang HY, Kazi H, Han LY, Bakshi KP, Stucky A, et al. Demonstrated brain insulin resistance in Alzheimer's disease patients is associated with IGF-1 resistance, IRS-1 dysregulation, and cognitive decline. J Clin Invest. 2012;122(4):1316-1338.

52.   Craft S. Alzheimer disease: Insulin resistance and AD--extending the translational path. Nat Rev Neurol. 2012;8(7):360-362.

53.   Poddar MK, Banerjee S, Chakraborty A, Dutta D. Metabolic disorder in Alzheimer's disease. Metab Brain Dis. 2021;36(5):781-813.

54.   Arnold SE, Arvanitakis Z, Macauley-Rambach SL, Koenig AM, Wang HY, Ahima RS, et al. Brain insulin resistance in type 2 diabetes and Alzheimer disease: concepts and conundrums. Nat Rev Neurol. 2018;14(3):168-181.

55.   Procaccini C, Santopaolo M, Faicchia D, Colamatteo A, Formisano L, de Candia P, et al. Role of metabolism in neurodegenerative disorders. Metabolism. 2016;65(9):1376-1390.

56.   Craft S. The role of metabolic disorders in Alzheimer disease and vascular dementia: two roads converged. Arch Neurol. 2009;66(3):300-305.

57.   Ge F, Zhu D, Tian M, Shi J. The Role of Thyroid Function in Alzheimer's Disease. J Alzheimers Dis. 2021;83(4):1553-1562.

58.   Bavarsad K, Hosseini M, Hadjzadeh MA, Sahebkar A. The effects of thyroid hormones on memory impairment and Alzheimer's disease. J Cell Physiol. 2019;234(9):14633-14640.

59.   Mullur R, Liu YY, Brent GA. Thyroid hormone regulation of metabolism. Physiol Rev. 2014;94(2):355-382.

60.   Fekete C, Lechan RM. Central regulation of hypothalamic-pituitary-thyroid axis under physiological and pathophysiological conditions. Endocr Rev. 2014;35(2):159-194.

61.   Bianco AC, da Conceicao RR. The Deiodinase Trio and Thyroid Hormone Signaling. Methods Mol Biol. 2018;1801:67-83.

62.   Sabatino L, Vassalle C, Del Seppia C, Iervasi G. Deiodinases and the Three Types of Thyroid Hormone Deiodination Reactions. Endocrinol Metab (Seoul). 2021;36(5):952-964.

63.   Eslami-Amirabadi M, Sajjadi SA. The relation between thyroid dysregulation and impaired cognition/behaviour: An integrative review. J Neuroendocrinol. 2021;33(3):e12948.

64.   Khaleghzadeh-Ahangar H, Talebi A, Mohseni-Moghaddam P. Thyroid Disorders and Development of Cognitive Impairment: A Review Study. Neuroendocrinology. 2022;112(9):835-844.

65.   Nampoothiri S, Nogueiras R, Schwaninger M, Prevot V. Glial cells as integrators of peripheral and central signals in the regulation of energy homeostasis. Nat Metab. 2022;4(7):813-825.

66.   Waterson MJ, Horvath TL. Neuronal Regulation of Energy Homeostasis: Beyond the Hypothalamus and Feeding. Cell Metab. 2015;22(6):962-970.

67.   Schur EA, Melhorn SJ, Oh SK, Lacy JM, Berkseth KE, Guyenet SJ, et al. Radiologic evidence that hypothalamic gliosis is associated with obesity and insulin resistance in humans. Obesity (Silver Spring). 2015;23(11):2142-2148.

68.   Thaler JP, Yi CX, Schur EA, Guyenet SJ, Hwang BH, Dietrich MO, et al. Obesity is associated with hypothalamic injury in rodents and humans. J Clin Invest. 2012;122(1):153-162.

69.   Benzler J, Ganjam GK, Kruger M, Pinkenburg O, Kutschke M, Stohr S, et al. Hypothalamic glycogen synthase kinase 3beta has a central role in the regulation of food intake and glucose metabolism. Biochem J. 2012;447(1):175-184.

70.   Arrieta-Cruz I, Knight CM, Gutierrez-Juarez R. Acute Exposure of the Mediobasal Hypothalamus to Amyloid-beta25-35 Perturbs Hepatic Glucose Metabolism. J Alzheimers Dis. 2015;46(4):843-848.

71.   Rojas-Carranza CA, Bustos-Cruz RH, Pino-Pinzon CJ, Ariza-Marquez YV, Gomez-Bello RM, Canadas-Garre M. Diabetes-Related Neurological Implications and Pharmacogenomics. Curr Pharm Des. 2018;24(15):1695-1710.

72.   Li J, Zhang Y, Lu T, Liang R, Wu Z, Liu M, et al. Identification of diagnostic genes for both Alzheimer's disease and Metabolic syndrome by the machine learning algorithm. Front Immunol. 2022;13:1037318.

73.   Kouidhi S, Clerget-Froidevaux MS. Integrating Thyroid Hormone Signaling in Hypothalamic Control of Metabolism: Crosstalk Between Nuclear Receptors. Int J Mol Sci. 2018;19(7).

74.   Dores RM, Liang L, Davis P, Thomas AL, Petko B. 60 YEARS OF POMC: Melanocortin receptors: evolution of ligand selectivity for melanocortin peptides. J Mol Endocrinol. 2016;56(4):T119-133.

75.   Shen WJ, Yao T, Kong X, Williams KW, Liu T. Melanocortin neurons: Multiple routes to regulation of metabolism. Biochim Biophys Acta Mol Basis Dis. 2017;1863(10 Pt A):2477-2485.

76.   Butler AA. The melanocortin system and energy balance. Peptides. 2006;27(2):281-290.

77.   Butler AA, Cone RD. Knockout studies defining different roles for melanocortin receptors in energy homeostasis. Ann N Y Acad Sci. 2003;994:240-245.

78.   Lensing CJ, Adank DN, Doering SR, Wilber SL, Andreasen A, Schaub JW, et al. Ac-Trp-DPhe(p-I)-Arg-Trp-NH2, a 250-Fold Selective Melanocortin-4 Receptor (MC4R) Antagonist over the Melanocortin-3 Receptor (MC3R), Affects Energy Homeostasis in Male and Female Mice Differently. ACS Chem Neurosci. 2016;7(9):1283-1291.

79.   Belgardt BF, Bruning JC. CNS leptin and insulin action in the control of energy homeostasis. Ann N Y Acad Sci. 2010;1212:97-113.

80.   Gautron L, Elmquist JK. Sixteen years and counting: an update on leptin in energy balance. J Clin Invest. 2011;121(6):2087-2093.

81.   Cowley MA, Smart JL, Rubinstein M, Cerdan MG, Diano S, Horvath TL, et al. Leptin activates anorexigenic POMC neurons through a neural network in the arcuate nucleus. Nature. 2001;411(6836):480-484.

82.   Park HK, Ahima RS. Physiology of leptin: energy homeostasis, neuroendocrine function and metabolism. Metabolism. 2015;64(1):24-34.

83.   Shimizu H, Inoue K, Mori M. The leptin-dependent and -independent melanocortin signaling system: regulation of feeding and energy expenditure. J Endocrinol. 2007;193(1):1-9.

84.   Abraham MA, Rasti M, Bauer PV, Lam TKT. Leptin enhances hypothalamic lactate dehydrogenase A (LDHA)-dependent glucose sensing to lower glucose production in high-fat-fed rats. J Biol Chem. 2018;293(11):4159-4166.

85.   da Silva AA, Hall JE, do Carmo JM. Leptin reverses hyperglycemia and hyperphagia in insulin deficient diabetic rats by pituitary-independent central nervous system actions. PLoS One. 2017;12(11):e0184805.

86.   Engin A. Diet-Induced Obesity and the Mechanism of Leptin Resistance. Adv Exp Med Biol. 2017;960:381-397.

87.   Brown JA, Bugescu R, Mayer TA, Gata-Garcia A, Kurt G, Woodworth HL, Leinninger GM. Loss of Action via Neurotensin-Leptin Receptor Neurons Disrupts Leptin and Ghrelin-Mediated Control of Energy Balance. Endocrinology. 2017;158(5):1271-1288.

88.   Gamber KM, Huo L, Ha S, Hairston JE, Greeley S, Bjorbaek C. Over-expression of leptin receptors in hypothalamic POMC neurons increases susceptibility to diet-induced obesity. PLoS One. 2012;7(1):e30485.

89.   Qureshi D, Collister J, Allen NE, Kuzma E, Littlejohns T. Association between metabolic syndrome and risk of incident dementia in UK Biobank. Alzheimers Dement. 2024;20(1):447-458.

90.   Zhou Z, Ryan J, Tonkin AM, Zoungas S, Lacaze P, Wolfe R, et al. Association Between Triglycerides and Risk of Dementia in Community-Dwelling Older Adults: A Prospective Cohort Study. Neurology. 2023;101(22):e2288-e99.

91.   Piaggi P, Thearle MS, Krakoff J, Votruba SB. Higher Daily Energy Expenditure and Respiratory Quotient, Rather Than Fat-Free Mass, Independently Determine Greater ad Libitum Overeating. J Clin Endocrinol Metab. 2015;100(8):3011-3020.

92.   Porter J, Thompson H, Tjahyo AS. Understanding total energy expenditure in people with dementia: A systematic review with directions for future research. Australas J Ageing. 2021;40(3):243-251.

93.   Bondi MW, Edmonds EC, Jak AJ, Clark LR, Delano-Wood L, McDonald CR, et al. Neuropsychological criteria for mild cognitive impairment improves diagnostic precision, biomarker associations, and progression rates. J Alzheimers Dis. 2014;42(1):275-289.

94.   Petersen RC. Mild Cognitive Impairment. Continuum (Minneap Minn). 2016;22(2 Dementia):404-418.

95.   Aggarwal NT, Wilson RS, Beck TL, Bienias JL, Bennett DA. Motor dysfunction in mild cognitive impairment and the risk of incident Alzheimer disease. Arch Neurol. 2006;63(12):1763-1769.

96.   Boyle PA, Buchman AS, Wilson RS, Leurgans SE, Bennett DA. Association of muscle strength with the risk of Alzheimer disease and the rate of cognitive decline in community-dwelling older persons. Arch Neurol. 2009;66(11):1339-1344.

97.   Gustafson D, Rothenberg E, Blennow K, Steen B, Skoog I. An 18-year follow-up of overweight and risk of Alzheimer disease. Arch Intern Med. 2003;163(13):1524-1528.

98.   Lin YS, Lin FY, Hsiao YH. Myostatin Is Associated With Cognitive Decline in an Animal Model of Alzheimer's Disease. Mol Neurobiol. 2019;56(3):1984-1991.

99.   Lee SJ. Regulation of muscle mass by myostatin. Annu Rev Cell Dev Biol. 2004;20:61-86.

100.   Tsuchida K. The role of myostatin and bone morphogenetic proteins in muscular disorders. Expert Opin Biol Ther. 2006;6(2):147-154.

101.   Benabdallah BF, Bouchentouf M, Rousseau J, Bigey P, Michaud A, Chapdelaine P, et al. Inhibiting myostatin with follistatin improves the success of myoblast transplantation in dystrophic mice. Cell Transplant. 2008;17(3):337-350.

102.   Saitoh M, Takayama K, Hitachi K, Taguchi A, Taniguchi A, Tsuchida K, Hayashi Y. Discovery of a follistatin-derived myostatin inhibitory peptide. Bioorg Med Chem Lett. 2020;30(3):126892.

103.   Iskenderian A, Liu N, Deng Q, Huang Y, Shen C, Palmieri K, et al. Myostatin and activin blockade by engineered follistatin results in hypertrophy and improves dystrophic pathology in mdx mouse more than myostatin blockade alone. Skelet Muscle. 2018;8(1):34.

104.   Abe S, Soejima M, Iwanuma O, Saka H, Matsunaga S, Sakiyama K, Ide Y. Expression of myostatin and follistatin in Mdx mice, an animal model for muscular dystrophy. Zoolog Sci. 2009;26(5):315-320.

105.   Sartori R, Romanello V, Sandri M. Mechanisms of muscle atrophy and hypertrophy: implications in health and disease. Nat Commun. 2021;12(1):330.

106.   Smith RC, Lin BK. Myostatin inhibitors as therapies for muscle wasting associated with cancer and other disorders. Curr Opin Support Palliat Care. 2013;7(4):352-360.

107. Kotecha AM, Correa ADC, Fisher KM, Rushworth JV. Olfactory Dysfunction as a Global Biomarker for Sniffing out Alzheimer's Disease: A Meta-Analysis. Biosensors (Basel). 2018;8(2).

108. Roalf DR, Moberg MJ, Turetsky BI, Brennan L, Kabadi S, Wolk DA, Moberg PJ. A quantitative meta-analysis of olfactory dysfunction in mild cognitive impairment. J Neurol Neurosurg Psychiatry. 2017;88(3):226-232.

109. Jung HJ, Shin IS, Lee JE. Olfactory function in mild cognitive impairment and Alzheimer's disease: A meta-analysis. Laryngoscope. 2019;129(2):362-369.

110. Jagust W. Imaging the evolution and pathophysiology of Alzheimer disease. Nat Rev Neurosci. 2018;19(11):687-700.

111. Dalton RM, Krishnan HS, Parker VS, Catanese MC, Hooker JM. Coevolution of Atomic Resolution and Whole-Brain Imaging for Tau Neurofibrillary Tangles. ACS Chem Neurosci. 2020;11(17):2513-2522.

112. Villemagne VL, Dore V, Burnham SC, Masters CL, Rowe CC. Imaging tau and amyloid-beta proteinopathies in Alzheimer disease and other conditions. Nat Rev Neurol. 2018;14(4):225-236.

113. Thal DR, Rub U, Orantes M, Braak H. Phases of A beta-deposition in the human brain and its relevance for the development of AD. Neurology. 2002;58(12):1791-800.

114. Grothe MJ, Barthel H, Sepulcre J, Dyrba M, Sabri O, Teipel SJ, Alzheimer's Disease Neuroimaging I. In vivo staging of regional amyloid deposition. Neurology. 2017;89(20):2031-2038.

115. Mattsson N, Palmqvist S, Stomrud E, Vogel J, Hansson O. Staging beta-Amyloid Pathology With Amyloid Positron Emission Tomography. JAMA Neurol. 2019;76(11):1319-1329.

116. Crary JF, Trojanowski JQ, Schneider JA, Abisambra JF, Abner EL, Alafuzoff I, et al. Primary age-related tauopathy (PART): a common pathology associated with human aging. Acta Neuropathol. 2014;128(6):755-766.

117. Esteban JA. Living with the enemy: a physiological role for the beta-amyloid peptide. Trends Neurosci. 2004;27(1):1-3.

118. Kamenetz F, Tomita T, Hsieh H, Seabrook G, Borchelt D, Iwatsubo T, et al. APP processing and synaptic function. Neuron. 2003;37(6):925-937.

119.   Parihar MS, Brewer GJ. Amyloid-beta as a modulator of synaptic plasticity. J Alzheimers Dis. 2010;22(3):741-763.

120.   Lawrence JL, Tong M, Alfulaij N, Sherrin T, Contarino M, White MM, et al. Regulation of presynaptic Ca2+, synaptic plasticity and contextual fear conditioning by a N-terminal beta-amyloid fragment. J Neurosci. 2014;34(43):14210-14218.

121.   Palmeri A, Ricciarelli R, Gulisano W, Rivera D, Rebosio C, Calcagno E, et al. Amyloid-beta Peptide Is Needed for cGMP-Induced Long-Term Potentiation and Memory. J Neurosci. 2017;37(29):6926-6937.

122.   Abramov E, Dolev I, Fogel H, Ciccotosto GD, Ruff E, Slutsky I. Amyloid-beta as a positive endogenous regulator of release probability at hippocampal synapses. Nat Neurosci. 2009;12(12):1567-1576.

123.   Morley JE, Farr SA, Banks WA, Johnson SN, Yamada KA, Xu L. A physiological role for amyloid-beta protein:enhancement of learning and memory. J Alzheimers Dis. 2010;19(2):441-449.

124.   Puzzo D, Privitera L, Fa M, Staniszewski A, Hashimoto G, Aziz F, et al. Endogenous amyloid-beta is necessary for hippocampal synaptic plasticity and memory. Ann Neurol. 2011;69(5):819-830.

125.   Lopez-Toledano MA, Shelanski ML. Neurogenic effect of beta-amyloid peptide in the development of neural stem cells. J Neurosci. 2004;24(23):5439-5444.

126.   Plant LD, Boyle JP, Smith IF, Peers C, Pearson HA. The production of amyloid beta peptide is a critical requirement for the viability of central neurons. J Neurosci. 2003;23(13):5531-5535.

127.   Plummer S, Van den Heuvel C, Thornton E, Corrigan F, Cappai R. The Neuroprotective Properties of the Amyloid Precursor Protein Following Traumatic Brain Injury. Aging Dis. 2016;7(2):163-179.

128.   Thornton E, Vink R, Blumbergs PC, Van Den Heuvel C. Soluble amyloid precursor protein alpha reduces neuronal injury and improves functional outcome following diffuse traumatic brain injury in rats. Brain Res. 2006;1094(1):38-46.

129.   Van Nostrand WE. The influence of the amyloid ss-protein and its precursor in modulating cerebral hemostasis. Biochim Biophys Acta. 2016;1862(5):1018-1026.

130.   Hefter D, Draguhn A. APP as a Protective Factor in Acute Neuronal Insults. Front Mol Neurosci. 2017;10:22.

131.   Hardy JA, Higgins GA. Alzheimer's disease: the amyloid cascade hypothesis. Science. 1992;256(5054):184-185.

132.   Evin G, Weidemann A. Biogenesis and metabolism of Alzheimer's disease Abeta amyloid peptides. Peptides. 2002;23(7):1285-1297.

133.   Bayer TA, Cappai R, Masters CL, Beyreuther K, Multhaup G. It all sticks together--the APP-related family of proteins and Alzheimer's disease. Mol Psychiatry. 1999;4(6):524-528.

134.   Thinakaran G, Koo EH. Amyloid precursor protein trafficking, processing, and function. J Biol Chem. 2008;283(44):29615-29619.

135.   Xu X. Gamma-secretase catalyzes sequential cleavages of the AbetaPP transmembrane domain. J Alzheimers Dis. 2009;16(2):211-224.

136.   Chen GF, Xu TH, Yan Y, Zhou YR, Jiang Y, Melcher K, Xu HE. Amyloid beta: structure, biology and structure-based therapeutic development. Acta Pharmacol Sin. 2017;38(9):1205-1235.

137.   Johnson GV, Hartigan JA. Tau protein in normal and Alzheimer's disease brain: an update. J Alzheimers Dis. 1999;1(4-5):329-351.

138.   Johnson GV, Stoothoff WH. Tau phosphorylation in neuronal cell function and dysfunction. J Cell Sci. 2004;117(Pt 24):5721-5729.

139.   Rawat P, Sehar U, Bisht J, Selman A, Culberson J, Reddy PH. Phosphorylated Tau in Alzheimer's Disease and Other Tauopathies. Int J Mol Sci. 2022;23(21).

140.   Oakley SS, Maina MB, Marshall KE, Al-Hilaly YK, Harrington CR, Wischik CM, Serpell LC. Tau Filament Self-Assembly and Structure: Tau as a Therapeutic Target. Front Neurol. 2020;11:590754.

141.   Alonso AD, Cohen LS, Corbo C, Morozova V, ElIdrissi A, Phillips G, Kleiman FE. Hyperphosphorylation of Tau Associates With Changes in Its Function Beyond Microtubule Stability. Front Cell Neurosci. 2018;12:338.

142.   Mansuroglu Z, Benhelli-Mokrani H, Marcato V, Sultan A, Violet M, Chauderlier A, et al. Loss of Tau protein affects the structure, transcription and repair of neuronal pericentromeric heterochromatin. Sci Rep. 2016;6:33047.

143.   Decker JM, Kruger L, Sydow A, Zhao S, Frotscher M, Mandelkow E, Mandelkow EM. Pro-aggregant Tau impairs mossy fiber plasticity due to structural changes and Ca(++) dysregulation. Acta Neuropathol Commun. 2015;3:23.

144.   Combs B, Mueller RL, Morfini G, Brady ST, Kanaan NM. Tau and Axonal Transport Misregulation in Tauopathies. Adv Exp Med Biol. 2019;1184:81-95.

145.   Zhang H, Cao Y, Ma L, Wei Y, Li H. Possible Mechanisms of Tau Spread and Toxicity in Alzheimer's Disease. Front Cell Dev Biol. 2021;9:707268.

146.   Bodea LG, Eckert A, Ittner LM, Piguet O, Gotz J. Tau physiology and pathomechanisms in frontotemporal lobar degeneration. J Neurochem. 2016;138 Suppl 1(Suppl Suppl 1):71-94.

147.   Obulesu M, Lakshmi MJ. Apoptosis in Alzheimer's disease: an understanding of the physiology, pathology and therapeutic avenues. Neurochem Res. 2014;39(12):2301-2312.

148.   Martin LJ. Neuronal cell death in nervous system development, disease, and injury (Review). Int J Mol Med. 2001;7(5):455-478.

149.   Swerdlow RH, Burns JM, Khan SM. The Alzheimer's disease mitochondrial cascade hypothesis. J Alzheimers Dis. 2010;20 Suppl 2(Suppl 2):S265-279.

150.   Tonnies E, Trushina E. Oxidative Stress, Synaptic Dysfunction, and Alzheimer's Disease. J Alzheimers Dis. 2017;57(4):1105-1121.

151.   Hauptmann S, Keil U, Scherping I, Bonert A, Eckert A, Muller WE. Mitochondrial dysfunction in sporadic and genetic Alzheimer's disease. Exp Gerontol. 2006;41(7):668-673.

152.   Hauptmann S, Scherping I, Drose S, Brandt U, Schulz KL, Jendrach M, et al. Mitochondrial dysfunction: an early event in Alzheimer pathology accumulates with age in AD transgenic mice. Neurobiol Aging. 2009;30(10):1574-1586.

153.   Kerr JS, Adriaanse BA, Greig NH, Mattson MP, Cader MZ, Bohr VA, Fang EF. Mitophagy and Alzheimer's Disease: Cellular and Molecular Mechanisms. Trends Neurosci. 2017;40(3):151-166.

154.   Pavlov PF, Hansson Petersen C, Glaser E, Ankarcrona M. Mitochondrial accumulation of APP and Abeta: significance for Alzheimer disease pathogenesis. J Cell Mol Med. 2009;13(10):4137-4145.

155.   Espino de la Fuente-Munoz C, Rosas-Lemus M, Moreno-Castilla P, Bermudez-Rattoni F, Uribe-Carvajal S, Arias C. Age-Dependent Decline in Synaptic Mitochondrial Function Is Exacerbated in Vulnerable Brain Regions of Female 3xTg-AD Mice. Int J Mol Sci. 2020;21(22).

156.   Strazielle C, Jazi R, Verdier Y, Qian S, Lalonde R. Regional brain metabolism with cytochrome c oxidase histochemistry in a PS1/A246E mouse model of autosomal dominant Alzheimer's disease: correlations with behavior and oxidative stress. Neurochem Int. 2009;55(8):806-814.

157.   Dunn AR, O'Connell KMS, Kaczorowski CC. Gene-by-environment interactions in Alzheimer's disease and Parkinson's disease. Neurosci Biobehav Rev. 2019;103:73-80.

158.   Sasaguri H, Hashimoto S, Watamura N, Sato K, Takamura R, Nagata K, et al. Recent Advances in the Modeling of Alzheimer's Disease. Front Neurosci. 2022;16:807473.

159.   Yokoyama M, Kobayashi H, Tatsumi L, Tomita T. Mouse Models of Alzheimer's Disease. Front Mol Neurosci. 2022;15:912995.

160.   Chen ZY, Zhang Y. Animal models of Alzheimer's disease: Applications, evaluation, and perspectives. Zool Res. 2022;43(6):1026-1040.

161.   Esquerda-Canals G, Montoliu-Gaya L, Guell-Bosch J, Villegas S. Mouse Models of Alzheimer's Disease. J Alzheimers Dis. 2017;57(4):1171-1183.

162.   Takeda T, Hosokawa M, Higuchi K. Senescence-accelerated mouse (SAM): a novel murine model of senescence. Exp Gerontol. 1997;32(1-2):105-109.

163.   Porquet D, Andres-Benito P, Grinan-Ferre C, Camins A, Ferrer I, Canudas AM, et al. Amyloid and tau pathology of familial Alzheimer's disease APP/PS1 mouse model in a senescence phenotype background (SAMP8). Age (Dordr). 2015;37(1):9747.

164.   Lawlor PA, Bland RJ, Das P, Price RW, Holloway V, Smithson L, et al. Novel rat Alzheimer's disease models based on AAV-mediated gene transfer to selectively increase hippocampal Abeta levels. Mol Neurodegener. 2007;2:11.

165.   Klementiev B, Novikova T, Novitskaya V, Walmod PS, Dmytriyeva O, Pakkenberg B, et al. A neural cell adhesion molecule-derived peptide reduces neuropathological signs and cognitive impairment induced by Abeta25-35. Neuroscience. 2007;145(1):209-224.

166.   Dmytriyeva O, Belmeguenai A, Bezin L, Soud K, Drucker Woldbye DP, Gotzsche CR, Pankratova S. Short erythropoietin-derived peptide enhances memory, improves long-term potentiation, and counteracts amyloid beta-induced pathology. Neurobiol Aging. 2019;81:88-101.

167. Baerends E, Soud K, Folke J, Pedersen AK, Henmar S, Konrad L, et al. Modeling the early stages of Alzheimer's disease by administering intracerebroventricular injections of human native Abeta oligomers to rats. Acta Neuropathol Commun. 2022;10(1):113.

168. Narasimhan S, Lee VMY. The use of mouse models to study cell-to-cell transmission of pathological tau. Methods Cell Biol. 2017;141:287-305.

169. Robert A, Scholl M, Vogels T. Tau Seeding Mouse Models with Patient Brain-Derived Aggregates. Int J Mol Sci. 2021;22(11).

170. Clavaguera F, Bolmont T, Crowther RA, Abramowski D, Frank S, Probst A, et al. Transmission and spreading of tauopathy in transgenic mouse brain. Nat Cell Biol. 2009;11(7):909-913.

171. Ulm BS, Borchelt DR, Moore BD. Remodeling Alzheimer-amyloidosis models by seeding. Mol Neurodegener. 2021;16(1):8.

172. Ahmed Z, Cooper J, Murray TK, Garn K, McNaughton E, Clarke H, et al. A novel in vivo model of tau propagation with rapid and progressive neurofibrillary tangle pathology: the pattern of spread is determined by connectivity, not proximity. Acta Neuropathol. 2014;127(5):667-683.

173. Nies SH, Takahashi H, Herber CS, Huttner A, Chase A, Strittmatter SM. Spreading of Alzheimer tau seeds is enhanced by aging and template matching with limited impact of amyloid-beta. J Biol Chem. 2021;297(4):101159.

174. Leyns CEG, Gratuze M, Narasimhan S, Jain N, Koscal LJ, Jiang H, et al. TREM2 function impedes tau seeding in neuritic plaques. Nat Neurosci. 2019;22(8):1217-1222.

175. Yuan P, Condello C, Keene CD, Wang Y, Bird TD, Paul SM, et al. TREM2 Haplodeficiency in Mice and Humans Impairs the Microglia Barrier Function Leading to Decreased Amyloid Compaction and Severe Axonal Dystrophy. Neuron. 2016;90(4):724-739.

176. Guerreiro R, Wojtas A, Bras J, Carrasquillo M, Rogaeva E, Majounie E, et al. TREM2 variants in Alzheimer's disease. N Engl J Med. 2013;368(2):117-127.

177. Jonsson T, Stefansson H, Steinberg S, Jonsdottir I, Jonsson PV, Snaedal J, et al. Variant of TREM2 associated with the risk of Alzheimer's disease. N Engl J Med. 2013;368(2):107-116.

178. Zhou Y, Song WM, Andhey PS, Swain A, Levy T, Miller KR, et al. Human and mouse single-nucleus transcriptomics reveal TREM2-dependent and TREM2-independent cellular responses in Alzheimer's disease. Nat Med. 2020;26(1):131-142.

179. Zhang Z, Simpkins JW. An okadaic acid-induced model of tauopathy and cognitive deficiency. Brain Res. 2010;1359:233-246.

180. Baker S, Gotz J. A local insult of okadaic acid in wild-type mice induces tau phosphorylation and protein aggregation in anatomically distinct brain regions. Acta Neuropathol Commun. 2016;4:32.

181. Kumar A, Seghal N, Naidu PS, Padi SS, Goyal R. Colchicines-induced neurotoxicity as an animal model of sporadic dementia of Alzheimer's type. Pharmacol Rep. 2007;59(3):274-283.

182. Silva SSL, Tureck LV, Souza LC, Mello-Hortega JV, Piumbini AL, Teixeira MD, et al. Animal model of Alzheimer's disease induced by streptozotocin: New insights about cholinergic pathway. Brain Res. 2023;1799:148175.

183. Skaaraas G, Melbye C, Puchades MA, Leung DSY, Jacobsen O, Rao SB, et al. Cerebral Amyloid Angiopathy in a Mouse Model of Alzheimer's Disease Associates with Upregulated Angiopoietin and Downregulated Hypoxia-Inducible Factor. J Alzheimers Dis. 2021;83(4):1651-1663.

184. Jakel L, Van Nostrand WE, Nicoll JAR, Werring DJ, Verbeek MM. Animal models of cerebral amyloid angiopathy. Clin Sci (Lond). 2017;131(19):2469-2488.

185. Goate A, Chartier-Harlin MC, Mullan M, Brown J, Crawford F, Fidani L, et al. Segregation of a missense mutation in the amyloid precursor protein gene with familial Alzheimer's disease. Nature. 1991;349(6311):704-706.

186. Levy-Lahad E, Wasco W, Poorkaj P, Romano DM, Oshima J, Pettingell WH, et al. Candidate gene for the chromosome 1 familial Alzheimer's disease locus. Science. 1995;269(5226):973-977.

187. Sherrington R, Rogaev EI, Liang Y, Rogaeva EA, Levesque G, Ikeda M, et al. Cloning of a gene bearing missense mutations in early-onset familial Alzheimer's disease. Nature. 1995;375(6534):754-760.

188. Selkoe DJ, Podlisny MB. Deciphering the genetic basis of Alzheimer's disease. Annu Rev Genomics Hum Genet. 2002;3:67-99.

189.   Deng Y, Wang Z, Wang R, Zhang X, Zhang S, Wu Y, et al. Amyloid-beta protein (Abeta) Glu11 is the major beta-secretase site of beta-site amyloid-beta precursor protein-cleaving enzyme 1(BACE1), and shifting the cleavage site to Abeta Asp1 contributes to Alzheimer pathogenesis. Eur J Neurosci. 2013;37(12):1962-1969.

190.   Goate A. Segregation of a missense mutation in the amyloid beta-protein precursor gene with familial Alzheimer's disease. J Alzheimers Dis. 2006;9(3 Suppl):341-347.

191.   Zhang S, Cai F, Wu Y, Bozorgmehr T, Wang Z, Zhang S, et al. A presenilin-1 mutation causes Alzheimer disease without affecting Notch signaling. Mol Psychiatry. 2020;25(3):603-613.

192.   Hardy J, Selkoe DJ. The amyloid hypothesis of Alzheimer's disease: progress and problems on the road to therapeutics. Science. 2002;297(5580):353-356.

193.   Pimplikar SW. Reassessing the amyloid cascade hypothesis of Alzheimer's disease. Int J Biochem Cell Biol. 2009;41(6):1261-1268.

194.   Ryman DC, Acosta-Baena N, Aisen PS, Bird T, Danek A, Fox NC, et al. Symptom onset in autosomal dominant Alzheimer disease: a systematic review and meta-analysis. Neurology. 2014;83(3):253-260.

195.   Alzheimer's A. 2013 Alzheimer's disease facts and figures. Alzheimers Dement. 2013;9(2):208-245.

196.   Mullan M, Crawford F, Axelman K, Houlden H, Lilius L, Winblad B, Lannfelt L. A pathogenic mutation for probable Alzheimer's disease in the APP gene at the N-terminus of beta-amyloid. Nat Genet. 1992;1(5):345-347.

197.   Citron M, Oltersdorf T, Haass C, McConlogue L, Hung AY, Seubert P, et al. Mutation of the beta-amyloid precursor protein in familial Alzheimer's disease increases beta-protein production. Nature. 1992;360(6405):672-674.

198.   Murrell JR, Hake AM, Quaid KA, Farlow MR, Ghetti B. Early-onset Alzheimer disease caused by a new mutation (V717L) in the amyloid precursor protein gene. Arch Neurol. 2000;57(6):885-887.

199.   Murrell J, Farlow M, Ghetti B, Benson MD. A mutation in the amyloid precursor protein associated with hereditary Alzheimer's disease. Science. 1991;254(5028):97-99.

200. Kamino K, Orr HT, Payami H, Wijsman EM, Alonso ME, Pulst SM, et al. Linkage and mutational analysis of familial Alzheimer disease kindreds for the APP gene region. Am J Hum Genet. 1992;51(5):998-1014.

201. Levy E, Carman MD, Fernandez-Madrid IJ, Power MD, Lieberburg I, van Duinen SG, et al. Mutation of the Alzheimer's disease amyloid gene in hereditary cerebral hemorrhage, Dutch type. Science. 1990;248(4959):1124-1126.

202. Herzig MC, Winkler DT, Burgermeister P, Pfeifer M, Kohler E, Schmidt SD, et al. Abeta is targeted to the vasculature in a mouse model of hereditary cerebral hemorrhage with amyloidosis. Nat Neurosci. 2004;7(9):954-960.

203. Gandy S, Simon AJ, Steele JW, Lublin AL, Lah JJ, Walker LC, et al. Days to criterion as an indicator of toxicity associated with human Alzheimer amyloid-beta oligomers. Ann Neurol. 2010;68(2):220-230.

204. Lee JH, Bacskai BJ, Ayata C. Genetic animal models of cerebral vasculopathies. Prog Mol Biol Transl Sci. 2012;105:25-55.

205. Oakley H, Cole SL, Logan S, Maus E, Shao P, Craft J, et al. Intraneuronal beta-amyloid aggregates, neurodegeneration, and neuron loss in transgenic mice with five familial Alzheimer's disease mutations: potential factors in amyloid plaque formation. J Neurosci. 2006;26(40):10129-10140.

206. Frautschy SA, Yang F, Irrizarry M, Hyman B, Saido TC, Hsiao K, Cole GM. Microglial response to amyloid plaques in APPsw transgenic mice. Am J Pathol. 1998;152(1):307-317.

207. Mucke L, Masliah E, Yu GQ, Mallory M, Rockenstein EM, Tatsuno G, et al. High-level neuronal expression of abeta 1-42 in wild-type human amyloid protein precursor transgenic mice: synaptotoxicity without plaque formation. J Neurosci. 2000;20(11):4050-4058.

208. Chishti MA, Yang DS, Janus C, Phinney AL, Horne P, Pearson J, et al. Early-onset amyloid deposition and cognitive deficits in transgenic mice expressing a double mutant form of amyloid precursor protein 695. J Biol Chem. 2001;276(24):21562-21570.

209. Borchelt DR, Thinakaran G, Eckman CB, Lee MK, Davenport F, Ratovitsky T, et al. Familial Alzheimer's disease-linked presenilin 1 variants elevate Abeta1-42/1-40 ratio in vitro and in vivo. Neuron. 1996;17(5):1005-1013.

210.   Duff K, Eckman C, Zehr C, Yu X, Prada CM, Perez-tur J, et al. Increased amyloid-beta42(43) in brains of mice expressing mutant presenilin 1. Nature. 1996;383(6602):710-713.

211.   Citron M, Westaway D, Xia W, Carlson G, Diehl T, Levesque G, et al. Mutant presenilins of Alzheimer's disease increase production of 42-residue amyloid beta-protein in both transfected cells and transgenic mice. Nat Med. 1997;3(1):67-72.

212.   Tomita T, Maruyama K, Saido TC, Kume H, Shinozaki K, Tokuhiro S, et al. The presenilin 2 mutation (N141I) linked to familial Alzheimer disease (Volga German families) increases the secretion of amyloid beta protein ending at the 42nd (or 43rd) residue. Proc Natl Acad Sci U S A. 1997;94(5):2025-2030.

213.   Das U, Wang L, Ganguly A, Saikia JM, Wagner SL, Koo EH, Roy S. Visualizing APP and BACE-1 approximation in neurons yields insight into the amyloidogenic pathway. Nat Neurosci. 2016;19(1):55-64.

214.   Jonsson T, Atwal JK, Steinberg S, Snaedal J, Jonsson PV, Bjornsson S, et al. A mutation in APP protects against Alzheimer's disease and age-related cognitive decline. Nature. 2012;488(7409):96-99.

215.   Fortea J, Zaman SH, Hartley S, Rafii MS, Head E, Carmona-Iragui M. Alzheimer's disease associated with Down syndrome: a genetic form of dementia. Lancet Neurol. 2021;20(11):930-942.

216.   Drummond E, Wisniewski T. Alzheimer's disease: experimental models and reality. Acta Neuropathol. 2017;133(2):155-175.

217.   Braidy N, Munoz P, Palacios AG, Castellano-Gonzalez G, Inestrosa NC, Chung RS, et al. Recent rodent models for Alzheimer's disease: clinical implications and basic research. J Neural Transm (Vienna). 2012;119(2):173-195.

218.   Ohtsuka M, Ogiwara S, Miura H, Mizutani A, Warita T, Sato M, et al. Pronuclear injection-based mouse targeted transgenesis for reproducible and highly efficient transgene expression. Nucleic Acids Res. 2010;38(22):e198.

219.   Gossler A, Doetschman T, Korn R, Serfling E, Kemler R. Transgenesis by means of blastocyst-derived embryonic stem cell lines. Proc Natl Acad Sci U S A. 1986;83(23):9065-9069.

220. Ittner LM, Klugmann M, Ke YD. Adeno-associated virus-based Alzheimer's disease mouse models and potential new therapeutic avenues. Br J Pharmacol. 2019;176(18):3649-3665.

221. Daya S, Berns KI. Gene therapy using adeno-associated virus vectors. Clin Microbiol Rev. 2008;21(4):583-593.

222. Hall AM, Roberson ED. Mouse models of Alzheimer's disease. Brain Res Bull. 2012;88(1):3-12.

223. Kitazawa M, Medeiros R, Laferla FM. Transgenic mouse models of Alzheimer disease: developing a better model as a tool for therapeutic interventions. Curr Pharm Des. 2012;18(8):1131-1147.

224. Yan Y, Cook CN. Using mass spectrometry to validate mouse models of tauopathy. Mol Neurodegener. 2023;18(1):22.

225. Roberson ED. Mouse models of frontotemporal dementia. Ann Neurol. 2012;72(6):837-849.

226. Saito T, Matsuba Y, Mihira N, Takano J, Nilsson P, Itohara S, et al. Single App knock-in mouse models of Alzheimer's disease. Nat Neurosci. 2014;17(5):661-663.

227. Saito T, Mihira N, Matsuba Y, Sasaguri H, Hashimoto S, Narasimhan S, et al. Humanization of the entire murine Mapt gene provides a murine model of pathological human tau propagation. J Biol Chem. 2019;294(34):12754-12765.

228. Wenger K, Viode A, Schlaffner CN, van Zalm P, Cheng L, Dellovade T, et al. Common mouse models of tauopathy reflect early but not late human disease. Mol Neurodegener. 2023;18(1):10.

229. Oddo S, Caccamo A, Shepherd JD, Murphy MP, Golde TE, Kayed R, et al. Triple-transgenic model of Alzheimer's disease with plaques and tangles: intracellular Abeta and synaptic dysfunction. Neuron. 2003;39(3):409-421.

230. Myers A, McGonigle P. Overview of Transgenic Mouse Models for Alzheimer's Disease. Curr Protoc Neurosci. 2019;89(1):e81.

231. Javonillo DI, Tran KM, Phan J, Hingco E, Kramar EA, da Cunha C, et al. Systematic Phenotyping and Characterization of the 3xTg-AD Mouse Model of Alzheimer's Disease. Front Neurosci. 2021;15:785276.

232.   Goodwin LO, Splinter E, Davis TL, Urban R, He H, Braun RE, et al. Large-scale discovery of mouse transgenic integration sites reveals frequent structural variation and insertional mutagenesis. Genome Res. 2019;29(3):494-505.

233.   Carroll JC, Pike CJ. Selective estrogen receptor modulators differentially regulate Alzheimer-like changes in female 3xTg-AD mice. Endocrinology. 2008;149(5):2607-2611.

234.   Carroll JC, Rosario ER, Kreimer S, Villamagna A, Gentzschein E, Stanczyk FZ, Pike CJ. Sex differences in beta-amyloid accumulation in 3xTg-AD mice: role of neonatal sex steroid hormone exposure. Brain Res. 2010;1366:233-245.

235.   Yang JT, Wang ZJ, Cai HY, Yuan L, Hu MM, Wu MN, Qi JS. Sex Differences in Neuropathology and Cognitive Behavior in APP/PS1/tau Triple-Transgenic Mouse Model of Alzheimer's Disease. Neurosci Bull. 2018;34(5):736-746.

236.   Coughlan G, Coutrot A, Khondoker M, Minihane AM, Spiers H, Hornberger M. Toward personalized cognitive diagnostics of at-genetic-risk Alzheimer's disease. Proc Natl Acad Sci U S A. 2019;116(19):9285-9292.

237.   Coughlan G, Laczo J, Hort J, Minihane AM, Hornberger M. Spatial navigation deficits - overlooked cognitive marker for preclinical Alzheimer disease? Nat Rev Neurol. 2018;14(8):496-506.

238.   Lyketsos CG, Carrillo MC, Ryan JM, Khachaturian AS, Trzepacz P, Amatniek J, et al. Neuropsychiatric symptoms in Alzheimer's disease. Alzheimers Dement. 2011;7(5):532-539.

239.   Kosel F, Pelley JMS, Franklin TB. Behavioural and psychological symptoms of dementia in mouse models of Alzheimer's disease-related pathology. Neurosci Biobehav Rev. 2020;112:634-647.

240.   Hebda-Bauer EK, Simmons TA, Sugg A, Ural E, Stewart JA, Beals JL, et al. 3xTg-AD mice exhibit an activated central stress axis during early-stage pathology. J Alzheimers Dis. 2013;33(2):407-422.

241.   Hutton CP, Lemon JA, Sakic B, Rollo CD, Boreham DR, Fahnestock M, et al. Early Intervention with a Multi-Ingredient Dietary Supplement Improves Mood and Spatial Memory in a Triple Transgenic Mouse Model of Alzheimer's Disease. J Alzheimers Dis. 2018;64(3):835-857.

242.	Kapadia M, Mian MF, Ma D, Hutton CP, Azam A, Narkaj K, et al. Differential effects of chronic immunosuppression on behavioral, epigenetic, and Alzheimer's disease-associated markers in 3xTg-AD mice. Alzheimers Res Ther. 2021;13(1):30.

243.	Sterniczuk R, Antle MC, Laferla FM, Dyck RH. Characterization of the 3xTg-AD mouse model of Alzheimer's disease: part 2. Behavioral and cognitive changes. Brain Res. 2010;1348:149-155.

244.	Pairojana T, Phasuk S, Suresh P, Huang SP, Pakaprot N, Chompoopong S, et al. Age and gender differences for the behavioral phenotypes of 3xTg alzheimer's disease mice. Brain Res. 2021;1762:147437.

245.	St-Amour I, Pare I, Tremblay C, Coulombe K, Bazin R, Calon F. IVIg protects the 3xTg-AD mouse model of Alzheimer's disease from memory deficit and Abeta pathology. J Neuroinflammation. 2014;11:54.

246.	Tournissac M, Vu TM, Vrabic N, Hozer C, Tremblay C, Melancon K, et al. Repurposing beta-3 adrenergic receptor agonists for Alzheimer's disease: beneficial effects in a mouse model. Alzheimers Res Ther. 2021;13(1):103.

247.	Bories C, Arsenault D, Lemire M, Tremblay C, De Koninck Y, Calon F. Transgenic autoinhibition of p21-activated kinase exacerbates synaptic impairments and fronto-dependent behavioral deficits in an animal model of Alzheimer's disease. Aging (Albany NY). 2017;9(5):1386-1403.

248.	Nie L, He K, Xie F, Xiao S, Li S, Xu J, et al. Loganin substantially ameliorates molecular deficits, pathologies and cognitive impairment in a mouse model of Alzheimer's disease. Aging (Albany NY). 2021;13(20):23739-23756.

249.	Pietropaolo S, Feldon J, Yee BK. Age-dependent phenotypic characteristics of a triple transgenic mouse model of Alzheimer disease. Behav Neurosci. 2008;122(4):733-747.

250.	Pietropaolo S, Sun Y, Li R, Brana C, Feldon J, Yee BK. Limited impact of social isolation on Alzheimer-like symptoms in a triple transgenic mouse model. Behav Neurosci. 2009;123(1):181-195.

251.	Pietropaolo S, Feldon J, Yee BK. Environmental enrichment eliminates the anxiety phenotypes in a triple transgenic mouse model of Alzheimer's disease. Cogn Affect Behav Neurosci. 2014;14(3):996-1008.

252. Clinton LK, Billings LM, Green KN, Caccamo A, Ngo J, Oddo S, et al. Age-dependent sexual dimorphism in cognition and stress response in the 3xTg-AD mice. Neurobiol Dis. 2007;28(1):76-82.

253. Dennison JL, Ricciardi NR, Lohse I, Volmar CH, Wahlestedt C. Sexual Dimorphism in the 3xTg-AD Mouse Model and Its Impact on Pre-Clinical Research. J Alzheimers Dis. 2021;80(1):41-52.

254. Bruzsik B, Biro L, Sarosdi KR, Zelena D, Sipos E, Szebik H, et al. Neurochemically distinct populations of the bed nucleus of stria terminalis modulate innate fear response to weak threat evoked by predator odor stimuli. Neurobiol Stress. 2021;15:100415.

255. Staples LG. Predator odor avoidance as a rodent model of anxiety: learning-mediated consequences beyond the initial exposure. Neurobiol Learn Mem. 2010;94(4):435-445.

256. Le Moene O, Agmo A. Responses to positive and aversive stimuli in estrous female rats housed in a seminatural environment: Effects of yohimbine and chlordiazepoxide. Pharmacol Biochem Behav. 2019;179:43-54.

257. Hebb AL, Zacharko RM, Dominguez H, Trudel F, Laforest S, Drolet G. Odor-induced variation in anxiety-like behavior in mice is associated with discrete and differential effects on mesocorticolimbic cholecystokinin mRNA expression. Neuropsychopharmacology. 2002;27(5):744-755.

258. Wu N, Rao X, Gao Y, Wang J, Xu F. Amyloid-beta deposition and olfactory dysfunction in an Alzheimer's disease model. J Alzheimers Dis. 2013;37(4):699-712.

259. Alvarado-Martinez R, Salgado-Puga K, Pena-Ortega F. Amyloid beta inhibits olfactory bulb activity and the ability to smell. PLoS One. 2013;8(9):e75745.

260. Wesson DW, Levy E, Nixon RA, Wilson DA. Olfactory dysfunction correlates with amyloid-beta burden in an Alzheimer's disease mouse model. J Neurosci. 2010;30(2):505-514.

261. Puzzo D, Privitera L, Leznik E, Fa M, Staniszewski A, Palmeri A, Arancio O. Picomolar amyloid-beta positively modulates synaptic plasticity and memory in hippocampus. J Neurosci. 2008;28(53):14537-14545.

262.	Wesson DW, Borkowski AH, Landreth GE, Nixon RA, Levy E, Wilson DA. Sensory network dysfunction, behavioral impairments, and their reversibility in an Alzheimer's beta-amyloidosis mouse model. J Neurosci. 2011;31(44):15962-15971.

263.	Palop JJ, Mucke L. Amyloid-beta-induced neuronal dysfunction in Alzheimer's disease: from synapses toward neural networks. Nat Neurosci. 2010;13(7):812-818.

264.	Chernov Y. Handwriting Markers for the Onset of Alzheimer's Disease. Curr Alzheimer Res. 2024.

265.	Kluger A, Gianutsos JG, Golomb J, Ferris SH, George AE, Franssen E, Reisberg B. Patterns of motor impairement in normal aging, mild cognitive decline, and early Alzheimer's disease. J Gerontol B Psychol Sci Soc Sci. 1997;52B(1):P28-39.

266.	Reiserer RS, Harrison FE, Syverud DC, McDonald MP. Impaired spatial learning in the APPSwe + PSEN1DeltaE9 bigenic mouse model of Alzheimer's disease. Genes Brain Behav. 2007;6(1):54-65.

267.	Kuwabara Y, Ishizeki M, Watamura N, Toba J, Yoshii A, Inoue T, Ohshima T. Impairments of long-term depression induction and motor coordination precede Abeta accumulation in the cerebellum of APPswe/PS1dE9 double transgenic mice. J Neurochem. 2014;130(3):432-443.

268.	Van Dam D, D'Hooge R, Staufenbiel M, Van Ginneken C, Van Meir F, De Deyn PP. Age-dependent cognitive decline in the APP23 model precedes amyloid deposition. Eur J Neurosci. 2003;17(2):388-396.

269.	Sepulveda-Falla D, Barrera-Ocampo A, Hagel C, Korwitz A, Vinueza-Veloz MF, Zhou K, et al. Familial Alzheimer's disease-associated presenilin-1 alters cerebellar activity and calcium homeostasis. J Clin Invest. 2014;124(4):1552-1567.

270.	Russo R, Cattaneo F, Lippiello P, Cristiano C, Zurlo F, Castaldo M, et al. Motor coordination and synaptic plasticity deficits are associated with increased cerebellar activity of NADPH oxidase, CAMKII, and PKC at preplaque stage in the TgCRND8 mouse model of Alzheimer's disease. Neurobiol Aging. 2018;68:123-133.

271.	Ewers M, Morgan DG, Gordon MN, Woodruff-Pak DS. Associative and motor learning in 12-month-old transgenic APP+PS1 mice. Neurobiol Aging. 2006;27(8):1118-1128.

272. O'Leary TP, Robertson A, Chipman PH, Rafuse VF, Brown RE. Motor function deficits in the 12 month-old female 5xFAD mouse model of Alzheimer's disease. Behav Brain Res. 2018;337:256-263.

273. Hoxha E, Lippiello P, Zurlo F, Balbo I, Santamaria R, Tempia F, Miniaci MC. The Emerging Role of Altered Cerebellar Synaptic Processing in Alzheimer's Disease. Front Aging Neurosci. 2018;10:396.

274. Fukutani Y, Cairns NJ, Rossor MN, Lantos PL. Cerebellar pathology in sporadic and familial Alzheimer's disease including APP 717 (Val-->Ile) mutation cases: a morphometric investigation. J Neurol Sci. 1997;149(2):177-184.

275. Sepulveda-Falla D, Matschke J, Bernreuther C, Hagel C, Puig B, Villegas A, et al. Deposition of hyperphosphorylated tau in cerebellum of PS1 E280A Alzheimer's disease. Brain Pathol. 2011;21(4):452-463.

276. Hoxha E, Boda E, Montarolo F, Parolisi R, Tempia F. Excitability and synaptic alterations in the cerebellum of APP/PS1 mice. PLoS One. 2012;7(4):e34726.

277. Dineley KT, Xia X, Bui D, Sweatt JD, Zheng H. Accelerated plaque accumulation, associative learning deficits, and up-regulation of alpha 7 nicotinic receptor protein in transgenic mice co-expressing mutant human presenilin 1 and amyloid precursor proteins. J Biol Chem. 2002;277(25):22768-22780.

278. Jacobs HIL, Hopkins DA, Mayrhofer HC, Bruner E, van Leeuwen FW, Raaijmakers W, Schmahmann JD. The cerebellum in Alzheimer's disease: evaluating its role in cognitive decline. Brain. 2018;141(1):37-47.

279. Mavroudis I. Cerebellar pathology in Alzheimer's disease. Hell J Nucl Med. 2019;22 Suppl:174-179.

280. Alveal-Mellado D, Castillo-Mariqueo L, Gimenez-Llort L. Sex- and Neuropsychiatric-Dependent Circadian Alterations in Daily Voluntary Physical Activity Engagement and Patterns in Aged 3xTg-AD Mice. Int J Mol Sci. 2022;23(22).

281. Sawicka-Gutaj N, Zawalna N, Gut P, Ruchala M. Relationship between thyroid hormones and central nervous system metabolism in physiological and pathological conditions. Pharmacol Rep. 2022;74(5):847-858.

282. Fu AL, Zhou CY, Chen X. Thyroid hormone prevents cognitive deficit in a mouse model of Alzheimer's disease. Neuropharmacology. 2010;58(4-5):722-729.

283. Maglione AV, do Nascimento BPP, Ribeiro MO, de Souza TJL, da Silva REC, Sato MA, et al. Triiodothyronine Treatment reverses Depression-Like Behavior in a triple-transgenic animal model of Alzheimer's Disease. Metab Brain Dis. 2022;37(8):2735-2750.

284. Ren B, Ma J, Tao M, Jing G, Han S, Zhou C, et al. The disturbance of thyroid-associated hormone and its receptors in brain and blood circulation existed in the early stage of mouse model of Alzheimer's disease. Aging (Albany NY). 2023;15(5):1591-1602.

285. Chamas L, Seugnet I, Poirier R, Clerget-Froidevaux MS, Enderlin V. A Fine Regulation of the Hippocampal Thyroid Signalling Protects Hypothyroid Mice against Glial Cell Activation. Int J Mol Sci. 2022;23(19).

286. O'Barr SA, Oh JS, Ma C, Brent GA, Schultz JJ. Thyroid hormone regulates endogenous amyloid-beta precursor protein gene expression and processing in both in vitro and in vivo models. Thyroid. 2006;16(12):1207-1213.

287. Li Z, Liu J. Thyroid dysfunction and Alzheimer's disease, a vicious circle. Front Endocrinol (Lausanne). 2024;15:1354372.

288. AlAnazi FH, Al-Kuraishy HM, Alexiou A, Papadakis M, Ashour MHM, Alnaaim SA, et al. Primary Hypothyroidism and Alzheimer's Disease: A Tale of Two. Cell Mol Neurobiol. 2023.

289. Vancamp P, Butruille L, Demeneix BA, Remaud S. Thyroid Hormone and Neural Stem Cells: Repair Potential Following Brain and Spinal Cord Injury. Front Neurosci. 2020;14:875.

290. AlAnazi FH, Al-Kuraishy HM, Alexiou A, Papadakis M, Ashour MHM, Alnaaim SA, et al. Primary Hypothyroidism and Alzheimer's Disease: A Tale of Two. Cell Mol Neurobiol. 2023;43(7):3405-3416.

291. Joy Mathew C, Jose MT, Elshaikh AO, Shah L, Lee R, Cancarevic I. Is Hyperthyroidism a Possible Etiology of Early Onset Dementia? Cureus. 2020;12(9):e10603.

292. Little AG. Local Regulation of Thyroid Hormone Signaling. Vitam Horm. 2018;106:1-17.

293. Albrechet-Souza L, Gilpin NW. The predator odor avoidance model of post-traumatic stress disorder in rats. Behav Pharmacol. 2019;30(2 and 3-Spec Issue):105-114.

294. Varkonyi D, Torok B, Sipos E, Fazekas CL, Banrevi K, Correia P, et al. Investigation of Anxiety- and Depressive-like Symptoms in 4- and 8-Month-Old Male Triple Transgenic Mouse Models of Alzheimer's Disease. Int J Mol Sci. 2022;23(18).

295. Gould TD, Dao DT, Kovacsics CE. The open field test. Mood and anxiety related phenotypes in mice: Characterization using behavioral tests. Totowa, NJ, US: Humana Press/Springer Nature; 2009. p. 1-20.

296. Takeshita H, Yamamoto K, Nozato S, Inagaki T, Tsuchimochi H, Shirai M, et al. Modified forelimb grip strength test detects aging-associated physiological decline in skeletal muscle function in male mice. Sci Rep. 2017;7:42323.

297. Horvath G, Goloncser F, Csolle C, Kiraly K, Ando RD, Baranyi M, et al. Central P2Y12 receptor blockade alleviates inflammatory and neuropathic pain and cytokine production in rodents. Neurobiol Dis. 2014;70:162-178.

298. Kwakowsky A, Potapov K, Kim S, Peppercorn K, Tate WP, Abraham IM. Treatment of beta amyloid 1-42 (Abeta(1-42))-induced basal forebrain cholinergic damage by a non-classical estrogen signaling activator in vivo. Sci Rep. 2016;6:21101.

299. Baird AL, Meldrum A, Dunnett SB. The staircase test of skilled reaching in mice. Brain Res Bull. 2001;54(2):243-250.

300. Farkas S, Szabo A, Torok B, Solyomvari C, Fazekas CL, Banrevi K, et al. Ovariectomy-induced hormone deprivation aggravates Abeta(1-42) deposition in the basolateral amygdala and cholinergic fiber loss in the cortex but not cognitive behavioral symptoms in a triple transgenic mouse model of Alzheimer's disease. Front Endocrinol (Lausanne). 2022;13:985424.

301. Kuti D, Winkler Z, Horvath K, Juhasz B, Szilvasy-Szabo A, Fekete C, et al. The metabolic stress response: Adaptation to acute-, repeated- and chronic challenges in mice. iScience. 2022;25(8):104693.

302. Paxinos G, Franklin KBJ, Franklin KBJ. The mouse brain in stereotaxic coordinates. 2nd ed. San Diego: Academic Press; 2001.

303. Szegeczki V, Bauer B, Jungling A, Fulop BD, Vago J, Perenyi H, et al. Age-related alterations of articular cartilage in pituitary adenylate cyclase-activating polypeptide (PACAP) gene-deficient mice. Geroscience. 2019;41(6):775-793.

304. Schmittgen TD, Livak KJ. Analyzing real-time PCR data by the comparative C(T) method. Nat Protoc. 2008;3(6):1101-1108.

305. Wirth-Dzieciolowska E, Lipska A, Wesierska M. Selection for body weight induces differences in exploratory behavior and learning in mice. Acta Neurobiol Exp (Wars). 2005;65(3):243-253.

306. Konkoly J, Kormos V, Gaszner B, Sandor Z, Kecskes A, Alomari A, et al. The Role of TRPA1 Channels in the Central Processing of Odours Contributing to the Behavioural Responses of Mice. Pharmaceuticals (Basel). 2021;14(12).

307. Georgiadis M, Muller R, Schneider P. Techniques to assess bone ultrastructure organization: orientation and arrangement of mineralized collagen fibrils. J R Soc Interface. 2016;13(119).

308. Chen Z, Xie H, Yao L, Wei Y. Olfactory impairment and the risk of cognitive decline and dementia in older adults: a meta-analysis. Braz J Otorhinolaryngol. 2021;87(1):94-102.

309. Romano RR, 3rd, Carter MA, Monroe TB. Narrative Review of Sensory Changes as a Biomarker for Alzheimer's Disease. Biol Res Nurs. 2021;23(2):223-230.

310. Kurtz P, Schuurman T, Prinz H. Loss of smell leads to dementia in mice: is Alzheimer's disease a degenerative disorder of the olfactory system? J Protein Chem. 1989;8(3):448-451.

311. Mitrano DA, Houle SE, Pearce P, Quintanilla RM, Lockhart BK, Genovese BC, et al. Olfactory dysfunction in the 3xTg-AD model of Alzheimer's disease. IBRO Neurosci Rep. 2021;10:51-61.

312. Coronas-Samano G, Portillo W, Beltran Campos V, Medina-Aguirre GI, Paredes RG, Diaz-Cintra S. Deficits in odor-guided behaviors in the transgenic 3xTg-AD female mouse model of Alzheimer′s disease. Brain Res. 2014;1572:18-25.

313. Sancheti H, Patil I, Kanamori K, Diaz Brinton R, Zhang W, Lin AL, Cadenas E. Hypermetabolic state in the 7-month-old triple transgenic mouse model of Alzheimer's disease and the effect of lipoic acid: a 13C-NMR study. J Cereb Blood Flow Metab. 2014;34(11):1749-1760.

314. Marchese M, Cowan D, Head E, Ma D, Karimi K, Ashthorpe V, et al. Autoimmune manifestations in the 3xTg-AD model of Alzheimer's disease. J Alzheimers Dis. 2014;39(1):191-210.

315.   Adlimoghaddam A, Snow WM, Stortz G, Perez C, Djordjevic J, Goertzen AL, et al. Regional hypometabolism in the 3xTg mouse model of Alzheimer's disease. Neurobiol Dis. 2019;127:264-277.

316.   Friesen M, Ziegler-Waldkirch S, Egenolf M, d'Errico P, Helm C, Mezo C, et al. Distinct Abeta pathology in the olfactory bulb and olfactory deficits in a mouse model of Abeta and alpha-syn co-pathology. Brain Pathol. 2022;32(3):e13032.

317.   Zhang YL, Xing RZ, Luo XB, Xu H, Chang RC, Zou LY, et al. Anxiety-like behavior and dysregulation of miR-34a in triple transgenic mice of Alzheimer's disease. Eur Rev Med Pharmacol Sci. 2016;20(13):2853-2862.

318.   Yu NY, Chang SH. Characterization of the fine motor problems in patients with cognitive dysfunction - A computerized handwriting analysis. Hum Mov Sci. 2019;65.

319.   Liu X, Abudukeremu A, Jiang Y, Cao Z, Wu M, Sun R, et al. Fine or Gross Motor Index as a Simple Tool for Predicting Cognitive Impairment in Elderly People: Findings from The Irish Longitudinal Study on Ageing (TILDA). J Alzheimers Dis. 2021;83(2):889-896.

320.   Likhtik E, Stujenske JM, Topiwala MA, Harris AZ, Gordon JA. Prefrontal entrainment of amygdala activity signals safety in learned fear and innate anxiety. Nat Neurosci. 2014;17(1):106-113.

321.   Langford-Smith A, Malinowska M, Langford-Smith KJ, Wegrzyn G, Jones S, Wynn R, et al. Hyperactive behaviour in the mouse model of mucopolysaccharidosis IIIB in the open field and home cage environments. Genes Brain Behav. 2011;10(6):673-682.

322.   Catuzzi JE, Beck KD. Anxiety vulnerability in women: a two-hit hypothesis. Exp Neurol. 2014;259:75-80.

323.   Moser JS, Moran TP, Kneip C, Schroder HS, Larson MJ. Sex moderates the association between symptoms of anxiety, but not obsessive compulsive disorder, and error-monitoring brain activity: A meta-analytic review. Psychophysiology. 2016;53(1):21-29.

324.   Szabo A, Farkas S, Fazekas C, Correia P, Chaves T, Sipos E, et al. Temporal Appearance of Enhanced Innate Anxiety in Alzheimer Model Mice. Biomedicines. 2023;11(2).

325.   Scholtzova H, Do E, Dhakal S, Sun Y, Liu S, Mehta PD, Wisniewski T. Innate Immunity Stimulation via Toll-Like Receptor 9 Ameliorates Vascular Amyloid

Pathology in Tg-SwDI Mice with Associated Cognitive Benefits. J Neurosci. 2017;37(4):936-959.

326. Cai H, Qiao J, Chen S, Yang J, Holscher C, Wang Z, et al. MCU knockdown in hippocampal neurons improves memory performance of an Alzheimer's disease mouse model. Acta Biochim Biophys Sin (Shanghai). 2022;54(10):1528-1539.

327. Naik S, Katariya R, Shelke S, Patravale V, Umekar M, Kotagale N, Taksande B. Nattokinase prevents beta-amyloid peptide (Abeta(1-42)) induced neuropsychiatric complications, neuroinflammation and BDNF signalling disruption in mice. Eur J Pharmacol. 2023;952:175821.

328. Dixit MP, Rahmatkar SN, Raut P, Umekar MJ, Taksande BG, Kotagale NR. Evidences for agmatine alterations in Abeta(1-42)induced memory impairment in mice. Neurosci Lett. 2021;740:135447.

329. Kotagale N, Rahmatkar S, Chauragade S, Dixit M, Umekar M, Chopde C, Taksande B. Involvement of hippocampal agmatine in beta(1-42) amyloid induced memory impairment, neuroinflammation and BDNF signaling disruption in mice. Neurotoxicology. 2020;80:1-11.

330. Payrits M, Borbely E, Godo S, Ernszt D, Kemeny A, Kardos J, et al. Genetic deletion of TRPA1 receptor attenuates amyloid beta- 1-42 (Abeta(1-42))-induced neurotoxicity in the mouse basal forebrain in vivo. Mech Ageing Dev. 2020;189:111268.

331. Xian YF, Qu C, Liu Y, Ip SP, Yuan QJ, Yang W, Lin ZX. Magnolol Ameliorates Behavioral Impairments and Neuropathology in a Transgenic Mouse Model of Alzheimer's Disease. Oxid Med Cell Longev. 2020;2020:5920476.

332. Li HQ, Ip SP, Yuan QJ, Zheng GQ, Tsim KKW, Dong TTX, et al. Isorhynchophylline ameliorates cognitive impairment via modulating amyloid pathology, tau hyperphosphorylation and neuroinflammation: Studies in a transgenic mouse model of Alzheimer's disease. Brain Behav Immun. 2019;82:264-278.

333. Mani V, Jaafar SM, Azahan NSM, Ramasamy K, Lim SM, Ming LC, Majeed ABA. Ciproxifan improves cholinergic transmission, attenuates neuroinflammation and oxidative stress but does not reduce amyloid level in transgenic mice. Life Sci. 2017;180:23-35.

334. Bagaria J, Bagyinszky E, An SSA. Genetics, Functions, and Clinical Impact of Presenilin-1 (PSEN1) Gene. Int J Mol Sci. 2022;23(18).

335.   Mittal K, Mani RJ, Katare DP. Type 3 Diabetes: Cross Talk between Differentially Regulated Proteins of Type 2 Diabetes Mellitus and Alzheimer's Disease. Sci Rep. 2016;6:25589.

336.   de Paula JJ, Albuquerque MR, Lage GM, Bicalho MA, Romano-Silva MA, Malloy-Diniz LF. Impairment of fine motor dexterity in mild cognitive impairment and Alzheimer's disease dementia: association with activities of daily living. Braz J Psychiatry. 2016;38(3):235-238.

337.   Stover KR, Campbell MA, Van Winssen CM, Brown RE. Analysis of motor function in 6-month-old male and female 3xTg-AD mice. Behav Brain Res. 2015;281:16-23.

338.   Parsons SA, Millay DP, Sargent MA, McNally EM, Molkentin JD. Age-dependent effect of myostatin blockade on disease severity in a murine model of limb-girdle muscular dystrophy. Am J Pathol. 2006;168(6):1975-1985.

339.   Haidet AM, Rizo L, Handy C, Umapathi P, Eagle A, Shilling C, et al. Long-term enhancement of skeletal muscle mass and strength by single gene administration of myostatin inhibitors. Proc Natl Acad Sci U S A. 2008;105(11):4318-4322.

340.   Bagheri R, Rashidlamir A, Motevalli MS, Elliott BT, Mehrabani J, Wong A. Effects of upper-body, lower-body, or combined resistance training on the ratio of follistatin and myostatin in middle-aged men. Eur J Appl Physiol. 2019;119(9):1921-1931.

341.   Khalafi M, Aria B, Symonds ME, Rosenkranz SK. The effects of resistance training on myostatin and follistatin in adults: A systematic review and meta-analysis. Physiol Behav. 2023;269:114272.

342.   Fife E, Kostka J, Kroc L, Guligowska A, Piglowska M, Soltysik B, et al. Relationship of muscle function to circulating myostatin, follistatin and GDF11 in older women and men. BMC Geriatr. 2018;18(1):200.

343.   Zimmers TA, Davies MV, Koniaris LG, Haynes P, Esquela AF, Tomkinson KN, et al. Induction of cachexia in mice by systemically administered myostatin. Science. 2002;296(5572):1486-1488.

344.   Brandt C, Hansen RH, Hansen JB, Olsen CH, Galle P, Mandrup-Poulsen T, et al. Over-expression of Follistatin-like 3 attenuates fat accumulation and improves insulin sensitivity in mice. Metabolism. 2015;64(2):283-295.

345. Motevalli MS, Dalbo VJ, Attarzadeh RS, Rashidlamir A, Tucker PS, Scanlan AT. The effect of rate of weight reduction on serum myostatin and follistatin concentrations in competitive wrestlers. Int J Sports Physiol Perform. 2015;10(2):139-146.

346. Giuliani D, Ottani A, Zaffe D, Galantucci M, Strinati F, Lodi R, Guarini S. Hydrogen sulfide slows down progression of experimental Alzheimer's disease by targeting multiple pathophysiological mechanisms. Neurobiol Learn Mem. 2013;104:82-91.

347. Kim J, Seo S, Park JHY, Lee KW, Kim J, Kim JC. Ca(2+)-Permeable TRPV1 Receptor Mediates Neuroprotective Effects in a Mouse Model of Alzheimer's Disease via BDNF/CREB Signaling Pathway. Mol Cells. 2023;46(5):319-328.

348. Park SS, Park HS, Kim CJ, Kang HS, Kim DH, Baek SS, Kim TW. Physical exercise during exposure to 40-Hz light flicker improves cognitive functions in the 3xTg mouse model of Alzheimer's disease. Alzheimers Res Ther. 2020;12(1):62.

349. Sah SK, Lee C, Jang JH, Park GH. Effect of high-fat diet on cognitive impairment in triple-transgenic mice model of Alzheimer's disease. Biochem Biophys Res Commun. 2017;493(1):731-736.

350. Kim D, Cho J, Kang H. Protective effect of exercise training against the progression of Alzheimer's disease in 3xTg-AD mice. Behav Brain Res. 2019;374:112105.

351. Xu B, He Y, Liu L, Ye G, Chen L, Wang Q, et al. The Effects of Physical Running on Dendritic Spines and Amyloid-beta Pathology in 3xTg-AD Male Mice. Aging Dis. 2022;13(4):1293-1310.

352. Roda AR, Esquerda-Canals G, Marti-Clua J, Villegas S. Cognitive Impairment in the 3xTg-AD Mouse Model of Alzheimer's Disease is Affected by Abeta-ImmunoTherapy and Cognitive Stimulation. Pharmaceutics. 2020;12(10).

353. de Frutos-Lucas J, Cuesta P, Lopez-Sanz D, Peral-Suarez A, Cuadrado-Soto E, Ramirez-Torano F, et al. The relationship between physical activity, apolipoprotein E epsilon4 carriage, and brain health. Alzheimers Res Ther. 2020;12(1):48.

354. Valenzuela PL, Castillo-Garcia A, Morales JS, de la Villa P, Hampel H, Emanuele E, et al. Exercise benefits on Alzheimer's disease: State-of-the-science. Ageing Res Rev. 2020;62:101108.

355. Szegeczki V, Perenyi H, Horvath G, Hinnah B, Tamas A, Radak Z, et al. Physical Training Inhibits the Fibrosis Formation in Alzheimer's Disease Kidney Influencing the TGFbeta Signaling Pathways. J Alzheimers Dis. 2021;81(3):1195-1209.

356. Wagner JM, Sichler ME, Schleicher EM, Franke TN, Irwin C, Low MJ, et al. Analysis of Motor Function in the Tg4-42 Mouse Model of Alzheimer's Disease. Front Behav Neurosci. 2019;13:107.

357. Oore J, Fraser L, Brown R. AGE-RELATED CHANGES IN MOTOR ABILITY AND MOTOR LEARNING IN TRIPLE TRANSGENIC (3×TG-AD) AND CONTROL (B6129SF1/J) MICE ON THE ACCELERATING ROTAROD. Proceedings of the Nova Scotian Institute of Science 2013.

358. Filali M, Lalonde R, Theriault P, Julien C, Calon F, Planel E. Cognitive and non-cognitive behaviors in the triple transgenic mouse model of Alzheimer's disease expressing mutated APP, PS1, and Mapt (3xTg-AD). Behav Brain Res. 2012;234(2):334-342.

359. Garvock-de Montbrun T, Fertan E, Stover K, Brown RE. Motor deficits in 16-month-old male and female 3xTg-AD mice. Behav Brain Res. 2019;356:305-313.

360. Hirai K, Aliev G, Nunomura A, Fujioka H, Russell RL, Atwood CS, et al. Mitochondrial abnormalities in Alzheimer's disease. J Neurosci. 2001;21(9):3017-3023.

361. Keil U, Bonert A, Marques CA, Scherping I, Weyermann J, Strosznajder JB, et al. Amyloid beta-induced changes in nitric oxide production and mitochondrial activity lead to apoptosis. J Biol Chem. 2004;279(48):50310-50320.

362. Fernandez-Vizarra P, Fernandez AP, Castro-Blanco S, Serrano J, Bentura ML, Martinez-Murillo R, et al. Intra- and extracellular Abeta and PHF in clinically evaluated cases of Alzheimer's disease. Histol Histopathol. 2004;19(3):823-844.

363. Lustbader JW, Cirilli M, Lin C, Xu HW, Takuma K, Wang N, et al. ABAD directly links Abeta to mitochondrial toxicity in Alzheimer's disease. Science. 2004;304(5669):448-452.

364. Wright KM, Deighan AG, Di Francesco A, Freund A, Jojic V, Churchill GA, Raj A. Age and diet shape the genetic architecture of body weight in diversity outbred mice. Elife. 2022;11.

365. Jura M, Kozak LP. Obesity and related consequences to ageing. Age (Dordr). 2016;38(1):23.

366. Kurokawa M, Akino K, Kanda K. A new apparatus for studying feeding and drinking in the mouse. Physiol Behav. 2000;70(1-2):105-112.

367. Blundell JE, Caudwell P, Gibbons C, Hopkins M, Naslund E, King NA, Finlayson G. Body composition and appetite: fat-free mass (but not fat mass or BMI) is positively associated with self-determined meal size and daily energy intake in humans. Br J Nutr. 2012;107(3):445-449.

368. Ravussin E, Lillioja S, Anderson TE, Christin L, Bogardus C. Determinants of 24-hour energy expenditure in man. Methods and results using a respiratory chamber. J Clin Invest. 1986;78(6):1568-1578.

369. Peronnet F, Massicotte D. Table of nonprotein respiratory quotient: an update. Can J Sport Sci. 1991;16(1):23-29.

370. Even PC, Nadkarni NA. Indirect calorimetry in laboratory mice and rats: principles, practical considerations, interpretation and perspectives. Am J Physiol Regul Integr Comp Physiol. 2012;303(5):R459-476.

371. Tschop MH, Speakman JR, Arch JR, Auwerx J, Bruning JC, Chan L, et al. A guide to analysis of mouse energy metabolism. Nat Methods. 2011;9(1):57-63.

372. Frayn KN. Calculation of substrate oxidation rates in vivo from gaseous exchange. J Appl Physiol Respir Environ Exerc Physiol. 1983;55(2):628-634.

373. Roberts SB, Dallal GE. Energy requirements and aging. Public Health Nutr. 2005;8(7A):1028-1036.

374. Simpson SJ, Le Couteur DG, Raubenheimer D, Solon-Biet SM, Cooney GJ, Cogger VC, Fontana L. Dietary protein, aging and nutritional geometry. Ageing Res Rev. 2017;39:78-86.

375. Wang Z, Heshka S, Gallagher D, Boozer CN, Kotler DP, Heymsfield SB. Resting energy expenditure-fat-free mass relationship: new insights provided by body composition modeling. Am J Physiol Endocrinol Metab. 2000;279(3):E539-45.

376. Berglund ED, Li CY, Poffenberger G, Ayala JE, Fueger PT, Willis SE, et al. Glucose metabolism in vivo in four commonly used inbred mouse strains. Diabetes. 2008;57(7):1790-1799.

377. Wyatt P, Berry SE, Finlayson G, O'Driscoll R, Hadjigeorgiou G, Drew DA, et al. Postprandial glycaemic dips predict appetite and energy intake in healthy individuals. Nat Metab. 2021;3(4):523-529.

378. Roelfsema F, Veldhuis JD. Thyrotropin secretion patterns in health and disease. Endocr Rev. 2013;34(5):619-657.

379. Fekete C, Lechan RM. Central regulation of hypothalamic-pituitary-thyroid axis under physiological and pathophysiological conditions. Endocr Rev. 2014;35(2):159-194.

380. Kohrle J, Fradrich C. Deiodinases control local cellular and systemic thyroid hormone availability. Free Radic Biol Med. 2022;193(Pt 1):59-79.

381. Werneck de Castro JP, Fonseca TL, Ueta CB, McAninch EA, Abdalla S, Wittmann G, et al. Differences in hypothalamic type 2 deiodinase ubiquitination explain localized sensitivity to thyroxine. J Clin Invest. 2015;125(2):769-781.

382. Blouet C, Schwartz GJ. Hypothalamic nutrient sensing in the control of energy homeostasis. Behav Brain Res. 2010;209(1):1-12.

383. Valdearcos M, Xu AW, Koliwad SK. Hypothalamic inflammation in the control of metabolic function. Annu Rev Physiol. 2015;77:131-160.

384. Movsesyan N, Ghochikyan A, Mkrtichyan M, Petrushina I, Davtyan H, Olkhanud PB, et al. Reducing AD-like pathology in 3xTg-AD mouse model by DNA epitope vaccine - a novel immunotherapeutic strategy. PLoS One. 2008;3(5):e2124.

385. Ponomarenko EA, Krasnov GS, Kiseleva OI, Kryukova PA, Arzumanian VA, Dolgalev GV, et al. Workability of mRNA Sequencing for Predicting Protein Abundance. Genes (Basel). 2023;14(11).

386. Gebauer F, Hentze MW. Molecular mechanisms of translational control. Nat Rev Mol Cell Biol. 2004;5(10):827-835.

IX. Bibliography of the candidate's publications

IX.1. Candidate's publication related to the theme of the thesis

Szabo A, Farkas S, Fazekas CL, Correia P, Chaves T, Sipos E, Makkai B, Torok B, Zelena D. Temporal Appearance of Enhanced Innate Anxiety in Alzheimer Model Mice. Biomedicines. 2023;11(2). (IF: 3.9)

Farkas S, **Szabo A,** Torok B, Solyomvari C, Fazekas CL, Banrevi K, Correia P, Chaves T, Zelena D. Ovariectomy-induced hormone deprivation aggravates $A\beta_{1-42}$ deposition in the basolateral amygdala and cholinergic fiber loss in the cortex but not cognitive behavioral symptoms in a triple transgenic mouse model of Alzheimer's disease. Front Endocrinol (Lausanne). 2022;13:985424. (IF: 5.2)

Varkonyi D, Torok B, Sipos E, Fazekas CL, Banrevi K, Correia P, Chaves T, Farkas S, **Szabo A,** S. Martinez-Bellver, B. Hangya, and D. Zelena. Investigation of Anxiety- and Depressive-like Symptoms in 4- and 8-Month-Old Male Triple Transgenic Mouse Models of Alzheimer's Disease. Int J Mol Sci. 2022;23(18). (IF: 5.6)

IX.2. Candidate's publications not related to the theme of the thesis

Farkas S, **Szabo A,** Hegyi AE, Torok B, Fazekas CL, Ernszt D, Kovacs T, Zelena D. Estradiol and Estrogen-like Alternative Therapies in Use: The Importance of the Selective and Non-Classical Actions. Biomedicines. 2022;10(4). (IF: 4.7)

Fazekas CL, **Szabo A,** Torok B, Banrevi K, Correia P, Chaves T, Daumas S, Zelena D. A New Player in the Hippocampus: A Review on VGLUT3+ Neurons and Their Role in the Regulation of Hippocampal Activity and Behaviour. Int J Mol Sci. 2022;23(2). (IF: 5.6)

Szabo A, Schlett K, Szucs A. Conventional measures of intrinsic excitability are poor estimators of neuronal activity under realistic synaptic inputs. PLoS Comput Biol. 2021;17(9):e1009378 (IF: 4.779)

Torok B, Fazekas CL, **Szabo A,** Zelena D. Epigenetic Modulation of Vasopressin Expression in Health and Disease. Int J Mol Sci. 2021;22(17). (IF: 6,208)

Chaves T, Fazekas CL, Horvath K, Correia P, **Szabo A,** Torok B, Banrevi K, Zelena, D. Stress Adaptation and the Brainstem with Focus on Corticotropin-Releasing Hormone. Int J Mol Sci. 2021;22(16). (IF: 6.208)

X. Acknowledgment

This scientific work would not have been possible without those who were by my side on this bumpy, trying, sometimes very happy, sometimes very frustrating path, whether for the duration of an experiment or throughout the entire journey.

I am primarily grateful to my supervisor, Prof. Dr. Dóra Zelena, for taking me under her wing and providing the conditions for the implementation of the experiments. She introduced me to the world of behavioural science and supported my sometimes-absurd ideas.

I am indebted to my friend, Dr. Csilla Lea Fazekas, for helping me join the research group, as well as for her professional help and the support of many friends.

My heart is grateful to Dr. Bibiana Szocsics-Török for teaching me the secrets and tricks of stereotaxic surgery. She helped me with my work while accepting me as her friend.

I am indescribably grateful to Dr. Szidónia Farkas for being not only a fantastic colleague but also a special friend. A big part of working together is that we were always there for each other when we needed professional or friendly support.

I am grateful to the researchers and assistants I met at the Experimental Medicine Research Institute, especially group 71, for accepting me into their group.

I owe a debt of gratitude to the employees of the Institute of Physiology of the Faculty of General Medicine of the University of Pécs, who not only welcomed me into their community but also created a workplace atmosphere where it is a pleasure to work, even on the worst days.

I would like to thank Gergő Deák, who is the best animal caretaker I have worked with, for his professional work. Thanks to his expertise, experiments with animals went smoothly.

I am indebted to laboratory animals; without them, science would not be where it is today.

However, I cannot forget to thank my family and friends for believing in me, encouraging me when I was nervous, and always being there for me.

Thanks to everyone who contributed in any way to the preparation of this thesis. Wherever my journey takes me, the meetings and exchanges of ideas have shaped my research thinking, attitude, and vision, so they live on in me forever.

Thank you.